ENVIRONMENTAL TRACERS FOR QUANTIFYING SURFACE WATER-GROUNDWATER INTERACTION

Sarah Bourke, BSc. (Honours)

School of the Environment, Flinders University

For submission in fulfillment of the requirements of Doctor of Philosophy

Declaration of originality

I certify that this thesis does not incorporate without acknowledgment any material previously submitted for a degree or diploma in any university; and that to the best of my knowledge and belief it does not contain any material previously published or written by another person except where due reference is made in the text.

Sarah Anne Bourke

01 April, 2014

Corrected thesis submitted 13 August, 2014

Co-Authorship

Sarah A. Bourke is the primary author on all manuscripts in this thesis. On all submitted papers, the co-authors provided intellectual supervision and editorial content.

Acknowledgements

Summary

As demand for water resources intensifies, quantification of surface water-groundwater interaction has become increasingly important for effective water resource management. Various hydraulic and tracer techniques have been developed for quantifying these exchanges, each sensitive to particular scales or modes of exchange. In order to capture the entire spectrum of exchange fluxes in any given system, it is often necessary to employ several of these methods. Chapter 1 outlines the need for new methods, with different sensitivities than previously published methods, which will be valuable additions to the suite of available techniques. In this thesis, two new techniques are presented, using gas tracers to quantify 1) hyporheic exchange in losing streams, and 2) groundwater discharge to gaining streams. Additionally, groundwater age indicators and noble gases are applied in a novel setting to quantify the re-circulation of groundwater associated with mine dewatering operations.

Chapter 2 presents a new method for quantifying hyporheic exchange in losing streams based on measurements of radon-222 along the stream. A longitudinal mass balance approach is used to interpret measurements of streamflow and radon along the stream in terms of hyporheic (beneath the stream) and parafluvial (beside the stream) exchange fluxes. The results of this new method are compared to two existing methods; streambed radon disequilibrium and transient storage modeling of the breakthrough curves of an injected tracer. Transient storage modeling characterized rapid hyporheic exchange with a mean residence time of 4 minutes, storage zone area of 0.6 m^2 and storage exchange flux of 224 m^2 d^{-1}. This is consistent with the results of the streambed radon disequilibrium method, which suggest that the rapidly flushed hyporheic zone was at most 0.1 m thick. In contrast, the radon influx of 5.4 x 10^4 Bq m^{-1} d^{-1} was dominated by (≥80%) long-path parafluvial exchange with residence times of days, spatial scales of tens to hundreds of metres, and an exchange flux on the order of 10 m^2 d^{-1}. The new radon-based method is particularly sensitive to return flow paths on spatial scales of tens of meters, with sub-surface residence times of days or more, which were not captured by the pre-existing methods. Concurrent application of this new method, with existing methods using injected tracers, will provide a more complete estimate of the spectrum of return flows in losing stream systems.

In Chapter 3, the application of carbon-14 (^{14}C) in dissolved inorganic carbon (DIC) as a tracer of groundwater discharge to gaining streams is presented. A mass balance model for ^{14}C in DIC is developed, which allows for the isotopic equilibration rate to be expressed as an effective

transfer velocity for ^{14}C in DIC. A controlled experiment was conducted over 72 days to quantify the rate of isotopic equilibration of ^{14}C in DIC in groundwater exposed to the atmosphere. The method was then tested at an artificial groundwater discharge zone in the Pilbara region of Western Australia. The effective transfer velocities of these systems were as expected based on the pH and gas transfer velocity of CO_2, with values of 0.013 and 0.025 m d^{-1} respectively. The method was then applied across a previously mapped spring discharge zone in the Daly River, in northern Australia. The ^{14}C activity of DIC in the stream decreased from 83 to 76 pMC across the major discharge zone, which was used to estimate the ^{14}C activity of the discharging groundwater at between 60 and 66 pMC. The effective transfer velocity was estimated at between 0.09 and 0.15 m d^{-1}, which is between 8 and 13% larger than would be expected based on the gas transfer velocity of CO_2 and pH of this system. This increased rate of equilibration, above that predicted by carbonate speciation, is likely to be driven by in-stream CO_2 production through biotic respiration or the conversion of dissolved organic carbon to DIC. In spite of these additional sources of DIC in the stream, the signal of groundwater discharge in stream ^{14}C activity persisted for at least tens of kilometers. This persistence of the changes in ^{14}C activity caused by groundwater discharge over longer distances than other gaseous tracers allows for a larger spatial sampling interval and may allow for smaller groundwater fluxes to be quantified than is possible with other gaseous tracers.

In Chapter 4, groundwater age indicators (^{14}C and CFC-12) and noble gases are used as tracers of recharge by surplus mine water that is discharged to streams. In environments where groundwater is effectively re-circulated, quantification of the relative proportions of natural and anthropogenic recharge can be difficult. Groundwater age indicators, in particular gases, are likely to be more sensitive tracers of recharge than stable isotopes or chloride in this setting. This is because, unlike stable isotopes or chloride, they undergo a process of equilibration with the atmosphere, and historical atmospheric concentrations are known. Ternary mixing fractions were calculated based on ^{14}C and CFC-12 concentrations measured along three transects of piezometers perpendicular to the creeks, and from dewatering wells. The three end-members were defined to reflect the historical atmospheric concentrations of these tracers, and the history of mining operations. Uncertainty in calculated mixing fractions was estimated using a Monte Carlo approach. Recharge by mine water that had been discharged to the creeks was present in all samples, with the largest proportions within 250 m of the creeks. These results are supported by seepage estimates based on the chloride mass balance along the creeks, which suggests that between 85 and 90% of mine water discharged to the creeks recharges the aquifer. Based on the duration of discharge, recharge by mine

water is predicted to extend between 110 and 730 m from the creeks. Ternary mixing ratios in dewatering wells suggest that recharge by mine water accounted for between 10 and 87 % of water currently abstracted by dewatering wells. These results are supported by estimates of excess air and terrigenic helium-4 amounts, with correlations between the amount of mine water and excess air, and the amount of regional groundwater and terrigenic helium-4. These methods could also be used to quantify recharge associated with agricultural irrigation or wetland supplementation and will be most successful when the duration of the activity is short, relative to the timescale of variation in atmospheric tracer concentrations.

Chapter 5 discusses how the new methods demonstrated in this thesis can be used in conjunction with pre-existing methods to improve field-based estimates surface water-groundwater interaction. Future work will involve the further validation of these new methods and their application at other field sites.

Table of Contents

List of Figures

List of Tables

List of Appendices

Chapter 1   Introduction

1.1   Background

As water resources become increasingly scarce relative to demand, robust assessments of surface water-groundwater exchange have become critical for sustainable water resource management. Water fluxes between streams and aquifers occur over a range of spatial and temporal scales, and can be grouped into one of three modes of interaction; gaining, losing or through-flow (Winter et al., 1998). In gaining systems, the net exchange of water is from the aquifer to the surface water body; in losing systems the net exchange of water is from the surface water body to the aquifer; and in through-flow systems, water flows into the surface water body on the up-gradient side, and out on the down-gradient side. Superimposed onto this net gain or loss between stream and aquifer, are return flow paths, over a range of spatial and temporal scales, that can collectively be termed hyporheic exchange (Stonedahl et al., 2010). These return flow paths are particularly important for biogeochemical cycling in stream systems and are important drivers of nutrient distributions and contaminant fate and transport (Harvey and Wagner, 2000).

The mode and magnitude of exchange between a stream and the underlying aquifer can vary along its length, and through time (Kalbus et al., 2006). However, classification into one of these modes remains useful for management, with potential risks varying between exchange modes. Furthermore, the numerous methods that have been developed for quantifying surface water-groundwater interaction are often more suited to one mode of exchange than another. (Sophocleous, 2002, Kalbus et al., 2006).

Gaseous tracers are inherently suitable for quantifying surface water-groundwater interaction because they respond quickly to exposure to the atmosphere (Raymond and Cole, 2001). As a result, concentrations of gaseous tracers are often significantly different in groundwater and surface water. In this thesis, new methods of quantifying surface water-groundwater interaction are developed using environmental isotopes and groundwater age indicators that are gaseous, or equilibrate with the atmosphere in a similar way to gaseous tracers. The application of environmental isotopes as tracers relies on the rate of accumulation (for radiogenic isotopes) or decay (for radioactive isotopes) of the tracer to imply residence times, and therefore fluxes (Cook and Herczeg, 2000). Examples of environmental isotopes that can be used as tracers of surface water-groundwater interactions are radon-222, carbon-14, and

helium-4. Other groundwater age indicators, such as CFCs, SF_6, and thermonuclear carbon-14, have historical concentration distributions with periods of time where atmospheric concentrations were elevated due to anthropogenic activity, and can therefore be used as event markers (Cook and Herczeg, 2000).

Any tracer-based method for estimating surface water-groundwater interaction has inherent bias and uncertainty (Shanafield and Cook, 2014, Kalbus et al., 2006). Because of this, it is generally considered sound practice to employ more than one tracer whenever practicable (Scanlon et al., 2002, Shanafield and Cook, 2014). New tracer techniques, with different sensitivities to published techniques, will be valuable additions to the suite of available techniques for quantifying surface water-groundwater interaction.

1.2 Objectives

Three specific objectives were addressed, each focused on the development or application of isotopic gas tracers for quantifying a particular mode of surface water-groundwater interaction:

1. Develop analytical methods for using stream radon-222 to quantify hyporheic exchange in a losing stream.
2. Develop and test the use of carbon-14 as a tracer of groundwater discharge to streams.
3. Differentiate sources of recharge in environments with groundwater re-circulation using CFC-12, carbon-14 and noble gases

1.3 Thesis structure

This thesis consists of 5 chapters, beginning with this introduction, which outlines the research question and objectives and outlines the thesis structure. The following three chapters (Chapters 2, 3, and 4), present the main research work, and are written as manuscripts for publication in peer reviews journals. Each of these chapters can be read independently and are published or under review as follows:

Chapter 2:
Bourke, S.A. Cook, P.G., Shanafield, M., Dogramaci, S., (2014). Characterization of hyporheic exchange in losing streams using radon-222. Journal of Hydrology, 519, 94-105.

Chapter 3:

Bourke, S.A., Harrington, G.A., Cook, P.G., Post, V.E., Dogramaci, S., 2014, Carbon-14 in streams as a tracer of discharging groundwater. Journal of Hydrology, 519, 117-130.

Chapter 4:

Bourke, S.A., Cook, P.G., Dogramaci, S., Kipfer, R., In review, Differentiating sources of recharge in environments with groundwater re-circulation using CFC-12, carbon-14 and noble gases. Prepared for Journal of Hydrology, in CSIRO internal review at the time of thesis submission.

These manuscripts are followed by a conclusion (Chapter 5), which summarizes the broader implications of the research presented in this thesis and makes recommendations for future work. Abstracts of conference papers based on the work presented in this thesis are included in Appendix 3.

Chapter 2   Characterization of hyporheic exchange in a losing stream using radon-222

2.1   Introduction

Hyporheic exchange exerts an important influence on nutrient distribution, productivity and contaminant transport in streams (Boulton et al., 2010, Jones and Mulholland, 2000, Bencala, 1984, Findlay, 1995). While definitions of hyporheic exchange vary, the term generally refers to the cycling of water between a stream and the groundwater below and adjacent to it, creating an exchange zone with chemical properties that are different to both the stream and the aquifer. This cycling occurs at a range of scales and can be related to stream bed-forms, turbulent eddies, gravel bars and meanders (Stonedahl et al., 2010, Cardenas et al., 2004, Boano et al., 2011, O'Connor and Harvey, 2008).

A common technique for estimating hyporheic exchange is to inject a tracer into the stream and use a transient storage model to interpret the tracer breakthrough curves measured downstream (Harvey and Wagner, 2000, Bencala and Walters, 1983). The time scale of tracer injection and measurement is usually on the order of hours with breakthrough curves measured at locations within one kilometre of the injection point. The sensitivity of the method is limited to flow paths on smaller spatial and temporal scales than the injection experiment and so this scale of tracer injection captures fluxes with residence times of hours or less and usually spatial scales of hundreds of metres or less (Harvey et al., 1996). The use of transient storage modeling to resolve longer flow paths is time consuming and labour intensive, requiring tracer injection over a period of days (Dent et al., 2007, Triska et al., 1993). Transient storage modeling of breakthrough curves using a one-zone storage model is generally considered to capture the characteristic exchange scale in most systems, but is biased towards rapid exchange (Harvey et al., 1996, Choi et al., 2000). As a further limitation, the distribution of hyporheic flow paths is approximated as one storage zone that includes the effects of stagnant zones along the stream, and could over-estimate hyporheic exchange in streams with significant in-stream storage capacity.

While long flow paths with long residence times may not be a large component of the overall exchange flux, they may be important for solute transport and biogeochemical cycling (Dent et

al., 2007). The difficulty of capturing exchange fluxes with long residence times and flow paths has led some authors to suggest that hydraulic methods should be applied more often (Bencala et al., 2011). An alternative approach is to use measurements of radon -222 in the stream or streambed to infer hyporheic exchange parameters (Cook et al., 2006, Lamontagne and Cook, 2007, Mullinger et al., 2007, Mullinger et al., 2009).

Radon-222 (hereafter referred to as radon) is a radiogenic noble gas with a half-life of 3.8 days that is produced by most sediment through the decay of uranium series isotopes. Radon activity in surface water is low as radon is readily lost to the atmosphere through gas exchange. Water that enters the subsurface increases in radon activity over a period of around 20 days until equilibrium between radon production and decay is reached. In losing streams, radon activity in groundwater has previously been used to infer rates of infiltration (Bertin and Bourg, 1994, Hoehn and Von Gunten, 1989). Disequilibrium of radon activities within the streambed has been used to infer residence times in the hyporheic zone (Lamontagne and Cook, 2007). Streambed radon activities are relatively easy to measure but interpretation of streambed radon profiles requires an estimate of the radon production rate of the sediments, which can be highly variable in heterogeneous alluvial sediments. Also, calculation of hyporheic fluxes from streambed radon activities requires an independent estimate of the groundwater exchange flux.

In gaining stream systems, groundwater inflow rates and hyporheic exchange have been estimated based on stream radon activities using a 1D mass balance model (Cook et al., 2006, Cook et al., 2003). One of the major difficulties with this approach is separating the radon contribution through hyporheic exchange from the radon contribution of groundwater discharge.

In a losing stream where there is no groundwater inflow, the radon activity in the stream is effectively determined by the balance of losses to groundwater recharge, radioactive decay and gas exchange with the atmosphere, and additions through hyporheic exchange. If these loss terms are known, longitudinal stream radon activities in a losing stream can be used to estimate hyporheic exchange parameters (hyporheic zone depth, flux and residence time). In this chapter this new method for characterizing hyporheic exchange parameters based on longitudinal stream radon activities is applied in a losing stream. These results are compared to estimates from two existing methods with differing scales of sensitivity: streambed radon disequilibrium and transient storage modeling of tracer breakthrough curves.

2.2 Theory

Definitions of hyporheic exchange are many and varied (Gooseff, 2010). Hydrochemically, the hyporheic zone can be considered as a zone where the water composition is a mixture of stream water and groundwater, providing a habitat intermediate between stream and groundwater (Triska et al., 1993, Boulton et al., 2010, Hoehn and Cirpka, 2006). Hydrologists often define the hyporheic zone based on the extent of flow paths which originate from and return to the stream (Storey et al., 2003, O'Connor and Harvey, 2008, Stonedahl et al., 2010, Worman et al., 2002). In this context, hyporheic exchange can be considered to include a spectrum of flow paths ranging from shallow exchange between the stream and streambed on the scale of centimetres to longer return flows across stream meanders on the scale of tens to hundreds of metres (Stonedahl et al., 2010). In this chapter, it is useful to restrict the use of the term hyporheic to its literal meaning (*hypo* = beneath), using it refer to exchange fluxes between the stream and streambed directly beneath the stream. These fluxes are usually characterized by residence times of less than a day, spatial scales less than a metre, and are commonly captured by injected tracer experiments (Bencala and Walters, 1983, Harvey et al., 1996). Exchange fluxes with longer residence times of days to weeks and spatial scales of metres to tens of metres are not commonly captured by injected tracer experiments, and are not well resolved by radon profiles beneath the streambed. These longer flow paths are more likely to occur within the alluvium adjacent to the stream (but may also flow directly beneath it), and so the term parafluvial is used to refer to this type of exchange (*para* = beside).

2.2.1 Stream radon activity

In a losing stream, the change in streamflow with distance is a function of groundwater recharge and evaporation, and is given by:

$$\frac{\partial Q}{\partial x} = -q_{gw} - Ew \qquad\qquad (2.1)$$

where Q is the streamflow ($m^3\,d^{-1}$), q_{gw} is the groundwater recharge flux per metre length of stream ($m^2\,d^{-1}$), E is the evapotranspiration rate ($m\,d^{-1}$) and w is stream width (m). This groundwater recharge flux is related to the infiltration rate, I, of Cook et al. (2006) through the stream width: $q_{gw} = Iw$. This equation assumes steady state conditions, and can therefore only be applied if streamflow is constant for the duration of measurement and sample collection. Additional terms can be added to account for inflows from tributaries or drainage channels, provided that the flow rates (and inflow concentrations) can also be assumed to be constant for the duration of measurement and sample collection.

For dissolved gases in a stream the gas exchange rate is much greater than the evaporation rate and the evaporation term can be neglected in the tracer mass balance. Cook et al. (2006) expressed the mass balance of radon in a losing stream as:

$$\frac{\partial Qc}{\partial x} = q_h(c_h - c) - q_{gw}c - kwc - \lambda dwc \qquad (2.2)$$

where c is the radon activity within the stream, c_h is the radon activity within the hyporheic zone, q_h is the hyporheic exchange flux ($m^2\,d^{-1}$), k is the gas transfer velocity across the water surface ($m\,d^{-1}$), λ is the radioactive decay constant of radon (0.181 d^{-1}), and d is the stream depth (m).

In a one-layer, uniform, well-mixed hyporheic zone the steady state solute mass balance can be written:

$$q_h c - q_h c_h + q_{gw}c - q_{gw}c_h - \lambda wh\theta c_h + \gamma wh\theta = 0 \qquad (2.3)$$

where h is the hyporheic zone depth (m), γ is the radon production rate of the sediments (Bq $L^{-1}\,d^{-1}$) and ϑ is porosity (Lamontagne and Cook, 2007). This conceptual model implies an exponential distribution of hyporheic residence times with a mean residence time, t_h (d) given by:

$$t_h = \frac{wh\theta}{(q_h + q_{gw})} \qquad (2.4)$$

The concentration of radon within the hyporheic zone will increase as the hyporheic zone residence time increases, and hence the sensitivity of stream radon concentrations to the hyporheic exchange flux increases as the residence time increases. Therefore, when the exchange includes both very short (fast) and very long (slow) flow paths, it may be useful to explicitly differentiate between them. The mass balance of radon in the stream therefore becomes:

$$\frac{\partial Qc}{\partial x} = q_h(c_h - c) + q_p(c_p - c) - q_{gw}c - kwc - \lambda dwc \qquad (2.5)$$

where q_p is the fluid flux in or out of the parafluvial zone ($m^2\,d^{-1}$), and c_p is the concentration of water discharging from the parafluvial zone into the stream.

Although the exponential distribution of travel times implied by Equation 2.3 is perhaps appropriate for the shallow hyporheic zone beneath the streambed, and has been widely implemented in transient storage models (Runkel, 1998, Bencala and Walters, 1983, Harvey et al., 1996), it is less appropriate for longer flow paths which may travel some lateral distance

7

from the stream. Parafluvial flow paths are therefore represented as streamtubes, originating and ending in the stream, so that the radon activity of water leaving the parafluvial zone, c_p, is given by:

$$c_p = c_e - (c_e - c)e^{(-\lambda t_p)}$$
(2.6)

where t_p (d) is the parafluvial residence time and c_e (Bq L^{-1}) is the equilibrium radon activity. This equilibrium activity is related to the radon production rate, γ, by the relationship:

$$c_e = \frac{\gamma}{\lambda}$$
(2.7)

For any combination of parafluvial flux and residence time the total volume of alluvium swept by parafluvial flow paths into each metre length of stream can be calculated from:

$$V_p = \frac{q_p t_p}{\theta}$$
(2.8)

where V_p is the volume swept into each metre length of stream (m^2). V_p can be envisaged as the cross-sectional area of the parafluvial exchange zone.

Applying the chain rule of differentiation using Equations 2.1 and 2.5, substituting for c_h using equations 2.3 and 2.4, and substituting for c_p using Equations 2.6 and 2.7, the change in radon activity along the stream can be expressed as:

$$Q\frac{\partial c}{\partial x} = \left(\frac{\gamma}{\lambda} - c\right)\left(\frac{q_h t_h}{\lambda^{-1} + t_h}\right) + \left(\frac{\gamma}{\lambda} - c\right)q_p\left(1 - e^{-\lambda t_p}\right) - kwc - \lambda dwc$$
(2.9)

where the first term on the right hand side denotes the change in concentration due to hyporheic exchange and the second term denotes parafluvial exchange. This equation can be used to constrain the radon flux entering the stream through exchange with streambed hyporheic and parafluvial zones based on measurements of stream radon activity.

2.2.2 Streambed radon disequilibrium

Estimates of hyporheic residence time can be made from vertical profiles of radon activity through the hyporheic zone. Rearranging Equation 2.4 to solve for q_h and substituting this into Equation 2.3 gives:

$$t_h = \frac{c - c_h}{\lambda c_h - \gamma}$$
(2.10)

which can be used to estimate hyporheic residence times based on measurements of stream radon activity, hyporheic radon activity and the radon production rate of the sediments (Lamontagne and Cook, 2007). Once this residence time is known, if the groundwater recharge

flux, $q_{gw,}$ is also known, the hyporheic flux can be calculated by rearranging Equation 2.4 to solve for q_h.

2.2.3   Transient storage modeling

The breakthrough curves of a conservative artificial tracer can be interpreted using a transient storage model to infer the exchange flux between the stream and storage zone (Bencala and Walters, 1983, Harvey et al., 1996). While this exchange flux is sometimes equated with streambed hyporheic exchange it also includes parafluvial flow and the effects of stagnant zones along the stream channel that retard solute transport. In this chapter OTIS (One Dimensional Transport with Inflow and Storage), and OTIS-P are used to interpret tracer breakthrough curves (Runkel, 1998). OTIS-P is a modified version of OTIS, which couples the solution of the governing equation with a nonlinear regression package to estimate model parameters. These models assumes that solute concentrations vary only in the longitudinal direction, mass is conserved within the stream and storage zone, and transient storage is the only physical process affecting solute concentrations within the storage zone. In the absence of decay, sorption or lateral inflow, the concentration of solute in the stream channel and storage zone are described by:

$$\frac{\partial c}{\partial t} = -\frac{Q}{A}\frac{\partial c}{\partial x} + \frac{1}{A}\frac{\partial}{\partial x}\left(AD\frac{\partial c}{\partial x}\right) + \alpha(c_s - c) \qquad (2.11)$$

$$\frac{\partial c_s}{\partial t} = -\frac{A}{A_s}(\alpha(c_s - c)) \qquad (2.12)$$

where c is the solute concentration in the stream (mg L^{-1}), Q is the volumetric flow rate (m^{3}s^{-1}), D is the dispersion coefficient (m^{2}s^{-1}), A is the cross sectional area of the channel (m^2), c_s is the solute concentration in the storage zone (mg L^{-1}), A_s is the cross-sectional area of the storage zone (m^2) and α is the storage exchange coefficient (s^{-1}). The flux between the stream and the storage zone ($q_{s,}$ m^{2}s^{-1}) and the mean residence time ($t_{s,}$ s) within the storage zone can be calculated from:

$$q_s = \alpha A \qquad (2.13)$$

$$t_s = \frac{As}{\alpha A} \qquad (2.14)$$

2.3   Site description

Marillana Creek is a naturally ephemeral stream in the arid subtropical Pilbara region of Western Australia. The creek flows north east across the Hammersley Basin into the Fortescue Marsh, approximately 40 km downstream of the study site. The creek flows adjacent to a series of iron ore mines that dewater the ore body aquifer to maintain safe mining conditions. In addition to natural episodic flow events, the creek has received around 6 GL of mine water from dewatering operations per year for 13 years prior to this study. The alluvial deposit associated with Marillana Creek is between 50 and 300 m wide and approximately 5 m thick. This alluvial deposit is predominantly underlain by a palaeochannel deposit of fractured pisolitic goethite that extends to a depth of up to 50 m. Where the paleochannel deposit is absent, the creek alluvium is underlain by weathered banded iron formation and dolerite.

This study focuses on an 8 km long section of Marillana Creek immediately downstream of the mine water discharge outlet (Figure 2.1). Streamflow at the mine water discharge location is of the order of 0.3 $m^3 s^{-1}$ and is relatively constant throughout the year. Streamflow decreases along the 8 km section until there is no longer continuous flow, and the surface water expression is reduced to a series of disconnected pools. Stream stage is approximately 1 m above the water table in the alluvial aquifer, based on measurements in piezometers between 80 and 120 m from the stream. Thus, while the stream is clearly losing on a regional scale, this does not prohibit smaller scale exchange between the river and the adjacent alluvium, and the relationship between stream stage and aquifer hydraulic head on a smaller scale is likely to be quite complex. Similarly, the stream stage is 3 m above the hydraulic head in the underlying fractured bedrock aquifer (Figure 2.2).

The stream geomorphology is characterized by sequences of pools, riffles and glides. The majority of the 8 km section consists of glides; on average 0.5 m deep and ranging from 5 to 20 m wide. These glides are separated by riffles 5 m wide and up to 0.3 m deep and 10 m long. Pools are less than 5 m long and up to 1 m deep. In this chapter, all river distances refer to distances downstream of the mine water discharge location.
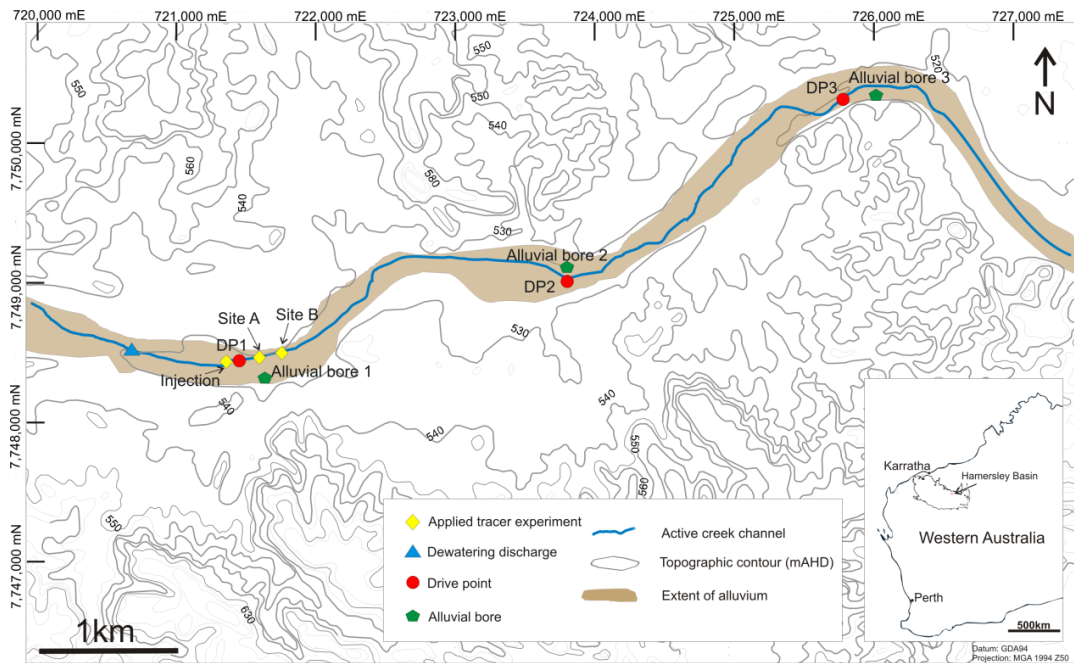
Figure 2.1 Map of the study site showing tracer injection, DP1, DP2, DP3 and alluvial bore locations. Arrow in locality map points to study site within the Hamersley Basin.
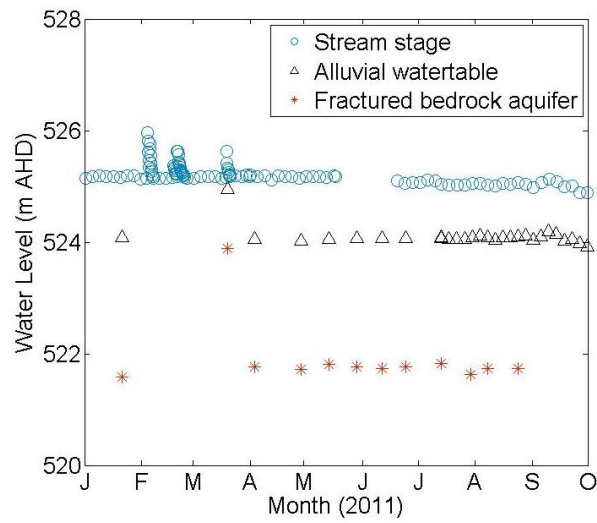
Figure 2.2 Stream stage and hydraulic head in the alluvial and underlying bedrock aquifers.

2.4   Methods

2.4.1   Radon production rate

Two methods were used to estimate the radon production rate of the sediments; water samples from alluvial bores and a glass jar emanation experiment. These methods provide estimates of equilibrium activity, which provide the basis for estimates of radon production rates (according to Equation 2.7). Water samples were collected from pre-existing wells screened across the watertable within the alluvium close to sites DP1, DP2 and DP3 (see Figure 2.1). In addition, sediment samples were collected from 5 sites along the creek at river distances of 0.3, 1.0, 2.2, 3.5 and 6.1 km. At each of these sites sediment was collected from; a) the surface of the stream, b) 0.5 m below the surface of the stream, and c) the dry alluvium adjacent to the stream, giving a total of 15 sediment samples. Porosity was measured volumetrically and bulk density calculated as the dry weight per total volume. Three split replicates from each sediment sample were then saturated with deionized water in sealed 500 mL glass jars (45 jars total) and allowed to reach an equilibrium radon activity over 29 days. Radon activities of the water were then determined based on 14 mL sub-samples. The radon activity of these samples was determined by liquid scintillation using a LKB Wallace Quantulus counter. The accuracy of this method varies with concentration, and in this study ranged from 0.15 Bq L^{-1} at a concentration of 2.7 Bq L^{-1} to 0.5 Bq L^{-1} at a concentration of 19.5 Bq L^{-1} with a precision of approximately 0.3 Bq L^{-1} (Leaney and Herczeg, 2006).

2.4.2   Longitudinal stream radon

Stream radon activity was measured at 12 sites along the stream between 17 and 19 May 2011, including directly from the mine water outlet. An additional stream sampling campaign was undertaken on 24-25 August 2011, during which water samples were collected at the mine water outlet and 18 sites along the stream approximately 500 m apart. Surface water samples for radon were initially collected in 1250 mL PET bottles. A 50 mL volume was removed from the bottle and 20 mL of mineral oil scintillant was added. The bottle was then shaken for 4 minutes before the scintillant oil was extracted into a pre-weighed PTFE scintillation vial. Radon activity was then determined by liquid scintillation as described in Section 2.4.1.

Stream velocity was measured on 23 August at 5 locations along the creek using an electromagnetic flow meter (Flowmate 2000). These locations were chosen for their accessibility, to be relatively evenly spaced along the study reach, and because the flow was

focused within a well-defined channel, allowing for a more accurate estimate of streamflow at these locations. Streamflow was calculated by integrating flow measurements recorded at 0.25 m intervals across the width of the stream following the method of Buchanan and Somers (1969).

A tracer injection of sulphur hexafluoride (SF_6) was conducted at the same location as the bromide injection on 25-26 August 2011 to estimate the gas transfer velocity (Wanninkhof et al., 1987). The SF_6 gas was released by diffusion through nylon tubing connected to a gas cylinder supplying an outlet pressure of 90 kPa, following the procedure of *Cook et al.* (2006). The gas was released continuously for 60 hours until sampling was complete. Water samples were collected in 15 mL glass vials at 8 locations over the 7 km downstream of the injection point. The first sample was collected 40 hours after the injection commenced, to allow stream concentrations to first reach equilibrium. If the SF_6 release was not long enough for the stream concentrations to have reached equilibrium, then the estimated gas exchange rate would be too large. Therefore, a longer SF_6 injection was conducted on 5-9 October 2012, during which samples were not collected for the first 5 days. Streamflow during this second experiment was comparable to the August 2011 release. SF_6 concentrations were measured using gas chromatography (Clark et al., 1995).

A 1D mass balance model of stream chemistry was built in EXCEL to interpret the longitudinal stream chemistry data based on Equation 2.9. This model explicitly solves the mass balance equation by finite difference approximation with a spatial discretization of 10 m. Parameters used in the mass balance model are summarized in Table 2-1. Stream geometry was held constant along the entire model with a width of 12 m and a depth of 0.5 m. These are average values based on field measurements and interpretation of aerial photographs. Streamflow losses to infiltration and evapotranspiration are constrained by fitting measured streamflow and chloride in the 1D mass balance model. The infiltration and evapotranspiration rates were constant along the entire model domain at values that provided the best fit to the streamflow and chloride data. The gas exchange rate was determined from the best fit to data from the SF_6 injection experiment. The radon production rate of the sediments was chosen based on the glass jar experiment and water samples from bores screened within the alluvium.

Table 2-1 Mass balance model parameters

Symbol	Description	Value	Units
E	evapotranspiration rate	0.014	m d^{-1}
k	gas transfer velocity	1.8	m d^{-1}
w	stream width	12	m
d	stream depth	0.5	m
ϑ	hyporheic zone porosity	0.3	v v^{-1}
λ	radon decay constant	0.181	d^{-1}
γ	radon production rate within hyporheic zone	1.5	Bq L^{-1} d^{-1}
q_{gw}	groundwater recharge flux	2.6	m^2 d^{-1}
q_h	hyporheic water flux		m^2 d^{-1}
q_p	parafluvial water flux		m^2 d^{-1}
t_h	hyporheic zone residence time		d
t_p	residence time of parafluvial flow		d
v_p	volume swept by parafluvial flow		m^3 m^{-1}

2.4.3 Streambed radon profiles

Vertical profiles of streambed radon activity were measured on 24 August 2011 at three locations along the creek; DP1, DP2 and DP3, located at 950, 3750 and 6330 m, respectively. Porewater samples were collected to a depth of up to 1.2 m using a 30 mm outer diameter drive point and a 20 mL syringe to sample 14 mL of water from each depth. These water samples were injected through a 0.4 μm disposable inline filter into pre-weighed Teflon coated PTFE scintillation vials containing 6mL of Packard NEN mineral oil. Radon activities were determined using liquid scintillation, as described in Section 2.4.1

Hyporheic residence times were estimated from Equation 2.10, based on the stream and hyporheic radon activities and the streambed radon production rate. Uncertainty in residence time estimates was assessed using a Monte Carlo analysis (10000 realizations). This analysis combined uncertainty in the laboratory measurement of radon activity (shown in Figure 2.3a) and uncertainty in the equilibrium activity (and therefore radon production rate).

2.4.4 Injected tracer and transient storage modeling

A tracer pulse of potassium bromide (KBr) was injected into the creek on 25 August 2011, at a river distance of 930 m. This tracer pulse consisted of approximately 40 L of water with a concentration of 72000 mg L^{-1}, injected over 90 seconds. The injection location was chosen such that slow moving glides that might retard solute for hours or longer were not included in

the experiment, and with a turbulent riffle between the point of injection and the first sampling station, to maximise solute mixing. Water samples were collected at two stations, 150 m (Site A) and 265 m (Site B) downstream of the injection point, over a 2 hour period immediately following the tracer injection. The average stream depth and width over the experimental reach were estimated by manual measurement at ten representative locations. Stream discharge at Site A was by integrating flow velocity measured at 0.25 m intervals across the stream using an electromagnetic flow meter. In-situ measurements of electrical conductivity were also made at these stations throughout the experiment to inform sample collection. Bromide concentrations were measured by ion chromatography.

Bromide breakthrough curves from the applied tracer experiment were interpreted using the OTIS transient storage model, with OTIS-P for parameter estimation (Runkel, 1998). The model consisted of one reach beginning at Site A and ending at Site B. This reach was divided into 1 m segments along the entire model domain. The time step was 1 minute with a total simulation time of 2 hours. Lateral outflow was included in the model to simulate infiltration at a rate of 0.22 m d^{-1} along the entire model domain. Streamflow at the upstream boundary was 0.2 m^3 s^{-1}. Concentrations at the upstream boundary were defined by measured data at sampling site A with linear interpolation between data points. The longitudinal dispersion coefficient (D), stream channel area (A) storage area (A_s) and storage exchange coefficient (α) were estimated using the inverse parameter estimation functionality of OTIS-P with a stopping value of 10^{-5} and unweighted residuals. The storage exchange flux and residence time were calculated from these parameters (A_s and α) using Equations 2.13 and 2.14.

2.5   Results

2.5.1   Radon production rate

Equilibrium activities in the alluvial wells were 8.0 ± 1.2 Bq L^{-1} (n=3) at DP1, 6.7 ± 0.4 Bq L^{-1} (n=3) at DP2 and 6.7 Bq L^{-1} (n=1) at DP3. Production rates at each well, calculated from Equation 2.7, were 1.5 ± 0.2 Bq L^{-1}d^{-1} at DP1, 1.2 ± 0.1 Bq L^{-1}d^{-1} at DP2, and 1.2 Bq L^{-1}d^{-1} at DP3. Equilibrium activities in the glass jar emanation tests (n=45) ranged from 2.7 to 19.5 Bq L^{-1} with a mean activity of 6.8 ± 3.8 Bq L^{-1} and a median of 5.6 Bq L^{-1}. The equilibrium activity of glass jar tests on sediment samples from DP1 was 8.4 ± 4.6 Bq L^{-1}, on sediment from DP2 was 4.8 ± 1.2 Bq L^{-1}, and on sediment from DP2 was 5.5 ± 0.5 Bq L^{-1}. Production rates calculated from these equilibrium activities were 2.4 ± 0.8 Bq L^{-1}d^{-1} at DP1, 0.9 ± 0.2 Bq L^{-1}d^{-1} at DP2, and

1.0 ± 0.1 Bq L^{-1} d^{-1} at DP3. Averaged across all samples including wells and glass jars (n=52), the equilibrium activity was 7.2 ± 3.8 Bq L^{-1}, which implies a production rate of 1.3 ± 0.7 Bq L^{-1} d^{-1}.

2.5.2 Streambed radon profiles

At site DP1, radon activities in the upper 0.1 m of the streambed ranged from 2.8 to 2.9 Bq L^{-1}, slightly higher than the radon activity of the stream, which was 2.4 Bq L^{-1} (Figure 2.3a). This suggests the presence of a rapidly flushed hyporheic zone in the upper 0.1 m of streambed at this site. In contrast, radon activities below 0.1 m at DP1, and throughout the profiles at DP2 and DP3 ranged from 3.9 to 8.7 Bq L^{-1}, suggesting residence times of days (Equation 2.10).

Confidence bounds on the hyporheic residence times were estimated using a Monte Carlo analysis that incorporates analytical measurement error and uncertainty in the radon production rate of the sediments. The distribution of equilibrium activities at each site was described by the mean and standard deviation across glass jar and bore water samples from each site (10.4 ± 4.0 Bq L^{-1} at DP1, 7.0 ± 1.6 Bq L^{-1} at DP2 and 7.0 ± 0.8 Bq L^{-1} at DP3). During the Monte Carlo analysis, if the generated radon activity in the streambed was less than the generated activity in the stream, a residence time of zero days was assigned to that realisation. As a result, where there is significant overlap between the distributions of streambed and stream radon activity, the upper bound of the 90% confidence interval hyporheic residence time can be estimated, but not the lower bound. Similarly, where there is significant overlap between the streambed radon distribution and the equilibrium activity distribution, the lower bound of the 90% confidence interval of hyporheic residence time can be estimated, but not the upper bound.

The median residence time within the upper 0.1 m at DP1 was 0.3 days, with a 90% confidence interval of 0 to 3 days (Figure 2.3b). Below 0.1 m the median residence times generally increased with depth from 6.3 days to 19.2 days, with the lower bounds of the 90% confidence intervals from 2.2 to 4.1 days. Median residence times were between 1.7 and 9.5 days at site DP2, and between 2.7 and 11.1 days at DP3. These data imply that at sites DP2 and DP3 the hyporheic zone is either absent, or shallower than the 0.05 m sampling interval at the top of each profile. Hyporheic exchange fluxes can theoretically be estimated based on the residence time using Equation 2.4, if the groundwater recharge flux and hyporheic zone geometry are

known. However, when the uncertainty in hyporheic residence times is considered, calculated flux estimates are effectively unbounded.
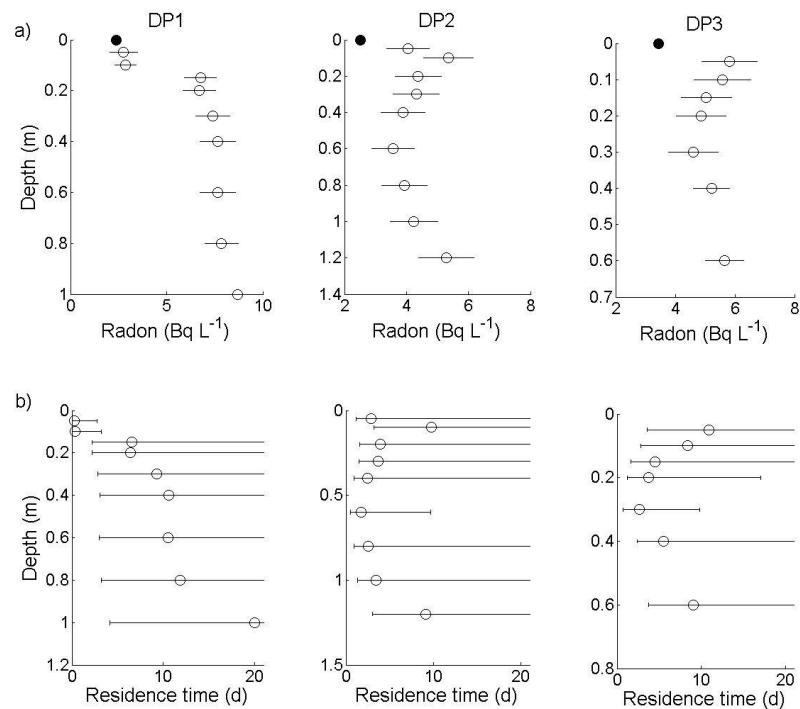
Figure 2.3 a) Streambed radon profiles. Dark circles are surface water samples, open circles are subsurface water samples. Error bars are 2σ based on laboratory measurement uncertainty. b) Median hyporheic residence time and 90% confidence interval based on Monte Carlo analysis.

2.5.3 Injected tracer and transient storage modeling

During the injected tracer experiment, stream discharge at Site A was measured at 0.2 m^3 s^{-1} (consistent throughout the experiment). The average depth over the experimental reach was approximately 0.25 m and the average width approximately 8 m. Bromide concentrations increased from a background concentration of 0.5 mg L^{-1} up to a peak of 35 mg L^{-1} at Site A approximately 10 minutes after the tracer injection (Figure 2.4). At site B the concentration peaked at 14 mg L^{-1} approximately 35 minutes after tracer injection. Integration of the bromide breakthrough curves showed that mass recovered at station B was 97.8% of the total mass at station A (the upstream model boundary). Losses to infiltration between stations A and B accounted for 1.2% of this mass loss (33 g), leaving 1.0% of the mass (30 g) as remaining in the storage zone at the end of the two hour simulation period.
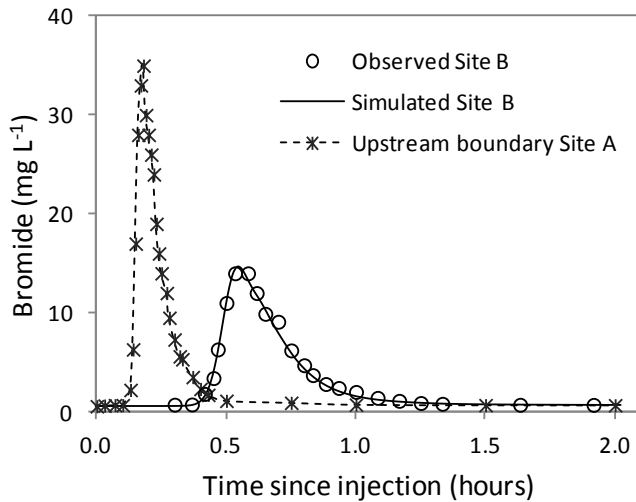
Figure 2.4 Bromide concentrations measured at site A and B, upstream boundary (linear interpolation of site A measured data) and OTIS simulated bromide concentration at site B.

OTIS-P was able to converge on a solution for all four parameters, with an RMSE of 0.3 mg L^{-1} and an R^2 value of 0.99. Stream channel area, storage area and the storage exchange coefficient were well constrained (Table 2-2). The stream channel area was estimated at 2.0 ± 0.1 m^2, the storage area estimated at 0.6 ± 0.1 m^2 and the storage exchange coefficient was estimated at 1.3 x 10^{-3} ± 4 x 10^{-4} s^{-1} (95% confidence limits). The longitudinal dispersion coefficient (*D*) was the least well constrained parameter, estimated at 3.8 x 10^{-2} ± 2.8 x 10^{-2} m^2 s^{-1}. Fluid flux between the stream channel and storage zone, was calculated based on Equation 2.13, giving an estimated storage flux (*q$_s$*) of 2.6 x 10^{-3} ± 0.4 x 10^{-3} m^2 s^{-1} (225 ± 35 m^2 d^{-1}). The average turnover rate, or mean residence time within this storage zone (*t$_s$*) was calculated by Equation 2.14, to be 230 ± 40 s (approximately 4 minutes or 0.003 days). The transient storage modeling approach simulates an exponential distribution of residence times within the storage zone. Therefore, this mean of 4 minutes corresponds to an exponential distribution of residence times with 90% of residence times less than 10 minutes (0.007 days) and 99.9% of residence times less than 28 minutes (0.02 days). If exchange with stagnant pools is assumed to be negligible, the storage area of 0.6 m^2 implies a storage zone depth of 0.25 m (based on stream width of 8 m and porosity of 0.3).

Table 2-2 OTIS-P parameter estimates

Model parameter	Units	Parameter estimate	Standard deviation
Longitudinal dispersion coefficient (D)	$m^2\,s^{-1}$	3.8×10^{-2}	1.3×10^{-2}
Stream channel area (A)	m^2	2.0	4.1×10^{-2}
Storage area (A_s)	m^2	0.6	4.0×10^{-2}
Storage exchange coefficient (α)	s^{-1}	1.3×10^{-3}	2.1×10^{-4}
Storage exchange flux (q_s)	$m^2\,s^{-1}$	2.6×10^{-3}	4.2×10^{-4}
Storage zone residence time (t_s)	s	230	40

2.5.4   Longitudinal stream radon

At the time of the August sampling campaign, streamflow decreased from 0.25 $m^3\,s^{-1}$ at the mine water discharge outlet to effectively zero at a distance of 7900 m, where the surface water had reduced to a series of disconnected pools (Figure 2.5). The chloride concentration increased along the stream from a minimum of 119 mg L^{-1} to 132 mg L^{-1}. Radon activities in the mine water discharge were 10.9 ± 0.6 Bq L^{-1} in May and 13.1 ± 0.7 Bq L^{-1} in August 2011. Flow at the discharge outlet was fast and highly turbulent. A pool of mine water was created immediately upstream of the mine water outlet so that the water flowing along the stream was likely to be a mixture of water from this pool and more recent mine water. As a result, stream radon activities immediately where the stream begins to flow are likely to be lower than the values measured directly from the mine water outlet. An initial stream radon activity of 8 Bq L^{-1} was used in the mass balance model that accounts for the enhanced degassing at the outlet location. Radon activities decreased to less than 5 Bq L^{-1} within 500 m. Radon activities along the subsequent 7400 m were between 2.0 and 4.9 Bq L^{-1} with an average of 3.3 ± 0.9 Bq L^{-1} (± std. dev).

Longitudinal streamflow and chemistry data were fit with the 1D mass balance model using a groundwater recharge flux of 2.6 $m^2\,d^{-1}$ and an evapotranspiration rate of 0.014 m d^{-1}. Pan evaporation measured by the Australian Bureau of Meteorology during the sampling period and evaporation estimates based on the Penman-Monteith equation both suggest evaporation rates on the order of 0.01 m d^{-1}. The simulated evapotranspiration rate is therefore considered to be reasonable with the excess above 0.01 m d^{-1} attributable to transpiration by riparian vegetation. Given a mean stream width of 12 m, the best fit to the SF_6 data was achieved with a gas exchange rate of 1.8 m d^{-1}. This is consistent with previous Australian studies that have used 1 – 1.6 m d^{-1} (Cook et al., 2006, Cook et al., 2003) and lies within the mid-range of literature values (Raymond and Cole, 2001).
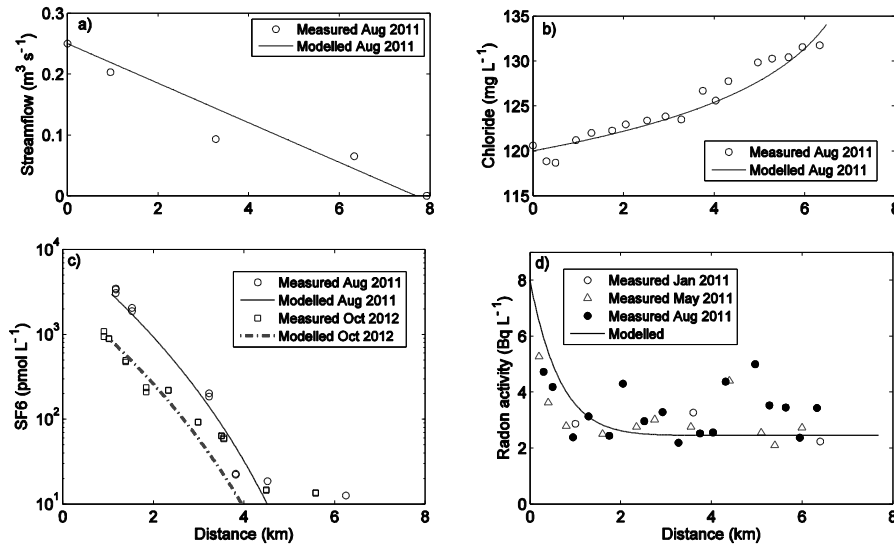
Figure 2.5 Measured and modelled a) streamflow, b) chloride, c) SF_6 and d) radon activity. Distances are downstream of the mine water outlet.

In the absence of streambed hyporheic and parafluvial fluxes, the stream radon activity would reduce to zero within 3.5 km of the mine water outlet. In order to maintain a stream radon activity of 2.4 Bq L^{-1} downstream of 3.5 km, a radon flux of 5.4 x 10^4 Bq m^{-1} d^{-1} is required to balance radon losses to groundwater recharge, gas exchange and radioactive decay. This radon flux must be derived from either hyporheic or parafluvial exchange or a combination of the two. However, without other information it is not possible to differentiate between them.

If the parafluvial exchange rate were zero, then the hyporheic flux that would be required to maintain the estimated radon flux can be calculated from Equation 2.9. Thus setting $\left(\frac{\gamma}{\lambda} - c\right)\left(\frac{q_h t_h}{\lambda^{-1} + t_h}\right)$ = 5.4 x 10^4 Bq m^{-1} d^{-1} and substituting for q_h using Equation 2.4, gives a hyporheic zone depth, h, of greater than 14 m. (The smallest possible value of h is obtained when t_h is small. Larger values of t_h give larger values of h.) Thus, if the parafluvial flux were zero, a hyporheic zone at least 14 m thick would be required to sustain stream radon activities of 2.4 Bq L^{-1} downstream of 3.5 km from the mine watering discharge outlet. This implied hyporheic zone depth is greater than the thickness of the alluvial deposit associated with the creek (approximately 5 m).

Alternatively, if hyporheic exchange is zero, then the magnitude of parafluvial flow required to maintain the same radon flux can be calculated from Equation 2.9. Thus setting

$\left(\frac{\gamma}{\lambda} - c\right) q_p \left(1 - e^{-\lambda t_p}\right)$ = 5.4 x 10^4 Bq m^{-1} d^{-1} and substituting for q_p using Equation 2.8 gives

V_p > 170 m^2. Again, the smallest possible value of V_p is associated with small values of t_h. This value of V_p is effectively equivalent to the cross-sectional area of the parafluvial zone. Given that the alluvial channel is approximately 5 m deep, V_p = 170 m^2 suggests that the parafluvial exchange zone was 34 m wide (or 17 m either side of the stream).

Combinations of hyporheic exchange and parafluvial exchange are, of course, also possible. However, the bromide injection experiment and streambed radon profiles together suggest a hyporheic zone of less than 0.1 m with residence time of less than three days. Literature values for hyporheic zone depth within the streambed are usually less than 1 m, with residence times of minutes to hours (Cranswick and Cook, *In review,* Lautz et al., 2010, Harvey and Wagner, 2000). If the mean hyporheic residence time is restricted to values of less than 1 day, and the depth of the hyporheic zone to less than 1 metre, then the highest radon flux that this can generate is 3.8 x 10^3 Bq m^{-1} d^{-1} (7 % of the total radon influx). This implies that the parafluvial radon influx must be at least 5.0 x 10^4 Bq m^{-1} d^{-1}, with the maximum parafluvial radon influx, of course, 5.4 x 10^4 Bq m^{-1} d^{-1}.

Although the minimum volume of the parafluvial zone is V_p = 170 m^2, both the volume swept and the parafluvial flux are a function of the residence time. If the parafluvial residence time were 3 days, the corresponding volume flushed by parafluvial flow paths would be between 170 and 220 m^3 m^{-1} (Figure 2.6). However if the parafluvial residence time were 10 days, then the flushed volume would be between 290 and 370 m^3 m^{-1}, or a 60–75 m wide parafluvial exchange zone (30–38 m either side of the stream). This is in comparison to hyporheic flow paths that probably flush a maximum volume of 10 m^3 per m length of stream (based on a hyporheic zone depth of 3 m, stream width of 12 m and porosity of 0.3). The parafluvial flux in these two examples would be 17 – 22 m^2 d^{-1} (residence time of 3 days) and 9 – 11 m^2 d^{-1} (residence time of 10 days).

Simulated stream radon activities were most sensitive to the equilibrium activity and gas exchange rate (Figure 2.7). They were only sensitive to stream width in the upstream 4 km of the model where the radon loss through degassing is greater than inputs from hyporheic and parafluvial fluxes. Similarly, the model is only sensitive to initial radon activity in the upstream 2 km. Radon simulations are not sensitive to infiltration or evapotranspiration rates (data not shown). The radon activity simulated downstream of 3.5 km was sensitive to the radon

production rate, which was constrained by measuring the equilibrium activities of the glass jar experiment and alluvial bores. The radon production rate in the model was fixed at 1.5 Bq^{-1} L^{-1} d^{-1}. The gas exchange rate was constrained by measuring stream width at multiple locations along the study reach and conducting an SF_6 tracer injection.
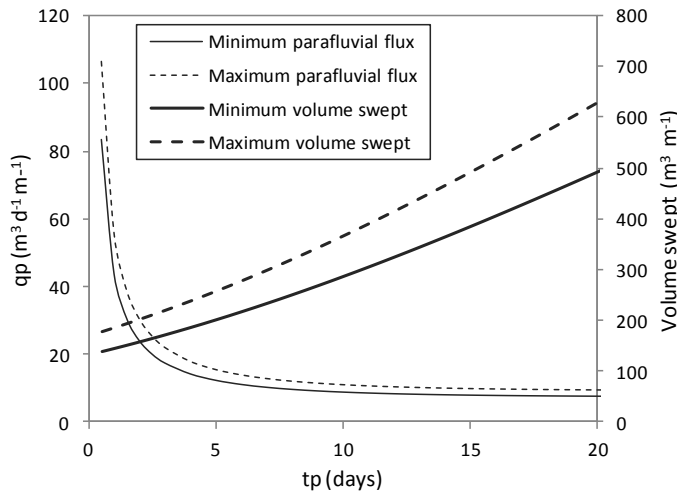
Figure 2.6 Parafluvial fluxes and corresponding volume of alluvium swept into each metre length of stream (m^3 m^{-1}) required to maintain radon activity in the stream at 2.4 Bq L^{-1} as a function of parafluvial residence time.
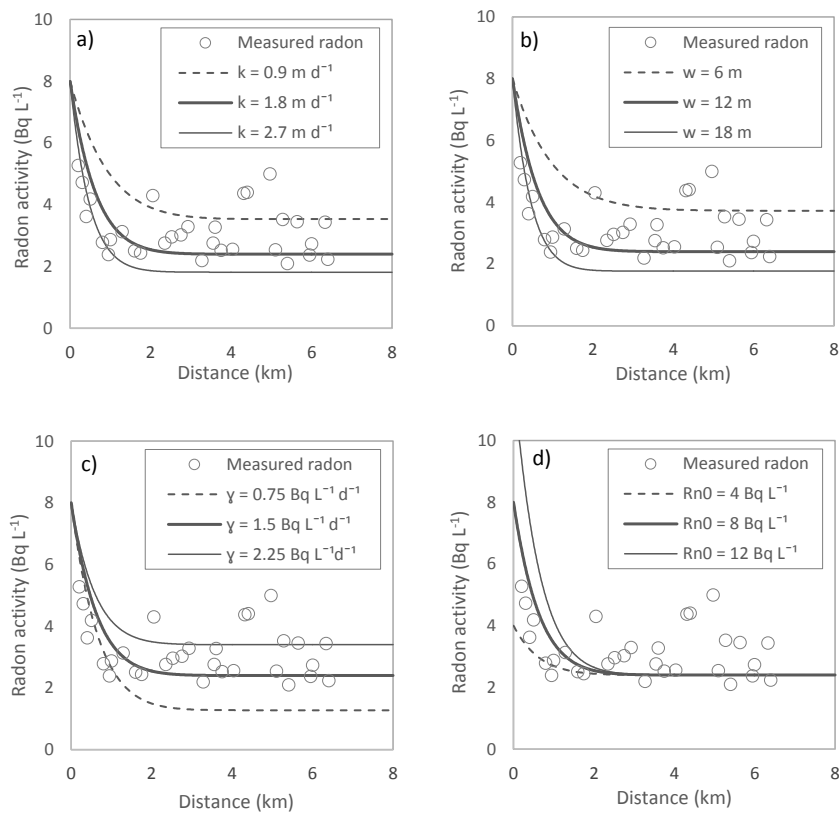
Figure 2.7 Sensitivity of radon simulations to a) gas exchange, b) stream width c) radon production rate and d) initial radon activity. Each parameter modelled at ±50% of base value.

Uncertainty in the parafluvial exchange flux, which dominated the radon influx, has been assessed using a Monte Carlo approach. When the stream radon activity is constant, the left hand side of Equation 2.8 can be set equal to zero. If the hyporheic exchange flux is assumed to be negligible, the equation can be rearranged to solve for the parafluvial flux, based on a given parafluvial residence time. The equilibrium radon activity is assumed to be log-normally distributed with the log-transformed values having a mean of 2.1 and standard deviation of 0.46, based on the measured values. The standard deviation of the mean is given by $0.46/\sqrt{n}$, where n = 52. Thus, for a parafluvial residence time of 5 days, if only uncertainty in the mean equilibrium activity of the sediment is considered, the mean parafluvial flux is 15.5 m^2 d^{-1}, with 90 % confidence interval of 13.6 to 18.0 m^2 d^{-1}. If uncertainty in the gas transfer velocity is also incorporated, which is estimated to be 20% of the value (±0.4 m d^{-1}), the 90 % confidence interval expands to 10.0 to 21.8 m^2 d^{-1}.

2.6   Discussion

Our ability to characterize the hyporheic zone is explicitly linked to the scale of sensitivity of the method that is applied, whether it is an environmental tracer, applied tracer experiment or a hydraulic approach (eg. Darcy's law, numerical modeling). In this chapter, a distinction was made between 1) short residence time, short flow path hyporheic fluxes that exchange water mostly between the stream and streambed, and 2) long residence time, long flow path, parafluvial fluxes mostly flowing through the alluvium adjacent to the stream. This distinction has been made to reflect the temporal and spatial sensitivities of the methods used, and the geometry of the stream and alluvial channel.

Transient storage modeling of breakthrough curves captured the fastest exchange fluxes, with residence times of minutes and spatial scales less than 0.5 m. The storage flux estimate from transient storage modeling in this study was an order of magnitude larger than estimates of hyporheic flux in the literature, which are generally between 10^{-6} and 10^{-4} m^2 s^{-1} (Bencala and Walters, 1983, Harvey et al., 1996, Lautz et al., 2010, Swanson and Cardenas, 2010). Stagnant zones were observed within the stream channel during the tracer injection and the relatively high storage flux measured in this study may be an artifact of exchange with in-stream storage zones. The influence of in-stream storage zones is likely to be most significant in strongly losing (or gaining) systems, in which the extent of the hyporheic zone decreases (Harvey et al., 1996, Cardenas, 2009).

For the radon disequilibrium method, the uncertainty in the radon production rate of the sediments is a significant limitation. As a result, the disequilibrium method was able to highlight the presence or absence of rapidly flushed zones beneath the stream, but was not able to constrain the exchange flux between stream and streambed. Extensive replication would be required to extrapolate these point-scale estimates of hyporheic zone depth to the reach scale. At the larger scales of application of the stream radon method, the mass balance model was also sensitive to the radon production rate, which must be estimated for the method to be applied, but this uncertainty was not prohibitive to the estimation of exchange parameters.

The longitudinal stream radon method provides information on hyporheic and parafluvial fluxes at regional scales. However, on its own, the method is not able to differentiate between these two fluxes. Nevertheless, if other methods can be used to put an upper limit on the hyporheic flux, then this method provides an estimate of the parafluvial exchange flux, which may be otherwise difficult to obtain. The sensitivity of stream radon concentrations to exchange flux increases as subsurface residence time increases (up to a residence time of approximately 7 days), and so the method is more sensitive to parafluvial exchange than hyporheic exchange. The injected tracer experiment in this study provided no indication of the longer flow path fluxes that were detected using the radon mass balance method, with 98% of the injected mass recovered over the 2 hour sampling interval. A tracer injection experiment of longer duration than was applied in this study (days at least) would be required to resolve these longer exchange fluxes using a transient storage modeling approach. However, information on flow paths with long residence times can only be obtained from the tail of the breakthrough curve, and injecting sufficient tracer to maintain large enough concentrations throughout this sampling period would be difficult.

The effectiveness of radon as a tracer of exchange fluxes with longer flow paths is linked to its production in the subsurface, which increases the difference between stream and hyporheic end-members with increasing residence time. The longitudinal radon mass balance identified a parafluvial exchange zone extending to a distance of tens of metres from the stream. This scale of parafluvial flow is consistent with estimates from other field sites that have inferred parafluvial flow paths on spatial scales of tens to hundreds of metres and residence times of days or greater based on tracer injection (Triska et al., 1993, Dent et al., 2007, Holmes et al., 1994), nutrient distributions (Lewis et al., 2007), dissolved oxygen (Deforet et al., 2009), stable

isotopes (Gooseff et al., 2003) and hydraulic gradients (Deforet et al., 2009, Peterson and Sickbert, 2006).

Much of the interest in hyporheic exchange is due to its role in nutrient cycling in streams. The extent of nutrient transformation is related to exchange zone residence time, which can vary over orders of magnitude depending on hydraulic gradients and the permeability of the sediments (Findlay, 1995). Highly permeable sediments like the coarse alluvium in this study can mean shorter residence times and therefore less chemical and biological transformation (Claret and Boulton, 2009). However, the parafluvial zone in this system extends over tens of metres with a residence time of days. The significance of this exchange zone for biogeochemical transformation depends on the residence time relative to reaction rates. If the reaction rates are fast (less than days) then biogeochemical cycling will still be dominated by rapid fluxes between the stream and streambed with residence times of hours or less.

Subsequent application of the longitudinal radon method in other losing streams, and in combination with more complex tracer injection methods (dilution gauging, estimates of gross gain and loss, eg. Payn et al. (2009)), will allow for stronger constraints on estimated residence times and fluxes. Radon activity in surface waters has also been used to characterize return flows in a tidal system, with channel residence times calculated from concurrent measures of radon and radium (Stieglitz et al., 2013). A multi-tracer approach may also be useful in losing stream systems, with additional tracers further constraining estimates of hyporheic exchange parameters.

2.7   Conclusion

In this chapter a new method for characterizing exchange flows in losing streams based on longitudinal stream radon activity was presented. The radon mass influx along an 8 km losing stream reach was interpreted to estimate streambed hyporheic and parafluvial exchange components. The radon mass balance in the stream was dominated by parafluvial flow paths that extend up to tens of metres from the stream. The major strength of this stream radon method is that it can provide an integrated measure of net exchange fluxes over kilometres of river, and is sensitive to exchange fluxes with long residence times and flow paths. While the parafluvial flux was constrained to within an order of magnitude, hyporheic exchange fluxes with short residence times and flow paths were not well constrained using this radon method. Application of this method in conjunction with transient storage modeling of injected tracer

breakthrough curves or hydraulic methods is recommended to fully characterize the spectrum

of hyporheic exchange in losing streams.

Chapter 3   Carbon-14 as a tracer of groundwater discharge to streams

3.1   Introduction

Knowledge of the provenance of groundwater discharging to streams is important for understanding the potential risk of stream depletion or contamination associated with the utilization of groundwater resources. Often groundwater discharge to streams originates from multiple aquifers, and has a range of aquifer residence times. By measuring multiple age indicators along a stream, each sensitive to a different range of groundwater residence times, it is theoretically possibly to identify groundwater contributions of different ages, and it is expected that older ages represent longer flow paths. Previous studies of groundwater discharge to streams have used radon-222 (^{222}Rn), which indicates groundwater discharge with residence times of days or greater (Gardner et al., 2011, Cook et al., 2003, Cook et al., 2006) to constrain the total groundwater discharge to the stream. Groundwater discharge with residence times less than 100 years has been detected using chlorofluorocarbons (CFCs), SF$_6$, tritium (^{3}H), or the ratio of tritium to helium-3 (^{3}H/^{3}He) (Smerdon et al., 2012, Stolp et al., 2010, Cook et al., 2003, Cook et al., 2006). The only groundwater age tracer that has been used to specifically quantify old groundwater discharge is terrigenic helium-4 (Gardner et al., 2011, Smerdon et al., 2012). Helium-4 ((^{4}He))can be used to measure groundwater residence times greater than 100 years, but is most sensitive to much longer residence times (≥10,000 years) (Cook and Herczeg, 2000).

A potential limitation of dissolved gasses as tracers of groundwater discharge to streams is that they degas rapidly to the atmosphere, and so the tracer concentration in the stream equilibrates with the atmosphere close to the groundwater discharge location. Therefore, detection of groundwater discharge using measured gas concentrations in the stream, requires a sufficient gradient between the stream concentration upstream of the discharge zone, and the groundwater discharge concentration. The rate of equilibration with the atmosphere also provides a limit on the sampling resolution required to detect groundwater discharge, with faster equilibration requiring finer sampling resolution (Cook, 2013). For carbon-14 (^{14}C), the process of equilibration is driven by CO_2 exchange across the air-water interface, and is effectively buffered by the other dissolved inorganic carbon species in solution. The rate of equilibration of ^{14}C is therefore likely to be much slower than the rate of equilibration of CO_2, and other gas tracers.

In this chapter, the hypothesis that ^{14}C activity of total dissolved inorganic carbon (TDIC) in a stream can be used to detect groundwater discharge to a stream is tested. If discharge of groundwater induces a detectable change in ^{14}C activity of TDIC along a stream reach, this can potentially be used to constrain either the quantity (if the groundwater ^{14}C activity is known), or the ^{14}C activity of groundwater discharging into the stream (if the quantity of groundwater discharge is known). Rates of carbon isotope equilibration are measured experimentally by exposing old (approximately 30ka) groundwater to the atmosphere. Next, the rate of carbon isotope equilibration in a naturally ephemeral creek channel receiving artificial groundwater discharge was measured. Finally, the application of ^{14}C as a tracer of groundwater discharge to streams is demonstrated in the Daly River in northern Australia.

3.2   Theory

3.2.1 Carbon isotopic equilibration mechanisms

Conceptually, begin with a stream containing dissolved inorganic carbon that is in chemical and isotopic equilibrium with the atmosphere. Suppose that groundwater with a different TDIC concentration and ^{14}C activity then enters the stream at a discrete location. At the location of groundwater discharge, the isotopic composition of the stream is determined by the mixing fractions of TDIC groundwater and surface water. Downstream of the location of groundwater discharge, there are two processes that can drive carbon isotopic re-equilibration between the stream and atmosphere; chemical exchange and isotopic exchange.

3.2.1.1   *Chemical exchange*

The dominant chemical exchange process that is relevant for carbon isotopic equilibration downstream of a groundwater discharge zone is the exchange of CO_2 between the stream and the atmosphere. Groundwater typically has high concentrations of dissolved CO_2 that will degas to the atmosphere through gas exchange upon discharge to a river. This degassing of CO_2 causes an increase in pH, which shifts the distribution of carbonate species in the TDIC pool (Appelo and Postma, 2005, Choi et al., 1998, Weiss, 1974). There is a fractionation effect associated with this CO_2 exchange because of the different molecular weights of $^{12}CO_2$, $^{13}CO_2$ and $^{14}CO_2$. As the CO_2 degasses, this fractionation causes an enrichment of the carbon isotopic signature of TDIC in the stream (Doctor et al., 2008, Choi et al., 1998).

The CO₂ exchange flux is driven by the degree of disequilibrium from the atmosphere, with the rate of change in CO₂ concentration in a volume, V (L^3), of water with surface area, A (L^2), given by;

$$\frac{\partial CO_2}{\partial t} = k_{CO2} \frac{A}{V} \left(CO_{2\ eq} - CO_2 \right) \tag{3.1}$$

where CO_2 is the concentration of dissolved CO_2 in solution (M L^{-3}) $CO_{2\ eq}$ is the concentration of dissolved CO_2 in equilibrium with the atmospheric CO_2 partial pressure (M L^{-3}), t is time (T), and k_{CO2} is the gas transfer velocity (L T^{-1}). This gas transfer velocity is a function of the diffusion coefficient of CO_2 and the turbulence in the boundary layer at the air-water interface (Raymond and Cole, 2001, Genereux and Hemond, 1992). Equations in the form of Equation 3.1 can also be written for each carbon isotopologue of CO_2, however, because ^{12}C is much more abundant than ^{13}C or ^{14}C, chemical exchange will be dominated by $^{12}CO_2$.

The enrichment caused by fractionation during CO_2 degassing can be simulated as a Rayleigh distillation process (Hendy, 1971), described by;

$$\delta \cong \varepsilon_T \ln(f) + \delta_0 \tag{3.2}$$

where δ is the carbon isotopic composition of the remaining solution, δ_0 is the initial carbon isotopic composition, f is the fraction of dissolved inorganic carbon remaining in solution, and ε_T is the total enrichment factor (Clark and Fritz, 1997). This enrichment factor is expressed relative to HCO_3^-, which dominates the dissolved carbon species in the pH range of 6.5 to 8.5. In this open system, where degassed CO_2 is continuously removed from the system, ε_T will be the sum of an equilibrium enrichment, ε_{g_HCO3-}, due to the different solubilities of each isotopologue of CO_2, and a kinetic enrichment, ε_k, driven by the different gas transfer velocities of each isotopologue (Zhang et al., 1995), such that $\varepsilon_T = \varepsilon_{g\_HCO3-} + \varepsilon_k$.

3.2.1.2   Isotopic exchange

There are two modes of isotopic exchange in this system: 1) between species within the TDIC pool, and 2) between dissolved CO_2 and atmospheric CO_2. Within the TDIC pool, isotopic equilibration is driven by isotopic exchange between $CO_{2(aq)}$, HCO_3^- and $CO3^{2-}$, and is achieved within minutes (Mills and Urey, 1940, Zeebe et al., 1999). As a result, isotopic equilibration of dissolved CO_2 and TDIC with the atmosphere will proceed at effectively same rate. Isotopic exchange between the atmosphere and the solution will occur whenever the isotopic composition of dissolved CO_2 is not in isotopic equilibrium with atmospheric CO_2. For $^{14}CO_2$ this exchange is described by;

$$^{14}CO_{2(g)} + {}^{12}CO_{2(aq)} \leftrightarrow {}^{12}CO_{2(g)} + {}^{14}CO_{2(aq)} \tag{3.3}$$
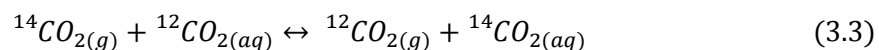
where $^{14}CO_{2(g)}$ is $^{14}CO_2$ gas in the atmosphere, $^{14}CO_{2(aq)}$ is $^{14}CO_2$ gas dissolved in the water, $^{12}CO_{2(g)}$ is $^{12}CO_2$ gas in the atmosphere and $^{12}CO_{2(aq)}$ is $^{12}CO_2$ gas dissolved in the water.

3.2.1.3   Achievement of isotopic equilibrium

Isotopic equilibration between the stream and the atmosphere can be driven by either chemical exchange or isotopic exchange, or a combination of the two. These two exchange processes are driven by different gradients (chemical concentration vs. isotopic composition), but they are not entirely independent. This is because CO_2 exchange alters the isotopic composition of the water, and hence changes the isotopic gradient between the water and the atmosphere, which drives the isotopic exchange process. This means that, although chemical equilibrium is not required for isotopic exchange to occur, isotopic equilibrium cannot be achieved while chemical (gas) exchange is ongoing.

3.2.2   Carbon isotope mass balance

A mass balance approach was used to simulate carbon isotope equilibration in 1) an evaporating pan of water, and 2) a gaining or losing stream. This allowed an effective transfer velocity to be estimated for each system, which describes the rate of equilibration with the atmosphere.

3.2.2.1   Mass balance of water exposed to the atmosphere

The water balance of an evaporating pan of water is given by;

$$\frac{\partial V}{\partial t} = -EA \qquad (3.4)$$

where V is the volume of water (L^3), E is the evaporation rate ($L\,T^{-1}$) and A is the surface area of the pan (L^2).

For a non-reactive, non-gaseous solute, the change in concentration in the pan over time is described by;

$$V\frac{\partial c}{\partial t} = cEA \qquad (3.5)$$

where c is the solute concentration in the water ($M\,L^{-3}$).

For a radioactive gas, the change in concentration in the pan over time is given by;

$$V\frac{\partial c}{\partial t} = EAc \ + kA(c_{eq} - c) - \lambda dAc \qquad (3.6)$$

where k is the gas transfer velocity (L T^{-1}), c_{eq} is the gas concentration of water in equilibrium with the atmosphere (M L^{-3}), λ is the radioactive decay constant (T^{-1}), and d is water depth (L). Equation 3.6 can be used to simulate changes in concentration for gases such as radon-222 as well as different CO_2 isotopologues.

For carbon isotopes, the exchange flux between TDIC and the atmosphere is controlled by the process of CO_2 exchange. In the carbon isotope mass balance, $^{12}CO_2$ is assumed to be in equilibrium with the atmosphere, which implies that chemical exchange is negligible. The flux of $^{12}CO_2$ out of the water to balance the influx of $^{14}CO_2$, as per Equation 3.3, will be negligible because of the much larger abundance of ^{12}C relative to ^{14}C. This means that for the mass balance of $^{12}C_{TDIC}$, the second and third terms of Equation 3.6 will be zero. The mass balance of ^{12}C in TDIC thus becomes;

$$V \frac{\partial}{\partial t} {}^{12}C_{TDIC} = {}^{12}C_{TDIC} AE \qquad (3.7)$$

For ^{14}C, the radioactive decay of ^{14}C is negligible at the timescale of the experiment, so that;

$$V \frac{\partial}{\partial t} {}^{14}C_{TDIC} = {}^{14}C_{TDIC} AE + \alpha_k k_{co_2} A({}^{14}CO_{2eq} - {}^{14}CO_2) \qquad (3.8)$$

where $^{14}C_{TDIC}$ is the concentration of ^{14}C in water (M L^{-3}), $^{14}CO_2$ is the concentration of $^{14}CO_2$ in the water (M L^{-3}), $^{14}CO_{2eq}$ is the $^{14}CO_2$ concentration of water in the pan when it is at isotopic equilibrium with the atmosphere (M L^{-3}), k_{CO2} is the gas transfer velocity of CO_2 (L T^{-1}) (as defined in Equation 3.1), and α_k is the kinetic fractionation factor to account for the different gas transfer velocities of $^{12}CO_2$ and $^{14}CO_2$. The value of this α_k is very close to 1 (0.9992 at 20°C) (Zhang et al., 1995), and so it is neglected in subsequent calculations.

The rate of change of the isotopic ratio $^{14}C/^{12}C$ in TDIC, referred to as R_{TDIC}, is described by;

$$\frac{\partial}{\partial t} R_{TDIC} = \frac{\partial}{\partial t} \frac{{}^{14}C_{TDIC}}{{}^{12}C_{TDIC}} \qquad (3.9)$$

By applying the quotient rule, and equating ^{12}C to TDIC, the change in isotopic ratio, R, of the TDIC in the water can be described by (full derivation in Appendix 1);

$$\frac{\partial}{\partial t} R_{TDIC} = k_{co_2} \frac{A}{V} \frac{CO_2}{TDIC} (R_{CO2eq} - R_{CO2}) \qquad (3.10)$$

where R_{CO2} is the ratio of $^{14}C/^{12}C$ in CO_2 (which is often expressed relative to a standard in either pMC or ‰) in the water at time t, and $R_{CO2\,eq}$ is the ratio of $^{14}C/^{12}C$ (either in pMC or ‰) of water in the pan when it is at isotopic equilibrium with the atmosphere. This equation can

be used to simulate the isotopic equilibration of water in the pan as a function of time. Equations for the change in ratio of $^{13}C/^{12}C$ in TDIC can also be rewritten, following the form of equations 3.9 and 3.10.

From Equation 3.10 it can be seen that the difference between the rate of isotopic change of R_{TDIC} relative to the gas transfer velocity of CO_2 is a function of the proportion of TDIC that is present as dissolved CO_2, which is in turn a function of pH (Appelo and Postma, 2005, Weiss, 1974). This effect of speciation is incorporated into a lumped parameter, k_e (L T^{-1}) that is the effective transfer velocity of ^{14}C in TDIC. The rate of change of isotopic ratio is then described by;

$$\frac{\partial}{\partial t} R_{TDIC} = k_e \frac{A}{V} \left(R_{CO2eq} - R_{CO2} \right) \tag{3.11}$$

where;

$$\frac{k_e}{k_{CO2}} = \frac{CO_2}{TDIC} \tag{3.12}$$

3.2.2.2 *Mass balance of a gaining or losing stream*

In a stream system, the mass is integrated over distance, rather than time. The water balance of a stream with groundwater discharge or recharge is given by;

$$\frac{dQ}{dx} = q_{gw} - Ew \tag{3.13}$$

where Q is stream discharge (L^3 T^{-1}), q_{gw} is groundwater flux into (positive values) or out of (negative values) the stream (L^2 T^{-1}), E is the evaporation rate (L T^{-1}), w is stream width (L) and x is the distance along the stream (L).

The equations for the change in concentration along a stream are different for gaining and losing streams. In the case of a gaining stream ($q_{gw} > 0$), the rate of change in concentration of a non-reactive, non-gaseous tracer is given by;

$$Q \frac{dc}{dx} = Ewc - q_{gw}(c_{gw} - c) \tag{3.14}$$

where c is the concentration in the stream (M L^{-3}), and c_{gw} is the concentration in the groundwater (M L^{-3}). This is comparable to Equation 3.5 for an evaporating pan of water. For a radioactive gas, the change in concentration along a gaining stream is described by Cook et al. (2003);

$$Q \frac{dc}{dx} = Ewc - q_{gw}(c - c_{gw}) + kw(c_{eq} - c) - \lambda dwc \tag{3.15}$$

Equation 3.15 is comparable to Equation 3.6 for the evaporating pan, and is used in the current study for simulating both radon-222 and CO_2 isotopologues.

The mass balance of ^{12}C in TDIC in a gaining stream that is at chemical equilibrium with the atmosphere such that there is no gas transfer of CO_2, is given by;

$$Q\frac{\partial}{\partial x}\,^{12}C_{TDIC} = Ew^{12}C_{TDIC} - q_{gw}\left(^{12}C_{TDIC} - ^{12}C_{TDICgw}\right)$$ (3.16)

Although the assumption of chemical equilibrium between the stream and the atmosphere is unlikely to hold in streams, this assumption is necessary to simplify the mathematics. The potential influence of chemical disequilibrium in this study is discussed in subsequent sections (Section 3.4 and 3.5).

For ^{14}C, the radioactive decay rate is slow and this term can be neglected, so that the rate of change of ^{14}C in TDIC along a gaining stream is given by;

$$Q\frac{d}{dx}\,^{14}C_{TDIC} = Ew^{14}C_{TDIC} - q_{gw}\left(^{14}C_{TDIC} - ^{14}C_{TDICgw}\right) +$$
$$k_{CO2}w(^{14}CO_{2eq} - ^{14}CO_2)$$ (3.17)

where $^{14}C_{TDICgw}$ is the concentration of ^{14}C in the groundwater (M L^{-3}).

Using R-notation (see Equation 3.9), applying the quotient rule to Equations 3.16 and 3.17, assuming that the $^{12}CO_2$ in the stream is in equilibrium with the atmosphere, and that the ^{12}C in solution is equal to the TDIC, and again using the effective transfer velocity, k_e, which incorporates the effect of speciation, the rate of change of isotopic ratio along the stream is given by (full derivation in Appendix II);

$$\frac{\partial}{\partial x}R_{TDIC} = k_e\frac{w}{Q}\left(R_{CO2eq} - R_{CO2}\right) - \frac{q_{gw}}{Q}\frac{TDIC_{gw}}{TDIC}\left(R_{TDIC} - R_{TDICgw}\right)$$ (3.18)

which can be used to simulate the carbon isotopic ratio along a stream in delta notation (‰) or pMC.

In a losing stream (or losing reach of a stream, $q_{gw} < 0$), the rate of change in concentration of a conservative ion along a losing stream is described in Chapter 2;

$$Q\frac{dc}{dx} = Ewc$$ (3.19)

the change in concentration of a radioactive gas tracer is described by;

$$Q\frac{dc}{dx} = Ewc + kw(c_{eq} - c) - \lambda dwc$$ (3.20)

and the change in isotopic ratio is given by:

$$\frac{\partial}{\partial x} R_{TDIC} = k_e \frac{w}{Q} \left(R_{CO2eq} - R_{CO2} \right) \tag{3.21}$$

In subsequent sections, the isotopic ratio of $^{14}C/^{12}C$ in TDIC is referred to as simply ^{14}C, and the isotopic ratio of $^{13}C/^{12}C$ in TDIC is referred to as ^{13}C.

3.3   Methods

The locations of the controlled equilibration experiment, and field applications at the artificial discharge location near Marandoo and along the Daly River are shown in (Figure 3.1).
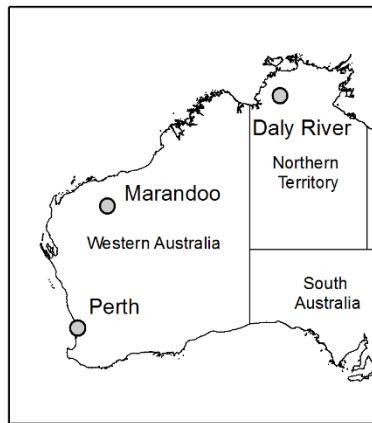
Figure 3.1 Locations of study sites in Perth (controlled equilibration experiment), Marandoo (artificial groundwater discharge) and the Daly River.

3.3.1   Controlled equilibration experiment

Groundwater from the Yarragadee aquifer in the Perth Basin, Australia (Figure 3.1) was used in a controlled experiment during which total dissolved inorganic carbon in the water is allowed to equilibrate with atmospheric CO_2. A circular pan (1.2 m in diameter, 0.25 m in height) containing 0.26 m^3 of groundwater was placed outside under cover and sheltered from direct rainfall input. The water was kept constantly circulating by pump (Aquagarden, 44W) without turbulence breaking the water surface. Water level and temperature were monitored continuously using a pressure transducer (Insitu level troll 300) corrected for barometric pressure (Insitu barotroll). Water samples (225 mL) were collected at intervals of hours to weeks for a period of 72 days between April 4th and June 14th, 2012. The water pH was measured using a WTW Multi 3420 Set D, and alkalinity was determined by titration using sulphuric acid (Hach Alkalintiy Digital Titration Kit). Chloride was measured by discrete analyser, and calcium was measured by ICP-OES (SGS laboratories, Perth).

Water samples were analysed for carbon isotopic composition using accelerator mass spectrometry (AMS) (Rafter radiocarbon laboratory, GNS Science, New Zealand). Dissolved inorganic carbon was converted to CO_2 through the addition of phosphoric acid. This CO_2 is then converted to graphite by reduction with hydrogen over an iron catalyst, and the isotopic composition of this graphite is determined by AMS. Carbon isotope data ($\delta^{13}C$ and $\delta^{14}C$) are reported in delta notation, as permil (‰), relative to an oxalic acid standard (Stuiver and Polach, 1977). The $\delta^{14}C$ is not corrected for sampling date or fractionation. Carbon-14 data are also reported as percent modern carbon (pMC), which are the units most commonly used for reporting the ^{14}C activity of groundwater. This pMC is calculated from;

$$pMC = \frac{A_{SN}}{A_{ABS}}$$ (3.22)

where A_{SN} is the activity of the sample normalized to $\delta^{13}C$ of -25‰ and A_{ABS} is the activity of the oxalic acid standard normalized with respect to $\delta^{13}C$ and corrected for radioactive decay since 1950 (Stuiver and Polach, 1977).

The effective transfer velocity of ^{14}C (and ^{13}C) was estimated using a mass balance approach to simulate isotopic equilibration using Equation 3.11. The parameters used in the mass balance are outlined in Table 3-1.

Determination of the gas transfer velocity for CO_2 (k_{CO2}) requires the consideration of the shifting speciation during CO_2 evasion (Equation 3.11). The k_{CO2} was estimated using a hydrochemical modeling approach (PHREEQC v2.18, Parkhurst and Appelo (1999)) to simulate CO_2 degassing, with the gas transfer velocity constrained by the measured pH and alkalinity during the chemical equilibration phase. PHREEQC solves the mass action equations for each species and simulates user-defined kinetic reactions. The kinetics of the CO_2 degassing were described by Equation 3.1, with an atmospheric CO_2 partial pressure of $10^{-3.4}$ atm (400 ppm). The simulated change in TDIC concentration during CO_2 degassing was used to calculate the enrichment associated with fractionation during this process. The fraction of TDIC remaining in solution after the CO_2 degassing phase was determined from the results of the hydrochemical model. This fraction remaining was then used to calculate the enrichment associated with CO_2 degassing using a Rayleigh distillation approach (Equation 3.2). Temperature dependant enrichment factors were applied, at a temperature of 20 °C, which was the average water temperature during the experiment. At this temperature, the kinetic enrichment factor for ^{13}C is -0.8‰ and equilibrium enrichment factor is -8.5‰, giving a total enrichment factor of -9.3‰

(Zhang et al., 1995). The enrichment of ^{14}C was assumed to be twice as large as the ^{13}C enrichment (Craig, 1957), resulting in a kinetic enrichment factor of -1.6‰, equilibrium enrichment factor of -17.0‰ and a total enrichment factor of -18.6‰.

3.3.2   Field application 1: Artificial groundwater discharge

The use of ^{14}C as a tracer of groundwater discharge was tested at a location of artificial groundwater discharge near Marandoo (Lower Fortescue River, Southern Branch) in the Pilbara region of north-western Australia. The Pilbara region has numerous iron ore mining operations that require dewatering of the mine pit to ensure safe mining conditions. Where dewatering volumes are in excess of water requirements for processing, this water is disposed of by discharging it to a nearby ephemeral creek line (which is normally dry). This water flows along the creek, until it is lost to evaporation and infiltration into the underlying alluvial aquifer associated with the creek. This system provides a proxy for groundwater discharge to a stream, with the relatively constant volume of mine water entering the creek at a fixed location, simulating a discrete groundwater discharge zone. The isotopic equilibration rate between the creek and the atmosphere is determined by measuring the ^{14}C activity in TDIC along the creek. Given that this ephemeral creek had recently wetted (within 7 weeks of sampling), in-stream CO_2 production is probably limited to bacterial synthesis and the effect of in-stream CO_2 production on isotopic equilibration is likely to be negligible (McIntyre et al., 2009). The mine water discharge had been abstracted from two production wells with the volume abstracted from each well consistent (13.9 to 14.2 ML d^{-1}) for the 4 days prior to sampling. Thus, although time-series data of the carbon-14 activity of the mine water discharge were not available, the variation over time is likely to have been as small as was operationally possible.

The stream channel was dry above the mine water discharge outlet and the only components of the water balance are streamflow losses to evaporation and infiltration. Water samples (1.5 L) were collected at six locations between 500 and 1500 m apart, along a 10 km reach downstream of the mine water discharge location on August 16th, 2012. Chloride, calcium and isotopic composition were measured using the methods outlined in Section 3.3.1. Streamflow was measured at each sampling location using an acoustic Doppler velocity meter (Sontec Flowtracker) following the methods described in Buchanan and Somers (1969). The data were fit using a mass balance model based on Equations 3.19, 3.20 and 3.21. The parameters used in the mass balance model are summarized in Table 3-2. The value of R_{CO2eq} was assumed to be

equal to the ^{14}C ratio in TDIC measured at the end of the controlled equilibration experiment, 108 pMC.

3.3.3 Field Application 2: Daly River

The Daly River flows north-west across the Ooloo Dolostone aquifer system in tropical northern Australia. A groundwater discharge zone with an estimated 10^6 m^3 d^{-1} of groundwater discharging along a 5 km stream reach (Cook et al., 2003, Smerdon et al., 2012) provided a location for testing the application of ^{14}C as a tracer of groundwater discharge. Stream flow measurements were taken at three locations along the creek (Streamflow ADCP). Water samples were collected at six locations along 120 km section of stream. Water samples were analysed for major ions using ICP-OES (Waite Laboratory, CSIRO, Adelaide). Radon activities were determined by liquid scintillation using a LKB Wallace Quantulus counter with a detection limit of 3 mBq L^{-1} (Leaney and Herczeg, 2006). Water samples were analysed for carbon isotopic composition by AMS as described in Section 3.3.1.

The data were analysed using a mass balance model as outlined in Section 3.2.2 using the parameters summarized in Table 3-3. Stream geometry, evaporation rate and radon gas transfer velocity were taken from previously published mass balance models of the Daly River (Cook et al., 2003, Smerdon et al., 2012). Measured stream flow and radon data were used to constrain groundwater discharge using manual calibration based on visual comparison of simulated and observed data. The measured ^{14}C data were used to constrain the effective transfer velocity and ^{14}C activity of the discharging groundwater based on visual comparison. The ^{14}C activity of discharging groundwater was assumed to be constant along the stream reach, which is reasonable based on the distribution of aquifers across the study site (Tickell, 2011). The estimated magnitude of the major groundwater discharge in this study is within 10% of published estimates (Cook et al., 2003, Smerdon et al., 2012).

Previous studies in the Daly River basin conducted at the same time of year as this study (October) measured the alkalinity of the groundwater in the Ooloo dolostone to be 410 ± 75 mg L^{-1} as HCO$_3^-$ (± stdev, n = 28), alkalinity of spring discharges to be 417 ± 7 mg L^{-1} as HCO$_3^-$ (n = 2) (Tickell, 2011). The alkalinity in the river during this was 374 ± 17 mg L^{-1} as HCO$_3^-$ (n = 6). Based on these data, the TDIC of the groundwater discharge is assumed to be similar to the TDIC in the Daly River and use a TDIC$_{gw}$/TDIC ratio of 1 in Equation 3.18.

3.4 Results

3.4.1 Controlled equilibration experiment

The volume of water in the pan decreased through evaporation from 0.26 to 0.15 m^3 over the 72 days of the experiment, implying an average evaporation rate of 0.0014 m d^{-1}. The concentrations of chloride, alkalinity and calcium all increased throughout the experiment, consistent with this reduction in water volume. Temperature ranged from 10.5 to 26.4 °C with a mean of 19.0 °C, and diel varation of ± 2.5 °C. Evasion of $CO_{2(g)}$ during the first 1.5 days increased the pH from 6.9 to 8.3 (Figure 3.2). The gas transfer velocity of $CO_{2(g)}$ during the controlled equilibration experiment was determined in a hydrochemical model (see Section 3.3.1), giving a k_{CO2} of 1.1 m d^{-1}.
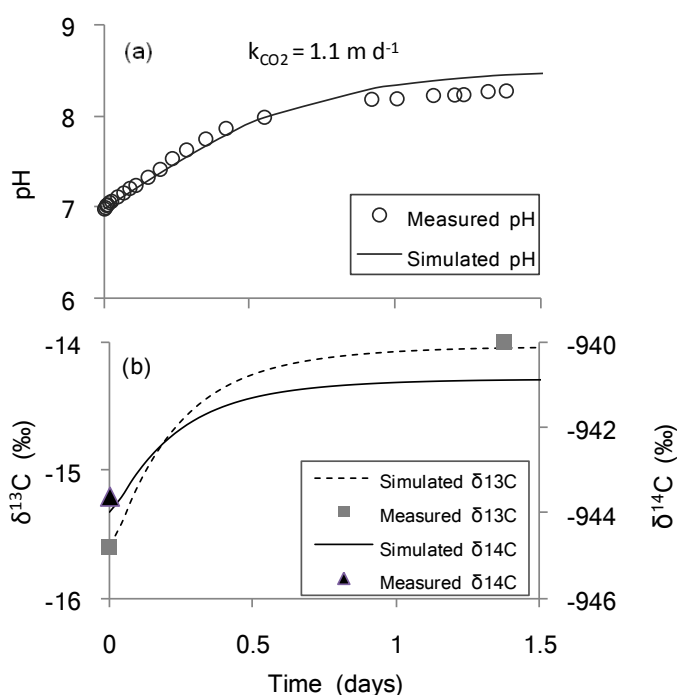
Figure 3.2 Controlled equilibration experiment degassing phase: a) simulated pH increase and b) associated isotopic enrichment of ^{13}C and ^{14}C in TDIC.

The enrichment associated with fractionation during CO_2 degassing was calculated using a Rayleigh distillation approach (Equation 3.2 and Section 3.3.1), giving an enrichment of 1.5‰ in $\delta^{13}C$ and 3.0‰ in $\delta^{14}C$, which equates to an increase of less than 1 pMC. This simulated enrichment correlates well with the observed enrichment in ^{13}C during the first 1.5 days of the experiment, but is much smaller than the observed enrichment in ^{14}C, which was -835‰ after 1.5 days (an increase of 109 ‰). This suggests that isotopic exchange dominated the

38

equilibration process for ^{14}C even while chemical exchange (i.e., CO_2 degassing) was ongoing. This is because the isotopic signature of ^{14}C was further from equilibrium with the atmosphere than ^{13}C and so the isotopic exchange flux for $^{14}CO_2$ was larger than for $^{13}CO_2$. Although saturation indices for calcite were greater than 1 during the experiment, the evolution of Ca^{2+} could be fully explained by evapo-concentration. This suggests that calcite was not precipitating and so fractionation effects associated with this process have been neglected.

Over the 72 days of the experiment $\delta^{13}C$ increased from -15.6 to -2.3‰, $\delta^{14}C$ increased from -943.6 to 77.2‰ and percent modern carbon increased from 5.5 to 107.7 pMC. The effective transfer velocity (k_e) of both ^{13}C and ^{14}C was determined using a mass balance approach (Table 3-1, Equation 3.11). The best fit to $\delta^{13}C$, $\delta^{14}C$ and pMC was achieved with an effective transfer velocity of 0.013 m d^{-1} (Figure 3.3). The sensitivity of the model to this effective transfer velocity is shown by plotting ±40% values on each plot.

The extent to which dissolved carbon speciation (which is a function of pH), determines the rate of equilibration in this system is assessed by comparing; 1) the ratio of the effective transfer velocity of ^{14}C to the gas transfer velocity of CO_2, and 2) the ratio of CO_2 to TDIC (see Equation 3.12). If these ratios are equal, this implies that carbon speciation was the major determinant of the rate of ^{14}C equilibration in TDIC in solution. The best-fit k_e (0.013 m d^{-1}) is 1.2% of the k_{CO2} (1.1 m d^{-1}). This correlates well with the expected proportion of TDIC that is CO_2 (0.7 – 1.1%), given the pH range measured during the experiment (8.3 – 8.5) (Table 3-4). The close agreement between these two ratios $\left(\frac{k_e}{k_{CO2}} \; vs. \frac{CO_2}{TDIC} \right)$ suggests that carbon speciation was the limiting factor for isotopic equilibration in this controlled equilibration experiment, and equilibration was dominated by isotopic exchange.

Table 3-1 Controlled equilibration experiment: Mass balance model parameters

Symbol	Description	Value	Units	Fitted to*
A	surface area	1.13	m^2	
E	evaporation rate	0.0014	m d^{-1}	Water volume, chloride
k_{CO2}	CO_2 gas transfer velocity	1.1	m d^{-1}	
k_e	effective transfer velocity	0.013	m d^{-1}	^{14}C, ^{13}C
$^{13}C_a$	^{13}C in equilibrium with atmosphere	-2.3	‰	
$^{14}C_a$	^{14}C in equilibrium with atmosphere	108	pMC	

*All other parameters fixed.
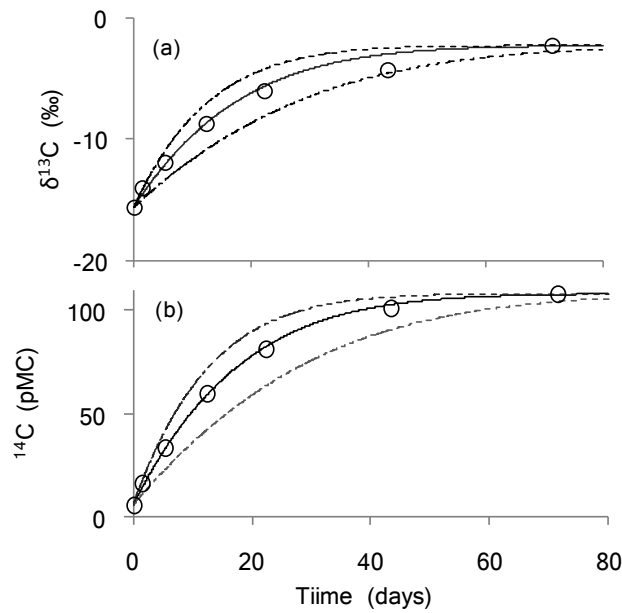
Figure 3.3 Evaporation pan experiment – isotopic equilibration: measured $\delta^{13}C$ a), and b) pMC. Simulated $\delta^{13}C$, and pMC using an effective transfer velocity of 0.013 m d^{-1} (solid line) and ± 40% of this value (dashed lines).

3.4.2   Field application 1: Artificial groundwater discharge

Streamflow decreased from 0.08 to 0.01 m^3 s^{-1} along the 10 km reach, driven by losses to evaporation and infiltration (Figure 3.4). Chloride increased from 110 to 116 mg L^{-1} due to evaporation along the 10 km reach. Carbon isotopic composition became more enriched with distance along the 10 km, with $\delta^{14}C$ increasing from -890 to -603‰ and percent modern carbon increasing from 11 to 31 pMC.

These data were analysed using a mass balance approach described by Equations 3.19 to 3.21, with an evaporation rate of 0.004 m d^{-1} and an infiltration flux of 0.6 m^2 d^{-1} (Table 3-2). The effective transfer velocity was calibrated to measured ^{14}C activity along the upstream 6 km by visual comparison. The best fit to the measured data was achieved with an effective transfer velocity, k_e, of 0.025 m d^{-1}. Given the stream geometry (stream width of 5 m, a stream depth of 0.3 m) and flow rate, this 6 km distance equates to a period of 1.7 days of exposure to the atmosphere. The measured ^{14}C activity at a distance of 10 km was not able to be fit with the same effective transfer velocity, which may reflect a different initial ^{14}C activity in the mine water discharge.

Table 3-2 Artificial groundwater discharge: Mass balance model parameters

Symbol	Description	Value	Units	Fitted to*
Q_0	Initial stream flow	0.08	$m^3 s^{-1}$	
w	stream width	5	m	
d	stream depth	0.3	m	
E	evaporation rate	0.01	$m\ d^{-1}$	Streamflow, chloride
q_{gw}	infiltration flux	-0.6	$m^3 d^{-1} m^{-1}$	Streamflow, chloride
k_e	^{14}C effective transfer velocity	0.025	$m\ d^{-1}$	^{14}C
$^{14}c_a$	atmospheric ^{14}C activity	108	pMC	

*All other parameters fixed.
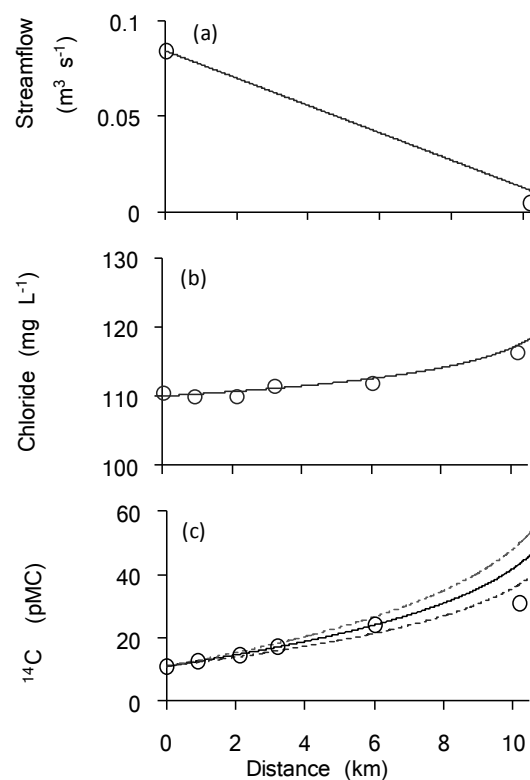
Figure 3.4 Artificial groundwater discharge: a) stream discharge, b) chloride and c) pMC. Measured (open circles) and simulated with an effective transfer velocity (k_e) of 0.025 m d^{-1} (solid line) and ± 20% of this value (dashed lines).

The CO_2 gas transfer velocity was not measured in this system, but k_{Rn} for a nearby stream (also ephemeral and receiving mine water discharge) was measured at 1.8 m d^{-1} (Bourke et al., 2014) Based on the difference in the diffusion coefficients of radon and CO_2, this implies a k_{CO2} of around 2.0 m d^{-1} (Genereux and Hemond, 1992). If the k_{CO2} for the Pilbara mine water discharge is between 1.6 and 2.4 m d^{-1} (± 20% of 2.0 m d^{-1}), the estimated k_e is between 1.0 and 1.6% of the k_{CO2} (Table 3-4). The pH of mine water discharge was 8.0 in August 2012, which

corresponds to $CO_{2(aq)}$ being 2% of TDIC. This correlates reasonably well with the ratio of k_e to k_{CO2}, suggesting that enrichment associated with fractionation during CO_2 degassing and CO_2 production within the stream are unlikely to be significant drivers of carbon isotopic equilibration in this system.

3.4.3 Field application 2: Daly River

Measured ^{14}C in stream TDIC along the Daly River, varied from 76 to 86 pMC ($\delta^{14}C$ from -230 to -161‰), while $\delta^{13}C$ varied from -10.6 to -11.6‰. Across the major groundwater discharge zone, stream flow increased from 12.3 to 25.5 $m^3 s^{-1}$, radon increased from 0.6 to 2.9 Bq L^{-1}, and ^{14}C decreased from 82.8 to 76.0 pMC, (Figure 3.5). Based on measured stream discharge and radon data from this and previous studies (Smerdon et al., 2012, Cook et al., 2003), the maximum estimated groundwater discharge was at a distance of 27 – 33 km, correlating well with the previously mapped location of the spring system. These data were simulated using a mass balance approach (Equation 3.21), with the parameters values described in Table 3-3.

Table 3-3 Daly River: Mass balance model parameters

Symbol	Description	Value	Units	Fitted to*
Q_0	Initial stream flow	12.3	$m^3 s^{-1}$	
d	stream depth	1.5	m	
w	stream width	50	m	
q_{gw}	groundwater discharge flux	10 - 200	$m^3 d^{-1} m^{-1}$	Streamflow, radon
E	evaporation rate	0.007	$m d^{-1}$	
k_e	^{14}C effective transfer velocity	0.09 – 0.15	$m d^{-1}$	^{14}C
k_{Rn}	radon gas transfer velocity	1	$m d^{-1}$	
λ_{Rn}	radon decay rate	0.181	d^{-1}	
c_{Rn}	groundwater radon concentration	7	Bq L^{-1}	
$^{14}c_a$	atmospheric ^{14}C activity	108	pMC	
$^{14}c_{gw}$	groundwater ^{14}C activity	61-66	pMC	^{14}C
$TDIC_{gw}/TDIC$	ratio of TDIC in groundwater:stream	1	-	

*All other parameters fixed.
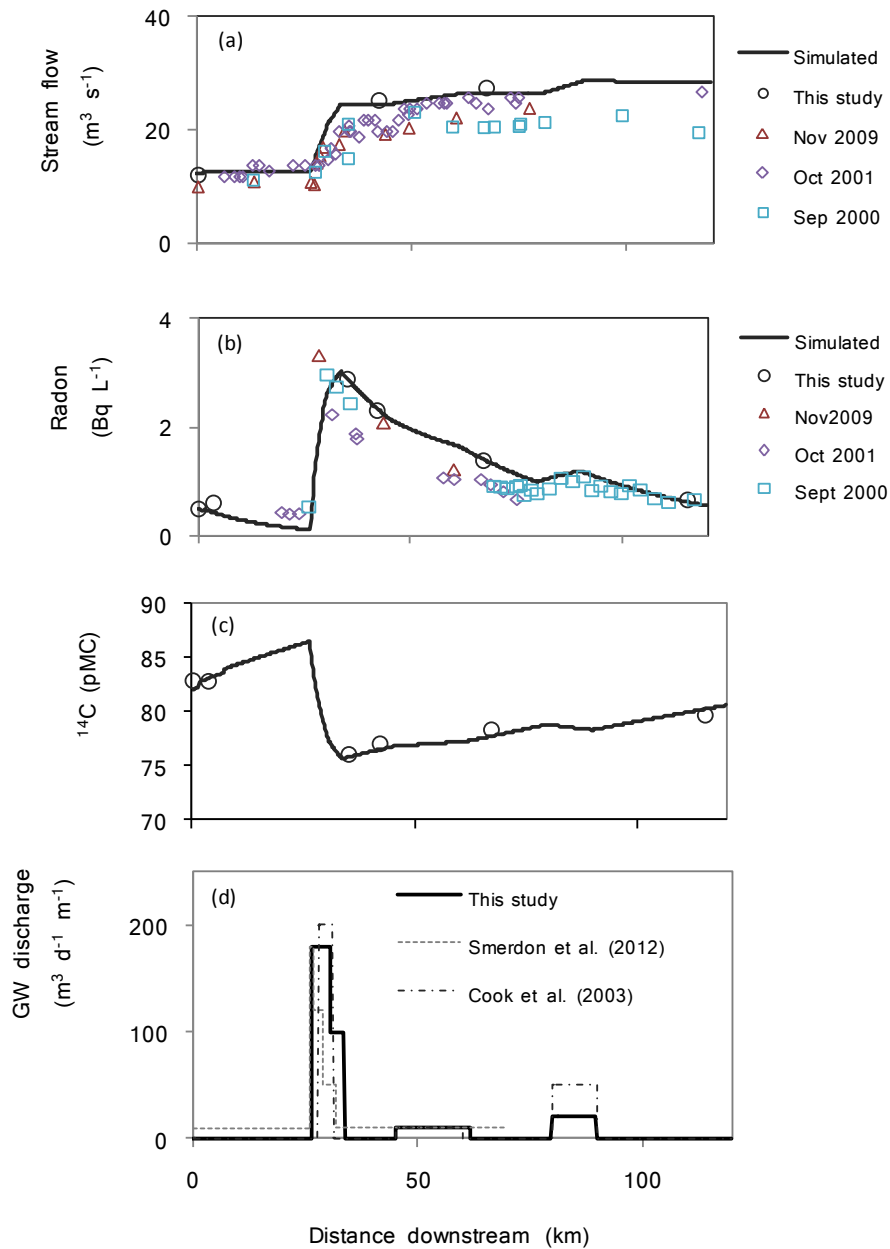
Figure 3.5 Daly River mass balance model a) Stream flow, b) radon, c) pMC and d) groundwater (GW) discharge.

The mass balance simulation of stream ^{14}C is most sensitive to the groundwater discharge flux, the ^{14}C activity (pMC) of the groundwater discharge and the effective transfer velocity (Figure 3.6). The groundwater discharge flux is well constrained by the measured variation in streamflow and radon activity. The measured variation in ^{14}C along the river was used to constrain the effective transfer velocity and the ^{14}C activity of the groundwater discharge. In the absence of a measured value immediately upstream of the groundwater discharge zone these two parameters cannot be fit independently, or uniquely. A similar fit to the data can be achieved using a range of gas transfer velocities and ^{14}C activities of groundwater discharge.

Figure 3.5 presents a k_e, of 0.13 m d^{-1}, 63 pMC, but other combinations are also possible. A larger k_e requires a correspondingly lower pMC, with possible values of k_e varying from 0.09 to 0.15 m d^{-1} and groundwater ^{14}C activity varying from 61 to 66 pMC (Table 3-3).
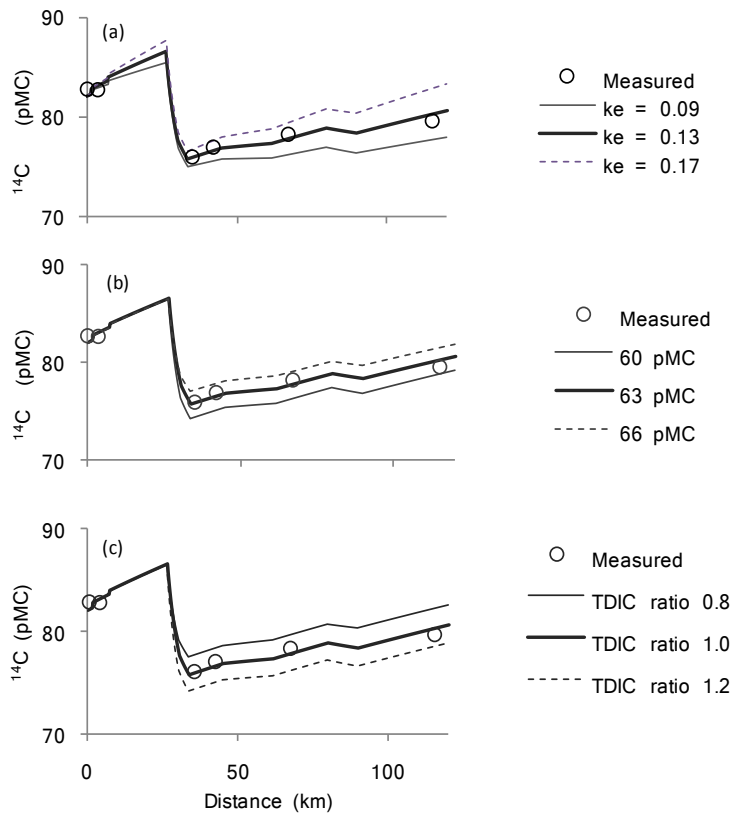
Figure 3.6 Daly River mass balance model: sensitivity to a) effective transfer velocity (ke), b) groundwater pMC and c) TDIC ratio (gw:sw).

The range of effective gas transfer velocities in the Daly River is between four and six times larger than the effective transfer velocity in artificial groundwater discharge study (Field application 1 at Marandoo), and an order of magnitude larger than the gas transfer velocity of the controlled equilibration experiment. Based on the in-situ pH of 7 measured in the Daly River, CO_2 would be around 4% of the total TDIC pool. The k_{Rn} in the Daly River has been previously estimated as 1 m d^{-1} (Cook et al., 2003), which, based on diffusion coefficients, implies a k_{CO2} of 1.2 m d^{-1}. If this is correct, then the effective transfer velocity is between 7.5 and 12.5% of the k_{CO2} (Table 3-4). The elevated k_e/k_{CO2} ratio, relative to the CO_2/TIDC ratio, suggests that either fractionation effects or in-stream CO_2 production are increasing the rate of isotopic equilibration in the Daly River, above what would be expected based on TDIC speciation.

Table 3-4 Relationships between pH, k_e and k_{co2}

Setting	pH	CO_2/DIC	k_{CO2} (m d^{-1})	k_e (m d^{-1})	k_e/k_{CO2}
Isotope exchange experiment	8.3	1 %	1.1	0.013	1.4%
Artificial groundwater discharge	8.0	2 %	1.4 – 2.2	0.025	1.4 – 2.5%
Daly River	7.8	4%	1.2	0.09 – 0.15	7.5 – 12.5%

3.5   Discussion

This is the first study to measure an effective transfer velocity for ^{14}C in TDIC. Although the equilibration of ^{14}C with the atmosphere is driven by $CO_{2(g)}$ exchange, it is buffered by the other carbonate species in solution and so the effective transfer velocity of ^{14}C in TDIC is much slower than the gas transfer velocity of CO_2. The effective gas transfer velocities measured in this study are between 0.16 and 14% of the reported range of values of k_{CO2}, which vary between 1 and 8 m d^{-1} (Butman and Raymond, 2011, Hagedorn and Cartwright, 2010, Richey et al., 2002, Raymond and Cole, 2001).

While this study is the first to apply ^{14}C in stream TDIC as a tracer of groundwater discharge to streams, ^{13}C has previously been used in this context (Doctor et al., 2008, Meredith and Kuzara, 2012). Data from this and previous studies show that the variation in δ^{14}C in natural waters can be an order of magnitude larger than the variation in δ^{13}C (Mayorga et al., 2005, Raymond et al., 2004, Cole and Caraco, 2001). The potential deviation of δ^{14}C from equilibrium with the atmosphere is up to 1060‰ (in the Southern Hemisphere), much larger than the potential disequilibrium of δ^{13}C ($\leq$ 23‰). For the Daly River samples, the measurement error for δ^{13}C was 0.2‰ (0.9% of maximum possible disequilibrium, and 20% of the measured variation in δ^{13}C), while for δ^{14}C the measurement error was 1.5‰ (0.1% of maximum possible disequilibrium). Given the larger variation between end-members relative to the measurement error, ^{14}C may be more sensitive as a tracer of groundwater discharge to streams than ^{13}C, and has the added benefit of providing information on the aquifer residence time of the groundwater discharge. If the total groundwater influx to the stream is constrained (in this chapter, stream gauging and ^{222}Rn were used), then the ^{14}C activity of the groundwater discharge can also be constrained through measurements of stream ^{14}C.

Previous authors have used ^{14}C mass balance calculations to calculate a constant flux of CO_2 between the ocean, streams or lakes and the atmosphere (Broecker et al., 1980, Wanninkhof et al., 1987, Broecker and Walton, 1959), which would result in a linear equilibration process. In this chapter, the $^{14}CO_2$ flux was simulated using a first order reaction driven by the deviation from equilibrium, which implies a larger flux change initially when the isotopic composition of the water is furthest from equilibrium. This approach has been verified in the controlled equilibration experiment, a modified losing stream (artificial groundwater discharge) and a natural gaining stream receiving groundwater discharge (Daly River).

Previous authors have suggested that carbon isotopic composition would be determined by fractionation associated with CO_2 degassing, suggesting that the effects of isotopic exchange would be negligible while there was chemical disequilibrium between the stream and the atmosphere (Doctor et al., 2008). This is in contrast with oceanographic studies that have highlighted the possibility of isotopic equilibration progressing in the opposite direction to chemical equilibration (Lynch-Stieglitz, 1995). During the first 1.5 days of the controlled equilibration experiment the CO_2 gradient was driving CO_2 evasion, which would have enriched the ^{14}C activity of the residual water by 3‰, or less than 1 pMC through fractionation effects. This is consistent with Choi et al. (1998), who observed an enrichment of between 3 and 5‰ associated with fractionation during CO_2 degassing from a stream. The ^{14}C enrichment observed in the evaporation pan experiment during this period of chemical equilibration was more than ten times larger than this predicted fractionation effect, with an increase of 109‰, or 11 pMC. In this simple system fractionation effects associated with other chemical exchange processes can be excluded, so this enrichment must have been driven by isotopic exchange of $^{14}CO_2$ in the opposite direction to the CO_2 evasion flux. This demonstrates that the process of isotopic equilibration in this system was 1) driven by isotopic exchange, 2) not dependent on chemical equilibrium to progress, and 3) resulted in a flux of $^{14}CO_2$ in the opposite direction to the CO_2 degassing flux.

The equation for the ^{14}C mass balance in a gaining stream, which was applied to the Daly River (Equation 3.18), assumes that the stream is in chemical equilibrium with the atmosphere, such that there was no net exchange of CO_2 across the air-water interface. However, chemical disequilibrium between the stream and atmosphere can also be caused by CO_2 influx associated with groundwater discharge. Furthermore, even in the absence of groundwater discharge, streams are generally supersaturated with respect to CO_2, which drives a net CO_2 evasion from the stream to the atmosphere (Richey et al., 2002, Butman and Raymond, 2011,

Raymond et al., 1997). This CO_2 excess is produced by plant respiration and other reactions that convert dissolved organic carbon (DOC) to dissolved inorganic carbon (DIC) (Cole et al., 2007). The effect of in-stream CO_2 production on the rate of carbon isotopic equilibration depends on the source. If respired CO_2 is in isotopic equilibrium with the atmosphere it will increase the rate of equilibration downstream of a groundwater discharge zone. The influence of CO_2 produced from DOC is less predictable, with many studies measuring predominantly modern ^{14}C signatures in stream DOC, (Hedges et al., 1986, Palmer et al., 2001, Raymond and Hopkinson, 2003, Mayorga et al., 2005), while depleted ^{14}C signatures were measured in stream DOC in some systems (Raymond and Bauer, 2001, Caraco et al., 2010, Raymond et al., 2004).

Although the assumption of chemical equilibrium in a stream is unlikely to hold, the magnitude of the effect of chemical exchange processes not explicitly accounted for in the [14]C_{TDIC} mass balance (Section 2.2) can be assessed by comparing the k_e/k_{CO2} ratio to the $CO_2/TDIC$ ratio. If the k_e/k_{CO2} ratio is much larger than $CO_2/TDIC$, then the rate of equilibration of carbon isotopes is greater than can be explained by isotopic exchange and speciation effects, and is likely to be enhanced by chemical exchange. In the controlled equilibration experiment and at the artificial discharge site (Marandoo) the ratio of k_e/k_{CO2} was similar to the proportion of CO_2 in TDIC, suggesting that the simplified conceptual model outlined in Section 2.2 adequately describe these systems. However, in Daly River, the ratio of k_e/k_{CO2} was up to three times larger than the proportion of CO_2 in TDIC. This suggests a significant enhancement of the rate of isotopic equilibration along the stream by chemical exchange processes and associated fractionation effects.

Furthermore, other fractionation processes, which were not explicitly considered in this study, could affect the isotopic equilibration rate in streams. Diurnal temperature variation within the stream will drive a cycle of CO_2 efflux and influx, with kinetic and equilibrium fractionation effects similar to those described in section 3.2.1. Calcite precipitation was not evident in this study, but may be significant in other stream systems and would act to deplete the stream ^{14}C signature (Keppel et al., 2012). Further studies are required to quantify the effects of degassing fractionation, diffusion, diurnal temperature variation, calcite precipitation and in-stream production of CO_2 in complex stream systems.

In spite of in-stream CO_2 production, and potential fractionation effects associated with chemical exchange, depleted ^{14}C signatures associated with groundwater discharge into the

stream persisted for tens of kilometres downstream of the mapped spring discharge location (0.5 to 3 days travel time). The equilibration rate of ^{14}C is on the order of 10 times slower than the equilibration rate of other gas tracers that have previously been applied as tracers of groundwater discharge, such as ^{4}He, CFCs, SF$_6$ and Rn, with reported gas transfer velocities ranging from 1.0 to 2.5 m d^{-1} (Smerdon et al., 2012, Gardner et al., 2011, Cook et al., 2003, Cook et al., 2006) . This may provide an advantage for using ^{14}C quantifying groundwater discharge in systems with small groundwater discharge volumes, or low concentrations of other gas tracers in the discharging groundwater.

The maximum optimal distance between samples can be described by the scale length, which is calculated as; $\frac{Q}{kw+dw\lambda}$ (Cook, 2013). Based on the range of simulated stream flow (12.3 – 33.0 m^3 s^{-1}), and the gas transfer velocities of radon and ^{4}He and stream geometry, the scale length in the Daly River for radon ranges from 17 to 45 km, and for ^{4}He ranges from 8 to 23 km. For ^{14}C, given the effective transfer velocity of ^{14}C in TDIC the Daly River, the scale length ranges from 151 to 407 km.

This persistence of the groundwater discharge signal over longer distances could limit the usefulness of ^{14}C to detect specific locations of discrete groundwater discharge in previously un-mapped systems. Preliminary sampling of streamflow and radon along the stream reach will allow for these discrete zones of discharge to be detected, and can be used to inform a secondary sampling campaign for measuring ^{14}C along the stream at larger spatial sampling intervals.

The application of ^{14}C as a tracer of groundwater discharge to streams, and the use of stream ^{14}C to constrain the ^{14}C activity of discharging groundwater, will be most successful when the groundwater discharge induces a significant depletion in stream ^{14}C activity relative to the ^{14}C activity of the stream in equilibrium with the atmosphere. The magnitude of the ^{14}C decrease in the stream is related to the ^{14}C activity of the groundwater, relative to the stream ^{14}C activity, and to the TDIC of the groundwater, relative to the stream TDIC (see Equation 3.18). Therefore, the sensitivity of this method will be greatest in systems with large gradients in ^{14}C activity between groundwater and the stream. However, a smaller gradient in ^{14}C activity between groundwater discharge and the stream can be offset by a strong gradient in TDIC, and vice versa.

The relationships between parameters in the groundwater discharge term and gas transfer term of Equation 3.18 are represented as nomograms in Figures 3.7 and 3.8 respectively. If three of the parameters represented in the nomogram are known, the fourth can be estimated by joining a line through the known parameter values to the pivot line, and then drawing a subsequent line to the third parameter value. This line will cross the axis of the fourth, unknown, parameter at the corresponding value. This process is demonstrated by the isopleths on each nomogram (dashed lines), which show the values for each parameter across the major discharge system in the Daly River. By comparing the resulting $\frac{\partial R}{\partial x}$ for each term, it is shown that the groundwater discharge value is 20 times larger than the gas transfer term, and therefore the decrease in ^{14}C across the groundwater discharge zone is likely to be measurable. More generally, these nomograms can be used to test the applicability of ^{14}C in TDIC as a tracer of groundwater discharge to a stream for a given field application. By making assumptions about the TDIC of groundwater and surface water and the likely groundwater inflow rate, the rate of change in carbon isotopic ratio along the stream can be predicted by visual inspection of the nomograms.

Pivot line

$-\delta R/\delta x$

$(permil \quad or \quad pMC)$

0.0001

0.0002

0.0003

0.0004
0.0005
0.0006
0.0007
0.0008
0.0009

0.0010

q_{gw}/Q

(L^{-1})

$TDIC_{gw}/TDIC$

0.00001

100.00

80.00
70.00
60.00
50.00
40.00
30.00

20.00

0.00002

0.00003

10.00

0.00004
0.00005
0.00006
0.00007
0.00008
0.00009

9.00
8.00
7.00
6.00
5.00

4.00

3.00

2.00

0.00010

1.00

0.90
0.80
0.70
0.60
0.50
0.40
0.30

0.20

$R_{TDIC} - R_{TDICgw}$

$(permil \quad or \quad pMC)$

1.0

2.0

3.0
4.0
5.0
6.0
7.0
8.0
9.0

10.0

20.0

30.0
40.0
50.0
60.0
70.0
80.0

100.0

200.0

300.0
400.0
500.0
600.0
700.0
800.0

1000.0

0.0020

0.0030

0.0040
0.0050
0.0060
0.0070
0.0080
0.0090

0.0100

0.0200

0.00020

0.00030

0.10

0.09
0.08
0.07
0.06
0.05
0.04

0.03

0.02

0.00040
0.00050
0.00060
0.00070
0.00080
0.00090

0.00100

0.01

0.0300

0.0400

0.0500

0.0600
0.0700
0.0800
0.0900

0.1000

$$-\delta R/\delta x = q_{gw}/Q \times TDIC_{gw}/TDIC \times (R_{TDIC} - R_{TDICgw})$$

Figure 3.7 Nomogram showing the relationships between parameters in the groundwater term of the equation for change in carbon isotope ratio along a gaining stream.

50
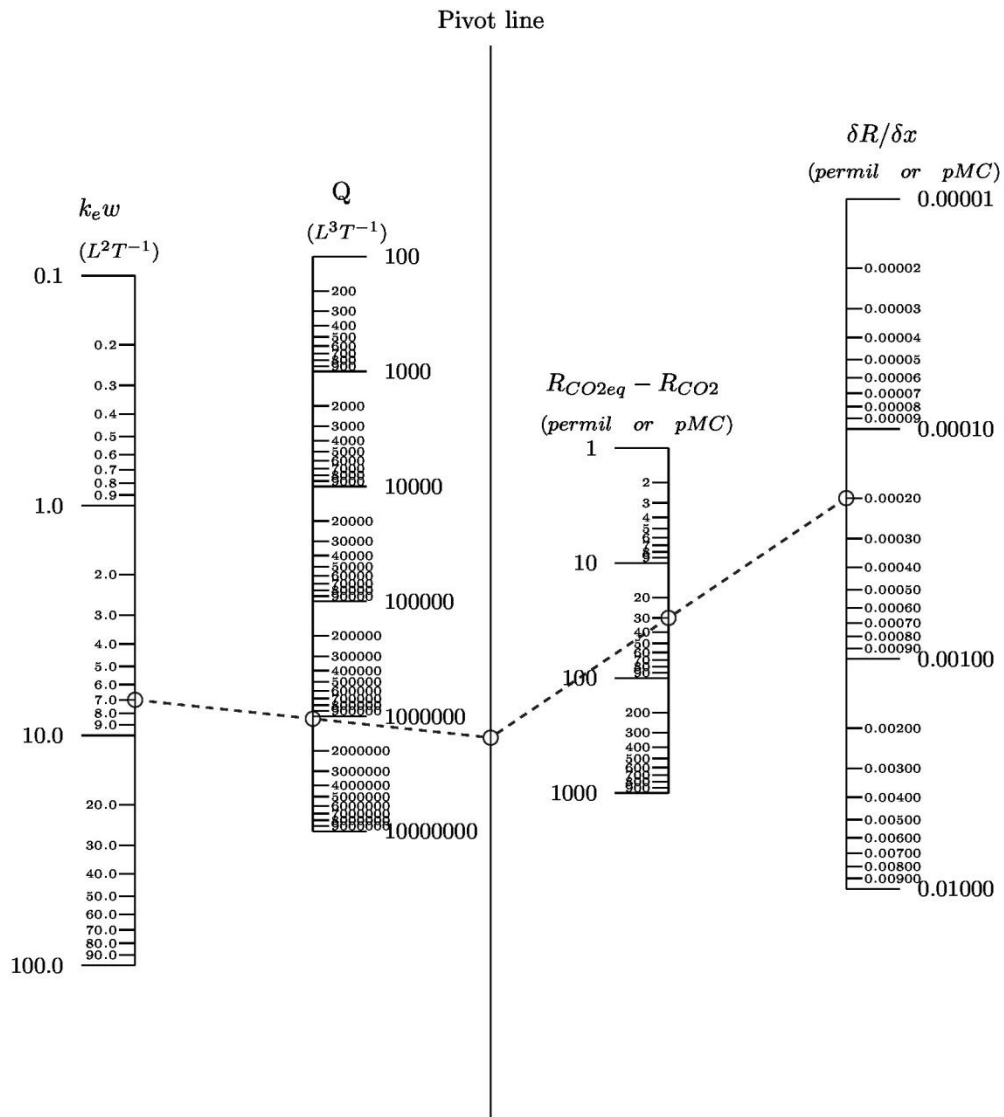
Figure 3.8 Nomogram showing the relationships between parameters in the gas transfer term of the equation for change in carbon isotope ratio along a gaining stream.

3.6   Conclusion

This chapter demonstrates that ^{14}C in streams can be used as a tracer of groundwater discharge. In contrast to other gas tracers the ^{14}C activity of the stream TDIC is a function of the entire TDIC pool, of which only CO_2 exchanges with the atmosphere. As a result, the effective transfer velocity of ^{14}C in TDIC is much slower than the CO_2 gas transfer velocity, and the signal of groundwater discharge can persist for hundreds of kilometres downstream. The effective transfer velocity of ^{14}C in TDIC is related to the gas transfer velocity of CO_2 through the stream pH, which determines the proportion of TDIC that is dissolved CO_2.

Because of this slower equilibration rate relative to other gas tracers, the signal of groundwater discharge in stream ^{14}C will persist further downstream than other gas tracers. This allows for a larger spatial sampling interval, and may provide for the detection of smaller groundwater discharge volumes, than is possible using other gas tracers. The application of ^{14}C as a tracer of groundwater discharge to streams is most likely to be effective in stream systems where the groundwater ^{14}C activity is significantly depleted relative to isotopic equilibrium with the atmospheric CO_2, and the groundwater TDIC is high relative to stream TDIC. Future application of ^{14}C in streams as a tracer of groundwater discharge should include in-situ measurement of stream pH and alkalinity, and estimates of the alkalinity of potential groundwater sources where possible.

Chapter 4   Differentiating sources of recharge in environments with groundwater re-circulation using CFC-12, carbon-14 and noble gases

4.1   Introduction

In environments where the surface waters have been derived from groundwater, differentiation of natural rainfall recharge and anthropogenic sources of recharge can be difficult. This recycling of groundwater between an aquifer and the land surface can be associated with irrigated agriculture (Brown et al., 2011), artificial wetland supplementation (Searle et al., 2011) or discharge of surplus mine water to streams (Kempe, 1983). In natural environments, water balance estimates are usually based on traditional hydrochemical and stable isotope methods. However, in a system where water is recycled between the aquifer and the surface, the application of major ions or stable isotopes as tracers can be limited by the lack of variation in potential end-members. In this setting, there are two potential advantages of groundwater age indicators as tracers for differentiating recharge sources. Firstly, the atmospheric concentrations of groundwater age indicators have varied over time and the distribution of atmospheric concentrations is known. Secondly, for gaseous groundwater age indicators, the process of equilibration through gas exchange with the atmosphere can cause significant changes in concentration. These changes may be larger than the enrichment of stable isotopes or the increase in chloride concentration caused by evapotranspiration.

The focus of this chapter is on the re-circulation of groundwater during mine dewatering operations. Surplus water produced during mine dewatering (hereafter referred to as mine water) can be discharged to natural drainage lines, allowing it to infiltrate into the underlying aquifer. This constitutes an anthropogenic source of recharge to adjacent aquifers that needs to be quantified in order to understand total impact of mining on the aquifer water balance. If the proximity of mining to natural creek lines requires dewatering between the creek and the pit, some fraction of the mine water that recharges to the aquifer through the creeks is potentially intercepted by dewatering wells. This may result in some of the mine water being re-circulated, potentially reducing the net change in the aquifer water balance associated with dewatering operations.

The study site is an iron-ore mine in the semi-arid Pilbara region of Western Australia. The conceptual framework for groundwater recharge in this mining-altered system is outlined in Figure (4.1). Prior to mining, recharge is dominated by episodic flood events along the creeks. Discharge of mine water causes the creek hydrology to shift from ephemeral to perennial flow regimes along the affected reaches. Over time, mine water discharge can produce a groundwater mound beneath the creeks, potentially changing them from disconnected to connected stream systems. As a result, natural episodic groundwater recharge through the creeks becomes superimposed onto the perennial recharge regime associated with the mine water discharge.
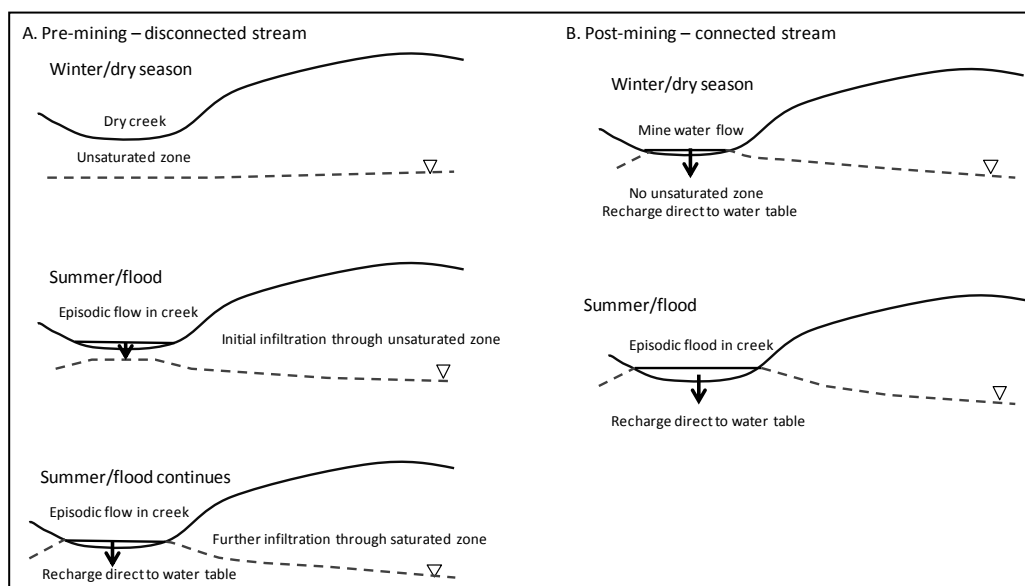
Figure 4.1 Conceptual diagram of recharge mechanisms, a) prior to mining and b) during mining.

This chapter tests the hypothesis that CFCs, ^{14}C and noble gases can be used as tracers to constrain the influence of mine dewatering operations on adjacent aquifers. At this study site, regional groundwater that recharged prior to 1960 is expected to have depleted ^{14}C activity, negligible CFC concentrations and elevated ^{4}He concentrations. Groundwater that recharged from mine water discharge along the creeks is expected to have a similar ^{14}C activity as regional groundwater (or slightly higher due to partial equilibration with the atmosphere), and CFC concentrations consistent with recharge since 1996. Water that recharged through the creek between 1960 and 1996, is termed pre-mining recharge, and is expected to have measurable CFC concentrations and ^{14}C activity greater than regional groundwater. Mine water recharge will have CFC concentrations in equilibrium with the atmosphere at the time of recharge, and ^{14}C activity that reflects the ^{14}C activity of the discharging mine water and partial

equilibration with the atmosphere. Where the discharge of mine water has led to a transition from disconnected to a connected stream system, low excess air amounts are expected that reflect the absence of an unsaturated zone during recharge (Massmann and Sültenfuß, 2008).

In this chapter, ternary mixing ratios are calculated from CFC and ^{14}C data to partition water samples into three recharge components. The lateral extent of recharge by mine water is inferred from mixing fractions in water samples collected from transects of piezometers installed perpendicular to the creeks. These results are compared with independent estimates of the potential extent of recharge by mine water based on the seepage flux from the creeks inferred from the stream chloride mass balance. The relative proportion of mine water discharge that is intercepted by dewatering wells is assessed by calculating ternary mixing fractions in samples from dewatering wells. These results are compared with excess air and terrigenic [4]He amounts in samples from the same wells.

4.2 Theory

4.2.1 Stable isotopes and chloride

Stable isotopes are widely used as hydrologic tracers to distinguish water sources, and can be used to partition recharge according to the distance from the coast, the rainfall amount, the abundance of snowmelt, or the amount of evaporation (Kendall and McDonnell, 1999). The major advantage of stable isotopes as tracers is that they are cheap and easy to measure, and because they are part of the water molecule they move in the same way as the water. Chloride concentration is also commonly applied as a conservative tracer in hydrologic studies (Mazor, 2003). The chloride mass balance can be used to quantify rates of diffuse recharge (based on evapo-concentration) and mixing processes, but this usually requires that steady state conditions are assumed (Scanlon et al., 2002, Harrington et al., 2002).

4.2.2 CFC-12 and ^{14}C as tracers

Chlorofluorocarbon (CFC) concentrations in groundwater can be used to date groundwater that recharged between about 1960 and 1990 (Beyerle et al., 1999, Busenberg and Plummer, 1992, Oster et al., 1996). Atmospheric concentrations of CFC-12 in the southern hemisphere increased from 6 in 1950 to a peak of 542 pptv in 2003, and since then have decreased to around 530 pptv in 2012 (AGAGE Station, Cape Grimm Australia). CFCs have previously been

used in combination with tritium and noble gases to estimate infiltration of river water into an alluvial aquifer (Beyerle et al., 1999).

Carbon-14 is a radioactive tracer with a half-life of 5730 years, which can be used to date groundwater up to around 20 000 years old, and has been used extensively as a tracer of groundwater flow (Cook and Herczeg, 2000). Atmospheric concentrations were relatively constant prior to the 1800's, when they began to decrease in response to the fossil fuel consumption, before increasing in response to thermonuclear testing during the 1950's and 1960's. In the Southern Hemisphere, atmospheric ^{14}C activities reached a peak of 164 pMC in 1965, before declining to the current value of around 110 pMC (Data from NIWAR, New Zealand). Previous studies have used ^{14}C as a tracer to investigate recharge from ephemeral streams in central Australia (Harrington et al., 2002, Shanafield and Cook, 2014).

The ^{14}C activity of groundwater is measured on dissolved inorganic carbon (DIC), which is composed of bicarbonate, carbonate and dissolved CO_2. Although ^{14}C is not technically a gaseous tracer, the dissolved CO_2 within the DIC pool is available for exchange with the atmosphere, and so the ^{14}C activity of water undergoes a process of equilibration when exposed to the atmosphere. In Chapter 3 it was shown that ^{14}C concentrations in streams equilibrate with the atmosphere slower than other gaseous tracers. This slower equilibration, and different temporal scale of change in atmospheric concentrations, means that ^{14}C should provide additional, complementary information, which may not be captured by CFC-12. Carbon isotope data as reported as percent modern carbon (pMC), which is calculated from;

$$pMC = \frac{A_{SN}}{A_{ABS}} \qquad (4.1)$$

where A_{SN} is the activity of the sample normalized to $\delta^{13}C$ of -25 ‰ and A_{ABS} is the activity of the oxalic acid standard corrected for radioactive decay since 1950 (Stuiver and Polach, 1977).

The influence of carbonate dissolution on ^{14}C activity can be constrained by the $\delta^{13}C$ following the method initially presented by Pearson (1965), modified by Clark and Fritz (1997), where the dilution factor, q, is given by;

$$q_{\delta^{13}C} = \frac{\delta^{13}C_{DIC} - \delta^{13}C_{carb}}{\delta^{13}C_{rech} - \delta^{13}C_{carb}} \qquad (4.2)$$

where $\delta^{13}C_{DIC}$ is the measured ^{13}C activity in the sample, $\delta^{13}C_{carb}$ is the ^{13}C activity of the dissolved carbonate and $\delta^{13}C_{rech}$ is the initial ^{13}C activity of the groundwater at the time of

recharge. The corrected (diluted) ^{14}C activity is then given by qA_0, where A_0 is the ^{14}C activity at the time of recharge.

4.2.3 Noble gases as tracers

Noble gases in groundwater have been used to infer paleo-temperatures, historical water level fluctuations and groundwater age (Aeschbach-Hertig et al., 2000, Castro et al., 2000, Ingram et al., 2007). The concentrations of noble gases in groundwater samples are a function of the gas concentrations in equilibrium with air at the time of recharge, which are, in turn, a function of temperature, pressure and salinity. In addition to this equilibrium component, there is usually also an "excess air" component that is produced by entrapment of air bubbles during recharge (Aeschbach-Hertig et al., 1999). The amount of excess air entrapped is a function of water table fluctuation into the unsaturated zone (Ingram et al., 2007, Holocher et al., 2002), and may be useful in tracking the transition of stream systems from disconnected to connected systems. Infiltration through an unsaturated zone beneath a disconnected stream would be expected to result in a larger excess air fraction than recharge directly to the saturated zone beneath a connected stream. The amount of excess air in each sample can be expressed as ΔNe (%), which describes the relative deviation of the measured concentration versus the expected equilibrium concentration, and is given by:

$$\Delta Ne = \left(\frac{Ne_{sample}}{Ne_{sat}} - 1\right) 100 \qquad (4.3)$$

where Ne_{sample} is the measured Ne concentration, Ne_{sat} is the concentration in air saturated water at the given temperature. Surface waters with breaking waves (eg. the ocean or turbulent streams) can have ΔNe values of up to 6 % while groundwater samples commonly have values of between 10 and 20 % (Kipfer et al., 2002, Cook and Herczeg, 2000).

In the case of helium-4 (^{4}He), there is also a terrigenic component that is produced by radioactive decay of U-Th bearing minerals within the aquifer (Kipfer et al., 2002, Solomon, 2000). This accumulation of ^{4}He over time can be used to infer groundwater residence times of 1000 to 100000 years (Cook and Herczeg, 2000) and may provide an additional tracer to differentiate between regional groundwater and more recent groundwater recharge. The amount of helium in groundwater ($^4He_{aq}$) will be the sum of the helium concentration in equilibrium with the atmosphere at the time of recharge ($^4He_{atm}$), excess air ($^4He_{excess}$) and terrigenic helium ($^4He_{terr}$), according to;

$$^4He_{aq} = \ ^4He_{atm} + \ ^4He_{excess} + \ ^4He_{terr} \qquad (4.4)$$

Once the excess air amount has been calculated, the terrigenic helium amount is calculated by rearranging Equation 4.4 to solve for $^4He_{terr}$.

4.2.4 Stream mass balance

The potential extent of recharge by mine water can be estimated from the loss rates of water from the creeks and increases in chloride concentrations downstream of the discharge location, as demonstrated in Chapters 2 and 3. The decrease in streamflow downstream is given by:

$$\frac{\partial Q}{\partial x} = -q_g - E \qquad (4.5)$$

where Q is streamflow (m^3 d^{-1}), x is distance downstream (m), q_g is the seepage flux into the aquifer per metre length of stream (m^2 d^{-1}) and E is evapotranspiration flux per metre length of stream (m^2 d^{-1}). The change in concentration, c, of a conservative, non-gaseous solute along the stream is given by:

$$Q\frac{\partial c}{\partial x} = Ec \qquad (4.6)$$

If the full thickness of the aquifer is assumed to be penetrated, the lateral extent of the aquifer penetrated by this seepage, on either side of the stream, y (m), is given by;

$$y = \frac{q_g \tau}{2b\theta} \qquad (4.7)$$

where τ is the duration of mine water discharge (d), θ is porosity and b is the aquifer thickness (m).

The rate of equilibration of gas tracers along the stream is important for predicting the concentrations of gas tracers in water at the time of recharge. For gaseous tracers (e.g. CFC-12), the change in concentration along the stream is described by;

$$Q\frac{\partial c}{\partial x} = Ec - kw(c - c_A) \qquad (4.8)$$

where k is the gas transfer velocity (m d^{-1}), w is the stream width and c is the gas concentration in the stream and c_A is the atmospheric gas concentration(Cook et al., 2003). If the gas transfer velocity and stream width are known then this equation can be combined with Equation 4.6 to determine the stream distance over which gas tracer concentrations will equilibrate with the atmosphere.

4.3　　　Site Description

This study was carried out in an area of iron ore mining in the Pilbara region of Western Australia (Figure 4.2). The average annual rainfall is around 300 mm yr^{-1} (313 mm yr^{-1} at Newman, 1971 to 2011, www.bom.gov.au) most of which falls during sporadic high rainfall events that coincide with the passage of cyclones across the coast during summer. Potential evaporation exceeds rainfall, with an average annual potential evaporation of around 3000 mm yr^{-1} (www.bom.gov.au)
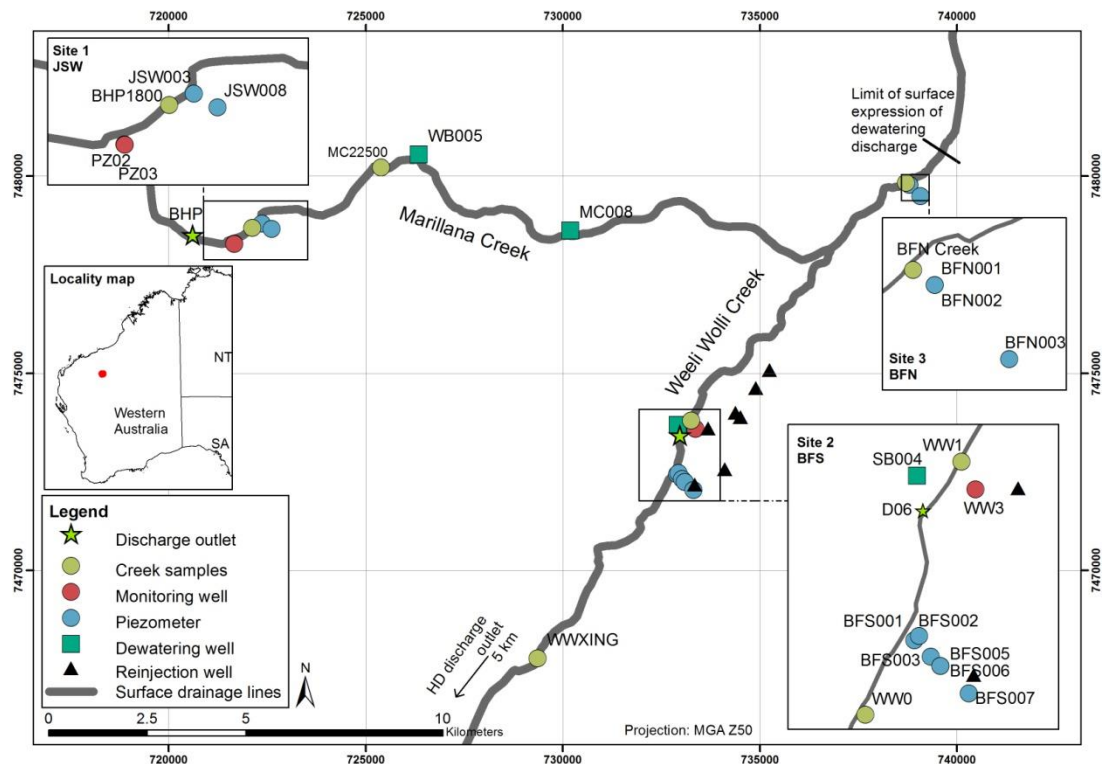
Figure 4.2 Map of study site.

The two major natural drainage features are Marillana and Weeli Wolli creeks, which flow east and north-east respectively across the Hamersley Basin, draining into the Fortescue Marsh. Stream flows associated with natural flood events are flashy, lasting up to 2-3 days, causing stream stage rises of up to 3 m. Surface water flow associated with the discharge of mine water extends up to 30 km from the mine water discharge outlets, and produces stream flows of up to 0.8 m^3 s^{-1} closest to the mine water discharge outlets. The regional groundwater flow direction is generally from the south-west to the north-east across the study site, sub-parallel to the direction of creek flow. Under natural conditions, rainfall recharge is dominated by recharge through the creeks during these heavy rainfall events with diffuse rainfall recharge considered to be negligible (Dogramaci et al., 2012). The target formation for iron ore mining

at the study site is a paleochannel deposit known as the channel iron deposit (CID). Abstracted water that is surplus to mine requirements is predominantly disposed of by allowing it to infiltrate along the creeks, with some re-injected into the CID aquifer using a series of re-injection wells in the south-east of the study site. There are three discharge outlets within the study site; the discharge outlet on Marillana Creek (BHP), and the Hope Downs (HD) and D06 discharge outlets on Weeli Wolli creek.

Geologically, the modern drainage lines consist of an alluvial channel between 50 and 200 m wide and approximately 5 m thick, of poorly sorted unconsolidated alluvium consisting of a fine fraction (silt and sand) interspersed within gravel, cobbles and boulders, which is incised into the underlying lithologies. In places, this alluvial channel is underlain by the CID, which consists of hematitic pisolites in a goethite cement and forms a fractured aquifer. Where not underlain by the CID, the creeks are underlain by a weathered alluvium that consists of moderately sorted silt, sand, clay and minor gravel size fractions. Outside of the creek-lines, this weathered alluvium overlies the CID, except where the CID outcrops at the surface. These three formations are hydraulically connected and are collectively underlain by the Weeli Wolli formation, which consists of banded iron formation (BIF) and dolomite.

Transects of nested piezometers were installed perpendicular to the creek at three locations (Table 4-1, Appendix 2). These locations were chosen to reflect differing hydraulic regimes and lithologies. Site 1 (JSW) is adjacent to Marillana Creek, which has been receiving around 5 GL yr^{-1} of mine water since 1996. The CID aquifer outcrops close to this location and mostly dominates the geology along this transect. A thin alluvium approximately 2 m thick overlies the CID, with a weathered channel horizon between these two units. Site 2 (BFS) is adjacent to Weeli Wolli Creek, which has been receiving around 30 GL yr^{-1} of mine water since 2007. This site is at the southern end (down hydraulic gradient) of the re-injection well-field, with the piezometer furthest from the creek at this site within 200 m of the southern-most re-injection well. The weathered alluvium at this site is 15 to 20 m thick, increasing in thickness away from the creek. This alluvium is underlain by the CID aquifer. Site 3 (BFN) is adjacent to Weeli Wolli creek, downstream of the confluence with Marillana Creek. This location is furthest from the active mining area, 1200 m upstream from the furthest extent of the surface expression of mine water in the creek. The weathered alluvium here is 25 to 30 m thick and is variably underlain by the CID or Weeli Wolli formation.

Table 4-1 Details of sampled wells

	Transect ID	Well ID	Screened interval (m bgl)	Depth to water (m bgl)	Distance from creek (m)
Alluvial aquifer	Site 1	PZ03	0 – 8	2.1	30
		JSW003	5 – 6	2.5	30
	Site 2	WW3	0 – 8	4.8	30
		BFS002	21 – 22	8.3	100
		BFS003	15 – 16	10.7	250
		BFS006	17 – 18	12.2	325
	Site 3	BFN001	19 – 20	3.5	100
		BFN002	5 – 6	3.6	100
		BFN003	19 – 20	12.3	500
CID aquifer	Site 1	PZ02	24 - 72	4.0	30
		JSW008	24 – 25	9.0	300
	Site 3	BFS001	26 – 27	7.6	100
		BFS005	30 – 31	19.5	325
		BFS007	17 – 18	21.7	550

4.4   Methods

4.4.1   Stable isotopes and major ions

Hydrochemical surveys were conducted in August 2011 along the creeks. Water samples were collected for chloride and stable isotope analysis at 18 locations along Marillana creek between 0.2 and 0.65 km apart on the 24th and 25th of August 2011. Samples were collected at 18 locations between 0.27 and 1.35 km apart along Weeli Wolli creek between the 22nd and 26th of August, 2011. Additional chloride data from samples along Weeli Wolli creek collected on 2 August 2011 are also presented (Dogramaci et al., *In prep.*). Water samples for stable isotope and major ion analysis also were collected during July, September and October 2012 from dewatering wells and piezometers (after purging at least 3 casing volumes) and from the creeks at locations adjacent to the piezometer transects. A rainfall sample collected during a cyclonic rainfall event on 13th January 2012 was also analyzed for stable isotopes and major ions. Stable isotopic composition (δ^2H and $\delta^{18}O$) was determined using an Isotopic Liquid Water and Continuous Water Vapor Analyzer Picarro L1102-I (West Australian Biogeochemistry Centre). Chloride was measured using a discrete analyser, with other major ions measured by ICP-OES (SGS laboratories, Perth).

4.4.2   CFC-12 and ^{14}C

Samples for CFC analysis were collected from wells using a stainless steel gas bailer (280 mL internal volume, 0.8 m in length) and nitrogen gas to uplift the sample to surface, with

triplicate glass sample bottles filled and capped while submerged. Piezometers were purged prior to sampling, with at least three casing volumes of water removed until in-situ temperature and electrical conductivity stabilized. CFC samples from dewatering wells were collected inline, with a pressure reducer and clear nylon tubing, ensuring that there were no visible bubbles along the line during sample collection. CFC samples were analyzed by gas chromatography (Waite Isotope Laboratory, Adelaide). For CFC-12 the measurement error depends on concentration and is ±2% at 500 pg kg^{-1}, ±10% at 100 pg kg^{-1}, and ±30 % at 30 pg kg^{-1}.

Piezometers were sampled for ^{14}C using either a Waterra power pack with nylon tubing (25 mm diameter piezometers) or submersible Tsunami pump (50 mm diameter piezometers). Carbon isotopic composition was determined using accelerating mass spectrometry (AMS) at the Rafter radiocarbon laboratory (GNS Science, New Zealand). Dissolved inorganic carbon was converted to CO_2 through the addition of phosphoric acid. This CO_2 was then converted to graphite by reduction with hydrogen over an iron catalyst, and the isotopic composition of this graphite determined by AMS. For the range of values measured in this study, the measurement error is approximately 0.2 pMC.

4.4.3   Noble gases

Samples were collected from three dewatering wells using nylon tubing connected directly to the dewatering well head via an in-line pressure reducer to fill copper tubes (internal volume 45 cm^3), which were immediately sealed with stainless steel clamps at both ends. Care was taken to ensure there were no visible bubbles along the nylon tubing during sample collection. Noble gas fractions (Xe, Kr, Ar, Ne and He) were determined by mass spectrometry (EAWAG isotope laboratory) (Kipfer et al., 1994).

Excess air amounts in each sample were calculated using the Noble90 Matlab script, as described by Aeschbach-Hertig et al. (1999). Recharge pressure was fixed at a value that reflected the elevation of the creek closest to the sample location (525 m AHD, 0.94 atm), and salinity was fixed at zero (fresh water). Terrigenic helium is calculated according to Equation 4.4, based on the recharge temperature and excess air amount. Recharge temperature, excess air and terrigenic ^{4}He amounts were estimated based on all four noble gasses (Xe, Kr, Ar and Ne (2 degrees of freedom) and also based only on measured Ar and Ne (zero degrees of freedom). Estimates of excess air and terrigenic helium were similar using both approaches

(see Appendix 2). For simplicity, the values based only on Ar and Ne are used in subsequent sections of this Chapter.

4.4.4 Ternary mixing ratios based on CFC-12 and ^{14}C

Ternary (three end-member) mixing ratios can be calculated from measurements of two tracers in a given sample. In this study CFC-12 and ^{14}C data are used as the basis for these calculations. The three end-members were defined to reflect the sensitivities of CFC-12 and ^{14}C and the history of mine operations at the study site: 1) mine water, 2) pre-mining recharge, and 3) regional groundwater.

The fraction of each end-member present in each sample is calculated by solving the following series of equations;

$$f_1 + f_2 + f_3 = 1 \tag{4.9}$$

$$CFC_s = f_1 CFC_1 + f_2 CFC_2 + f_3 CFC_3 \tag{4.10}$$

$$^{14}C_s = f_1 {}^{14}C_1 + f_2 {}^{14}C_2 + f_3 {}^{14}C_3 \tag{4.11}$$

where f_1, f_2 and f_3 are the fractions of each end-member in the sample, CFC_s is the CFC-12 concentration of the sample, CFC_1, CFC_2, CFC_3 are CFC-12 concentrations of the each end-member, $^{14}C_s$ is the ^{14}C activity of the sample, and $^{14}C_1$, $^{14}C_2$, $^{14}C_3$ are the ^{14}C activities of each end-member.

The fraction of each-member present in a given sample can be calculated using the solver function in EXCEL to solve Equations 4.9 to 4.11. For each end-member, there is a range of possible values for each tracer concentration, based on atmospheric concentrations and recharge conditions (eg. water temperature, dolomite dissolution). This uncertainty in the end-member definitions can be accounted for using a Monte Carlo approach (Bazemore et al., 1994, Joerin et al., 2002). Uncertainty in the end-member definitions was described by the probability distributions developed in Section 4.5.3. Mean and 70% confidence intervals for the mixing fractions of each sample were calculated on 1000 iterations. Iterations for which mixing fractions between 0 and 1 were not able to be determined were not included in the calculated mean and 70% confidence bounds.

Calculation of the ^{14}C mass balance requires consideration of the dissolved inorganic carbon (DIC) concentration in addition to the ^{14}C activity of each water source (as demonstrated in Chapter 3). In this chapter, we assume that differences in the DIC concentrations of the end-

members are negligible, and do not explicitly include DIC in the calculation of ternary mixing fractions. This assumption is supported by the small range of measured DIC concentrations in water samples collected from piezometers and the creeks. The measured bicarbonate concentration across all piezometers and creek samples ranged from 287 to 492 mg L^{-1}, with a mean of 359 mg L^{-1} and a standard deviation of 48 mg L^{-1}. If there was a variation in DIC between end-members, it would most likely be that the pre-mining end-member could have lower DIC concentrations than the mine water and regional groundwater end-members. However, the data suggest that this is not the case, with samples with the highest calculated fraction of pre-mining water (BFN transect) having bicarbonate values from 353 to 492 mg L^{-1}, in the upper range of the measured data.

4.4.5 Stream mass balance

A one-dimensional mass balance model of stream chemistry was built in EXCEL that explicitly solves the mass balance equations outlined in Section 4.2.4 using finite difference approximation with a spatial discretization of 10 m. This model was used to estimate the seepage flux from the creeks, and simulate CFC-12 concentrations along the creeks.

Predictions of the extent of recharge by mine water were made from estimates of seepage flux based on the chloride mass balance along the creeks. The total transmission loss, $\frac{\partial Q}{\partial x}$, is defined by the volume of discharge at the outlet and the extent of surface flow along the creek downstream of the discharge outlet. This transmission loss was apportioned into evapo-transpiration and seepage fluxes using visual best fit to the measured increase in chloride along each creek. The extent of recharge by mine water through the creeks was then calculated for each transect of piezometers using Equation 4.7. Aquifer thickness was 65 m at all Sites 1 and 2, and 75 m at Site 3, based on lithology logs recorded during the drilling of exploration holes. Porosity was assumed to vary between 0.1 and 0.3, which is considered to represent the likely range of porosity of the fractured CID and weathered alluvial aquifers (Freeze and Cherry, 1977).

Simulated CFC-12 concentrations along the creeks were used to test the validity of the assumption that CFC-12 concentrations in the creeks were in equilibrium with the atmosphere at the time of sampling. The gas transfer velocity of SF$_6$ was previously measured in Marillana creek using an SF$_6$ injection (k_{SF6} = 1.8 m d^{-1}), as described in Chapter 2. The gas transfer velocities of different gasses are related through their molecular diffusion coefficients (Bennett

and Rathbun, 1972, Genereux and Hemond, 1992). Given the measured gas transfer velocity of SF_6 and the diffusion coefficients of SF_6 and CFC-12, the gas transfer velocity of CFC-12 is calculated to be 1.6 m d^{-1}. Stream width is constant along model domain, with a width of 12 m in Marillana creek and 30 m in Weeli Wolli creek. The initial CFC-12 concentration was set to zero. The atmospheric concentration, C_A, was set to 150 pg kg^{-1}, which reflects the concentration of water in equilibrium with an atmospheric concentration of 530 pptv at 28 °C (Warner and Weiss, 1985).

4.5   Results

4.5.1   Stable isotopes and chloride

In August 2011, δ^{18}O in Marillana creek ranged from -8.1 to -7.2‰ and δ^2H ranged from -50.8 to -50.3‰ (Figure 4.3a). In Weeli Wolli creek, δ^{18}O ranged from -8.4 to -7.3‰ and δ^2H ranged from -59.7 to -53.6‰. Stable isotope signatures and chloride concentrations measured in Weeli Wolli creek in 2012 were consistent with these results, with δ^{18}O ranging from -8.2 to -7.6‰, δ^2H ranging from -55.8 to -55.1‰. Samples from piezometers and dewatering wells collected during 2012 had stable isotopic signatures that overlap with the range of stable isotopic composition measured in the creeks. Within piezometers and dewatering wells, δ^2H ranged from -51 to -59 ‰ and δ^{18}O ranged from -7.5 to -8.3 ‰.

The local meteoric water line (δ^2H = 7.03 δ^{18}O + 7.48) and local evaporation line (δ^2H = 5.16 δ^{18}O – 14.37) were determined by Dogramaci et al. (2012). The cyclonic rainfall sample had a δ^2H of -67 ‰ and δ^{18}O of –10.4 ‰, which is consistent with this previously determined local meteoric water line for rainfall events greater than 20 mm. The stable isotopic signatures of piezometers and dewatering wells plot close to the local evaporation line and are consistent with evaporation of less than 20%.
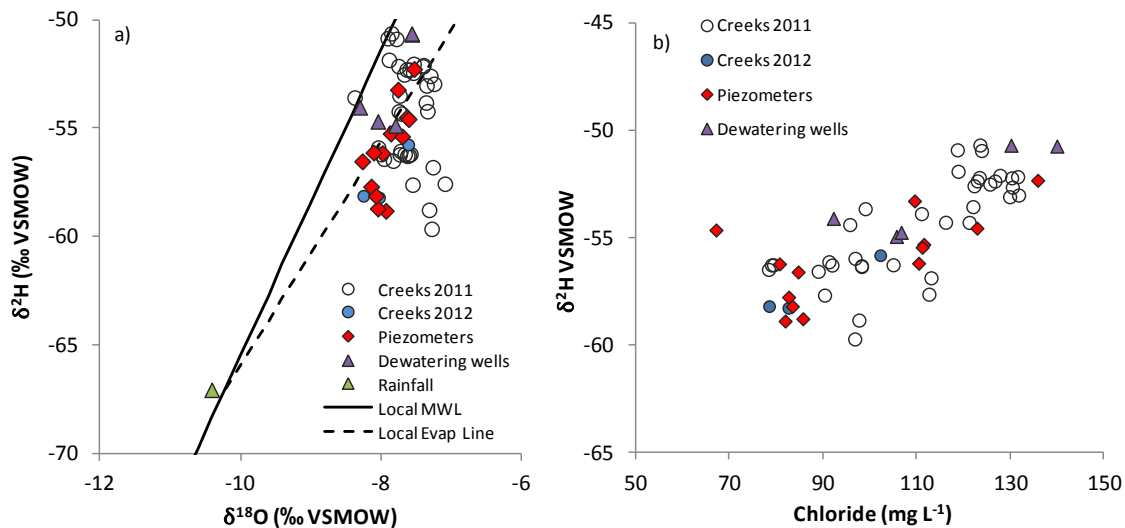
Figure 4.3 Stable isotope and chloride data.

Chloride concentrations in August 2011 ranged from 119 to 132 mg L^{-1} in Marillana creek, and 74 to 120 mg L^{-1} in Weeli Wolli creek (Figure 4. 3b and Figure 4.4). Chloride concentrations in Weeli Wolli creek in 2012 were consistent with the 2011 results, ranging from 78 to 102 mg L^{-1}. Chloride concentrations in piezometers ranged from 67 to 136 mg L^{-1}, and in dewatering wells ranged from 92 to 140 mg L^{-1}, overlapping significantly with the range of chloride concentrations in the creeks. Chloride concentrations were correlated with δ^2H (R^2 = 0.62) suggesting that they largely reflect evapo-concentration along the creek, but may also be affected by residual chloride that precipitates during ebbing flood events, originates from diffuse recharge, or enters the creeks from the broader landscape during runoff events.

In order to apply chloride or stable isotopes as tracers in this setting it would be necessary to define end-members that can distinguish between a) natural rainfall recharge that occurred prior to the commencement of mining, and b) recharge by excess water abstracted during mine dewatering operations. Given the significant overlap of chloride concentrations and stable isotopic signatures in piezometers and the creeks, definition of these end-members is not possible, and so they cannot be used as a basis for mixing ratio calculations.
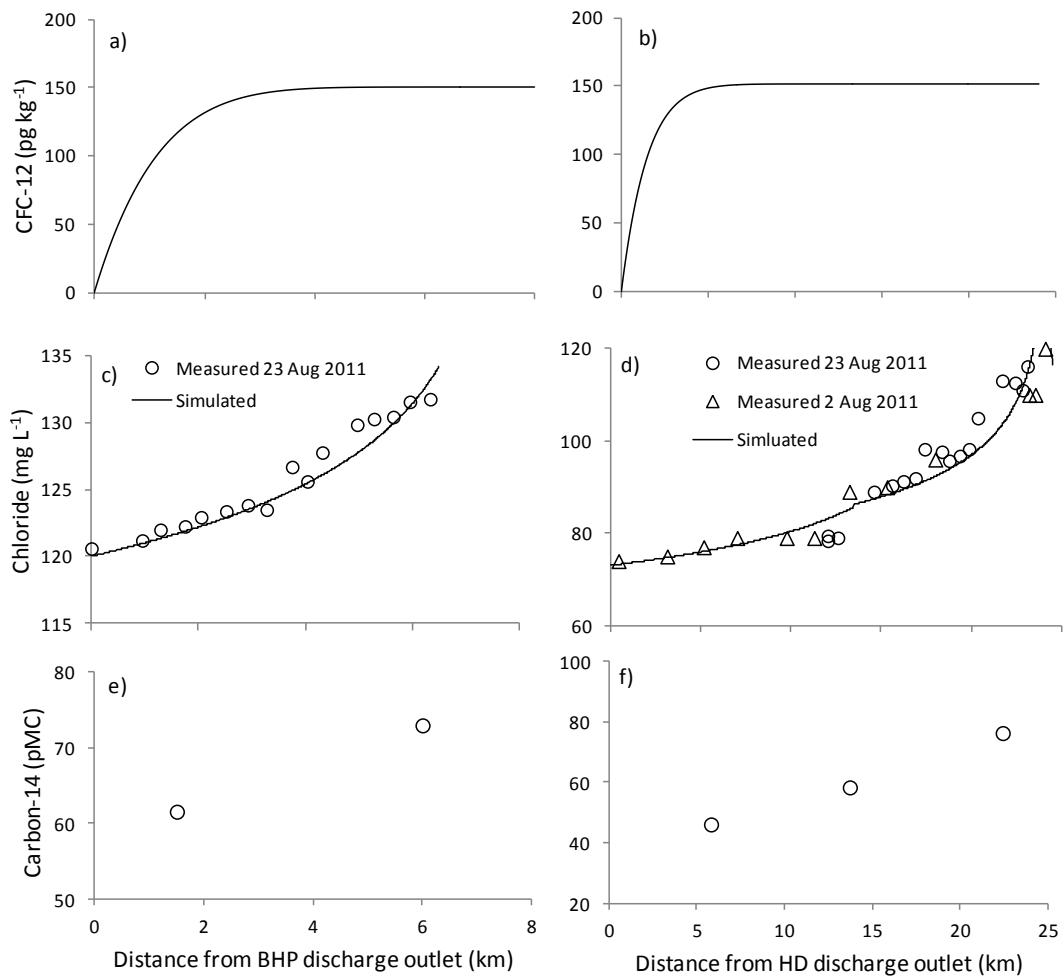
Figure 4.4 Simulated CFC-12 along a) Marillana creek and b) Weeli Wolli creek. Measured and simulated chloride along c) Marillana creek and d) Weeli Wolli creek. Measured ^{14}C along e) Marillana creek and f) Weeli Wolli creek.

4.5.2 CFC-12 and ^{14}C data

The CFC-11 data suggested atmospheric concentrations that were consistently lower than the atmospheric concentrations suggested by CFC-12 data. This implied that degradation was affecting the CFC-11 data and so they were excluded from further analysis. Only the CFC-12 data, which is less susceptible to degradation (Oster et al., 1996), is used to calculate mixing fractions. CFC-12 concentrations ranged from 105 to 566 pg kg^{-1} (Table 4-2). Measured ^{14}C activities ranged from 36 to 93 pMC, with δ^{13}C values ranging from -13.1 to -10.0 ‰. ^{14}C activities significantly lower than the ^{14}C activity of the mine water within the creeks (46 to 75 pMC), are likely to reflect the influence of regional groundwater. The only sample with ^{14}C activity lower than the mine water in the creeks was JSW008, for which the CFC-12 concentration was not determined (and therefore mixing ratios not calculated). Samples with

^{14}C activities higher than the ^{14}C activity of the mine water within the creeks are likely to reflect the influence of relatively recent (less than say 200 years ago) recharge during natural flood events. All samples at Site 3 had ^{14}C activities higher than the ^{14}C activities measured in the creeks.

Table 4-2 CFC and carbon isotope data

	Site ID	Sample	Distance from creek	CFC-12	δ^{13}C	^{14}C
			(m)	(pg kg^{-1})	permil	pMC
Creeks	Site 1	BHP1800*	0		-10.8	62
		MC22500*	0		-11.8	73
	Site 2	BFN Creek	0		-10.7	76
	Site 3	WW1	0		-10.0	58
		WWXING	0		-10.2	46
Alluvial aquifer	Site 1	PZ03	30	149	-11.1	61
		JSW003	30	106	-13.1	72
	Site 2	WW3	30		-11.2	68
		BFS002	250	107	-11.0	58
		BFS003	550	178	-10.7	67
		BFS006	325	68	-11.7	75
	Site 3	BFN001	100	108	-11.3	89
		BFN002	100	131	-12.2	93
		BFN003	500	126	-11.9	88
CID aquifer	Site 1	PZ02	100	93	-11.6	73
		JSW008	300		-11.4	36
	Site 2	BFS001	100	114	-11.6	69
		BFS005	325	33	-11.3	71
		BFS007	550	110	-11.1	81
Dewatering wells		SB004	150	125	-12.0	72
		PC005	50	146	-12.1	72
		MC008	0	79	-12.0	74

*Sample collected during August 2011, all other samples collected during July, September, or October of 2012.

4.5.3 Ternary mixing ratios: end-member definitions

4.5.3.1 Mine water

The mine water end-member represents groundwater that recharged through the creek since discharge to the creeks began in 1996. CFC-12 concentrations are assumed to be in equilibrium with the atmosphere at the time of recharge. Simulations show that the CFC-12 concentration of the creeks should be in equilibrium with the atmosphere within 3 km of the discharge outlet on Marillana creek, and within 5 km of the discharge outlet on Weeli Wolli creek (see Figure 4.4). This is supported by the CFC-12 concentration in PZ03, which samples the water table within the creek alluvium approximately 1.5 km downstream of a mine water discharge outlet,

and was in equilibrium with the atmosphere at the temperature of the well (149 pg kg^{-1}, with an equivalent atmospheric concentration of 530 pptv at 28 °C).

The relationship between atmospheric and dissolved CFC-12 concentrations in water recharging through the creek is largely a function of water temperature. Water temperature was measured in Marillana creek between 9 June 2010 and 8 October 2012 using a pressure transducer installed adjacent to PZ03 at Site 1. The water temperature time-series had an annual amplitude of around 12 °C, and a diurnal temperature variation with an amplitude of around 5 °C (Figure 4.5). A synthetic temperature time series was used to represent the measured temperature variations, generated from a composite of two sinusoidal functions; a diurnal cycle which represents the daily variation in temperature, and an annual cycle that represents the seasonal variation in mean daily temperature. Atmospheric concentrations of CFC-12 between 1996 and 2012 varied between 527 and 542 pptv. Given these distributions of recharge temperature and atmospheric concentrations, the range of values for CFC-12 in this end-member ranged from 123 to 221 pg kg^{-1} (Figure 4.6 and Figure 4.7).
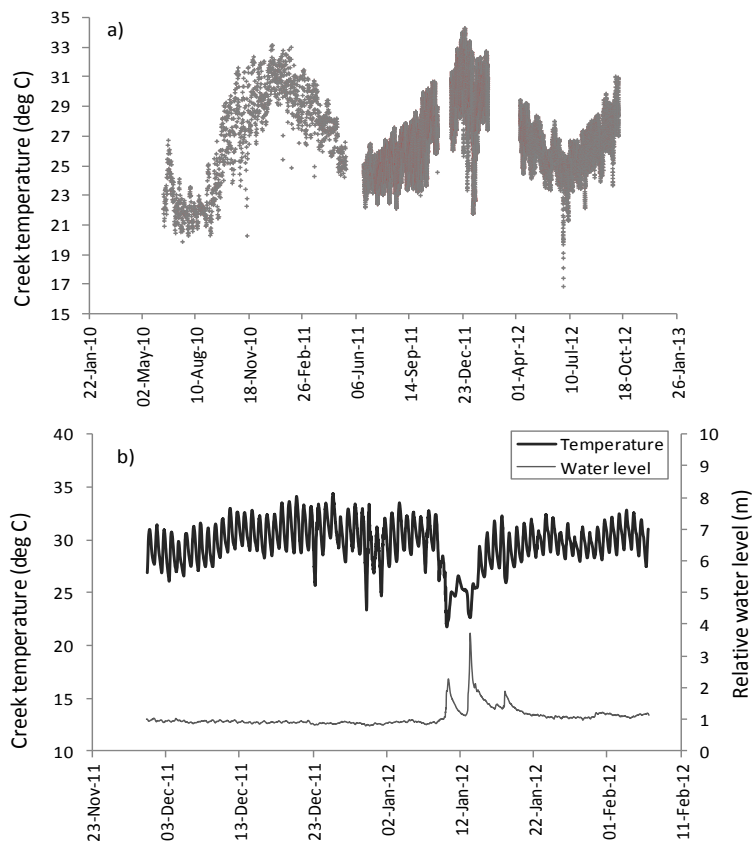
Figure 4.5a) Marillana Creek water temperatures at Site 1, and b) Marillana Creek water temperature and relative water level at Site 1 during a cyclone.

Carbon-14 activities in the creek during mining operations are a function of the initial activity of the mine water discharge, and gradual equilibration with the atmosphere as it flows downstream. Measured ^{14}C activities in the creeks, adjacent to the piezometer transects, ranged from 46 to 76 pMC, increasing with distance from the discharge outlets (see Figure 4.4). The lowest activity was measured 8 km up-gradient of the southern-most piezometer transect (Site 2). This measurement is therefore likely to underestimate the ^{14}C activity in mine water at the time of recharge in water intercepted by piezometers at Site 2 (because the ^{14}C activity will increase with increasing distance downstream as it equilibrates with the atmosphere). Linear interpolation suggests that by the time this water reaches Site 2 (12 km from the HD discharge location) the ^{14}C activity will have increased to 56 pMC. These waters were recently groundwater, which is reflected in their ion chemistry. Saturation indices for calcite and dolomite (the dominant form of carbonate in the catchment) were greater than zero in the mine water in the creeks, indicating supersaturation. These waters are therefore not likely to be further influenced by carbonate dissolution and so the range of measured ^{14}C activities of the mine water in the creeks was used without correction to define the end-member values. The range of ^{14}C in the mine water end-member is therefore allowed to vary randomly between 56 and 76 pMC (Figure 4.6 and Figure 4.7).

4.5.3.2   *Pre-mining recharge*

The pre-mining recharge end-member represents waters that recharged prior to the commencement of mining, but after 1960, so that they have measurable CFC-12 concentrations. The distribution of CFC-12 concentrations in recharge water for this end-member was based on the probability distribution of atmospheric CFC-12 concentrations between 1960 and 1996, and water temperatures randomly selected from within the range of temperatures measured in the creek during cyclonic flood events. Atmospheric CFC-12 concentrations between 1960 and 1996 increased from 30 to 526 pptv. Under natural conditions, recharge would have occurred in summer, during heavy rainfall events associated with the passage of cyclones. Water temperatures during these heavy flood events have been measured at this site and in other creeks not receiving mine water, with water temperatures varying between 20 and 30 °C, without a uniform diurnal variation in temperature. Given the distribution of atmospheric CFC-12 and recharge temperatures randomly selected between 20 and 30 °C, the CFC-12 concentrations in pre-mining recharge vary between 8 and 198 pg kg^{-1} (Figure 4.6 and Figure 4.7).

Carbon-14 activities in the pre-mining end-member would have initially been set by equilibrium with the atmosphere, but may have since been altered by dissolution of dolomite present in the creek catchment. Radioactive decay since 1960 will be less than 1 pMC and can be neglected. In the southern hemisphere, ^{14}C activities between 1960 and present have ranged from 110 to 170 pMC (NIWAR, Lower Hutt, New Zealand). Corrected ^{14}C activities are calculated using Equation 4.2. The sample δ^{13}C is constrained by the measured values in piezometers and dewatering wells, which ranged from -10 to -13 ‰. The δ^{13}C of DIC at the time of recharge is assumed to be between -14 and -15 ‰. This corresponds to dissolution of CO_2 produced by C_3 plants (which dominate the study site), in the pH range of 7.5 to 8.5 at a temperature of 25 °C (based on measured values in the creeks) (Clark and Fritz, 1997). This DIC assumed to have been altered by dissolution of marine dolomite with δ^{13}C values between -2 and +2 ‰ (Becker and Clayton, 1972). The resulting distribution of ^{14}C activities for the pre-mining end-member ranges from 72 to 150 pMC.

4.5.3.3   Regional groundwater

The regional groundwater end-member represents waters that recharged prior to 1960 and would therefore have CFC-12 concentrations below the background value of the measurement method (10 pg kg^{-1}). The CFC-12 concentration in this end-member is therefore assumed to be zero (Figure 4.6 and Figure 4.7).

The range of ^{14}C activities of this end-member is based on measured data at this and other sites in the Pilbara region (n = 14), where ^{14}C activity has been measured in groundwater wells situated away from creek lines, which are unlikely to be influenced by recharge after 1960. The ^{14}C activities in these wells ranged from 30 to 45 pMC. The lower bound of the distribution of ^{14}C in this end-member is defined by the lower limit of values measured in these wells. The upper bound of ^{14}C in regional groundwater is set equal to the lower bound of ^{14}C activities in pre-mining recharge. The distribution of ^{14}C activity in the regional groundwater end-member is therefore randomly selected from values between 30 and 72 pMC.
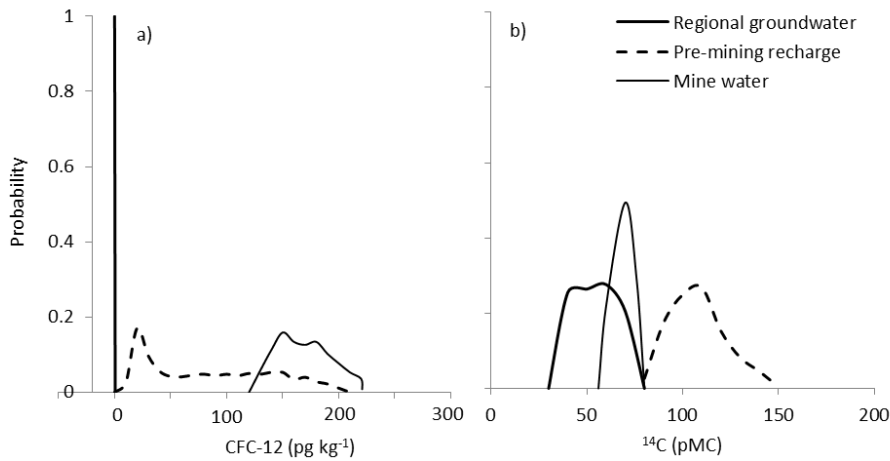
Figure 4.6 Probability distributions of end-member concentrations of a) CFC-12 and b) ^{14}C.
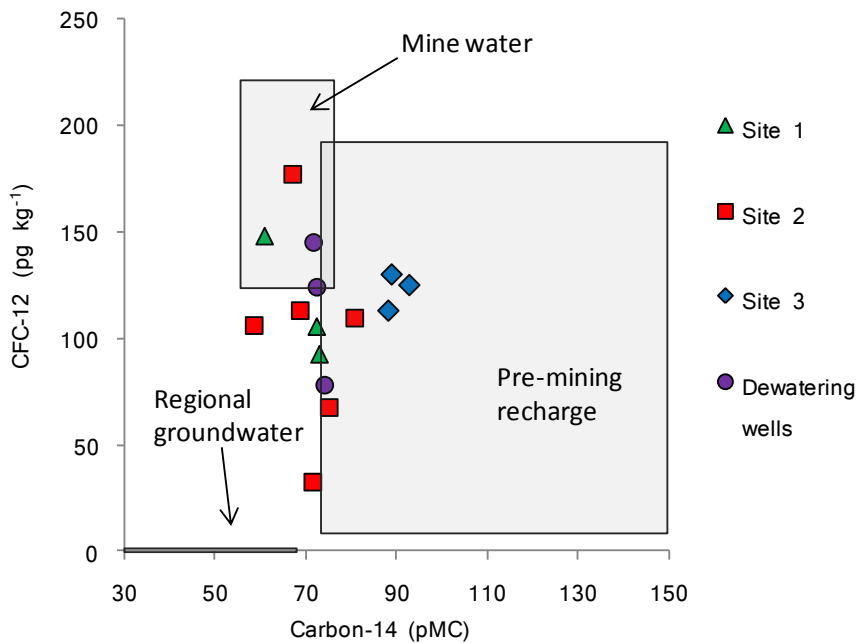
Figure 4.7 CFC-12 and ^{14}C data and the ranges of each end-member.

4.5.4 Calculated mixing fractions based on CFC-12 and ^{14}C

The mean calculated mixing fractions suggest that piezometers contained at most 55% regional groundwater, up to 69% pre-mining recharge and up to 80% mine water (Table 4-3, Figure 4.8). Mean mixing fractions in dewatering wells suggest they contained up to 32% regional groundwater, up to 40% pre-mining recharge and up to 67% mine water. Uncertainty in the calculated mixing fractions were between ± 15% and ± 127% of the mean. When this uncertainty is taken into consideration, piezometers contained from 0 to 76 % regional

groundwater, from 0 to 84 % pre-mining recharge and from 0 to 95 % mine water. Given the uncertainty in dewatering well mixing fractions, they contained from 0 to 48% regional groundwater, from 1 to 51% pre-mining recharge, and 10 to 87% mine water.

Table 4-3 Calculated mixing fractions: mean and range (70 % confidence interval) based on CFC-12 and ^{14}C data

	Site ID	Sample	Distance from creek	Regional groundwater		Pre-mining recharge		Mine water	
			(m)	Mean	Range	Mean	Range	Mean	Range
Alluvial aquifer	Site 1	PZ03	30	0.12	0.02 - 0.22	0.06	0 - 0.11	0.82	0.71 - 0.95
		JSW003	30	0.22	0.1 - 0.34	0.28	0.13 - 0.43	0.50	0.32 - 0.67
	Site 2	BFS002	250	0.32	0.22 - 0.41	0.06	0 - 0.13	0.62	0.51 - 0.74
		BFS003	550	0.05	0 - 0.12	0.11	0.01 - 0.2	0.84	0.77 - 0.94
		BFS006	325	0.38	0.2 - 0.55	0.39	0.25 - 0.52	0.24	0.02 - 0.39
	Site 3	BFN001	100	0.12	0.01 - 0.22	0.60	0.38 - 0.8	0.28	0 - 0.53
		BFN002	100	0.14	0.02 - 0.25	0.65	0.45 - 0.84	0.21	0 - 0.47
		BFN003	500	0.16	0.02 - 0.29	0.57	0.39 - 0.75	0.28	0 - 0.51
CID aquifer	Site 1	PZ02	100	0.31	0.06 - 0.53	0.31	0.14 - 0.48	0.38	0 - 0.68
	Site 2	BFS001	100	0.21	0.11 - 0.32	0.19	0.06 - 0.31	0.60	0.45 - 0.75
		BFS005	325	0.58	0.39 - 0.76	0.32	0.16 - 0.48	0.10	0 - 0.18
		BFS007	550	0.17	0.03 - 0.31	0.44	0.28 - 0.62	0.38	0.12 - 0.6
Dewatering wells		SB004	210	0.15	0.04 - 0.25	0.24	0.09 - 0.37	0.62	0.46 - 0.78
		PC005	130	0.09	0.01 - 0.18	0.19	0.05 - 0.31	0.72	0.58 - 0.87
		MC008	150	0.33	0.19 - 0.48	0.36	0.22 - 0.51	0.30	0.1 - 0.47
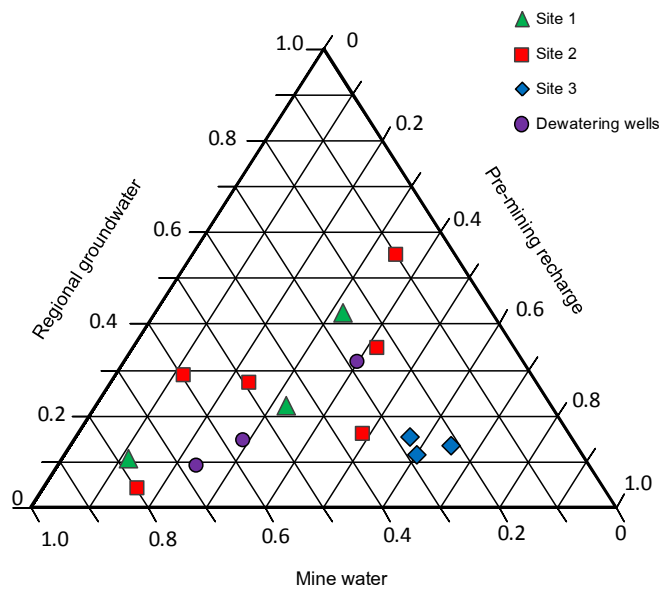
Figure 4.8 Ternary plot of mean mixing fractions for samples from piezometers along each transect, and from dewatering wells

All samples contained mine water, with the largest amounts within 250 m of the creek (Figure 4.9). In addition to this general trend, there were differences between transects. At Site 3 piezometer samples were dominated by pre-mining recharge (38 – 84%). At Site 1, the alluvial aquifer was dominated by mine water (32 – 95%), while in the CID aquifer the waters contained larger proportions of regional groundwater (6 – 53%) and pre-mining recharge (14 – 48%). Site 2, with the largest number of samples, had the most variation in calculated mixing fractions. The sample from the alluvium at a distance of 250 m (BFS003), had the highest calculated amount of mine water (77 – 94%), while the sample from the CID aquifer at 325 m (BFS005) had the largest calculated amount of regional groundwater (39 – 76%). These two aquifer units are hydraulically connected, and the variation along the transect, irrespective of aquifer, could, in part, reflect the influence of the re-injection well located 200 m from the piezometer BFS007 (550 m from the creek). While this re-injection well is down-gradient from the piezometer, a groundwater mound may have been created, resulting in flow from the re-injection well towards the piezometers. The water being re-injected is likely to be a mixture of regional groundwater, mine water and pre-mining recharge. The net effect on the tracer concentrations in the adjacent aquifer is therefore not easily predicted or quantified.
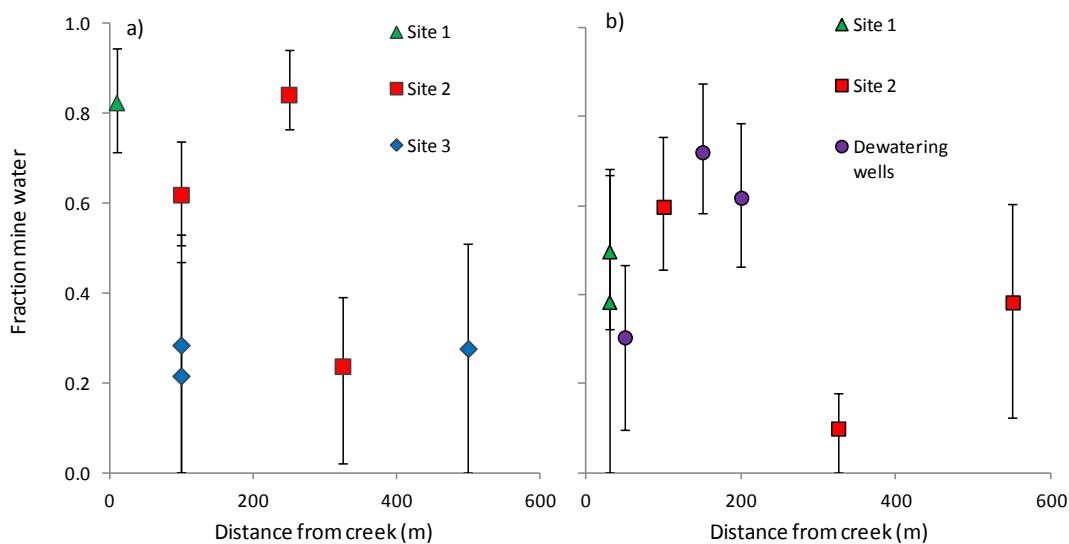
Figure 4.9 Fraction of mine water (mean and 70% confidence interval) versus distance from creek in a) the alluvial aquifer, and b) the CID aquifer.

4.5.5 Noble gases, excess air and terrigenic [4]He

Noble gas fractions of Ar ranged from 3.0 x 10^{-4} to 3.2 x 10^{-4} ccSTP gw^{-1}, Ne ranged from 2.1 x 10^{-7} to 2.2 x 10^{-7} ccSTP gw^{-1}, and He ranged from 9.1 x 10^{-8} to 4.1 x 10^{-7} ccSTP gw^{-1} (Table 4-4, Figure 4.10). Excess air amounts, expressed as ΔNe, ranged from 20 to 31 %. Terrigenic ^{4}He (^{4}He$_{Terr}$) ranged from 35 to 406 μccSTP kgw^{-1}. Excess air was negatively correlated with the mean calculated fraction of mine water (R^2 = 0.63), and terrigenic ^{4}He was positively correlated with the mean calculated fraction of regional groundwater (R^2 = 0.94).

Table 4-4 Noble gas data from dewatering wells

Sample	Distance from creek	Ar	Ne	He	ΔNe	^{4}He$_{Terr}$
	(m)	ccSTP gw^{-1}	ccSTP gw^{-1}	ccSTP gw^{-1}	‰	μccSTP kgw^{-1}
SB004	210	3.0 x 10^{-4}	2.2 x 10^{-7}	9.1 x 10^{-8}	29.6	35
PC005	130	3.2 x 10^{-4}	2.1 x 10^{-7}	9.1 x 10^{-8}	20.0	39
MC008	150	3.0 x 10^{-4}	2.2 x 10^{-7}	4.6 x 10^{-7}	30.5	406
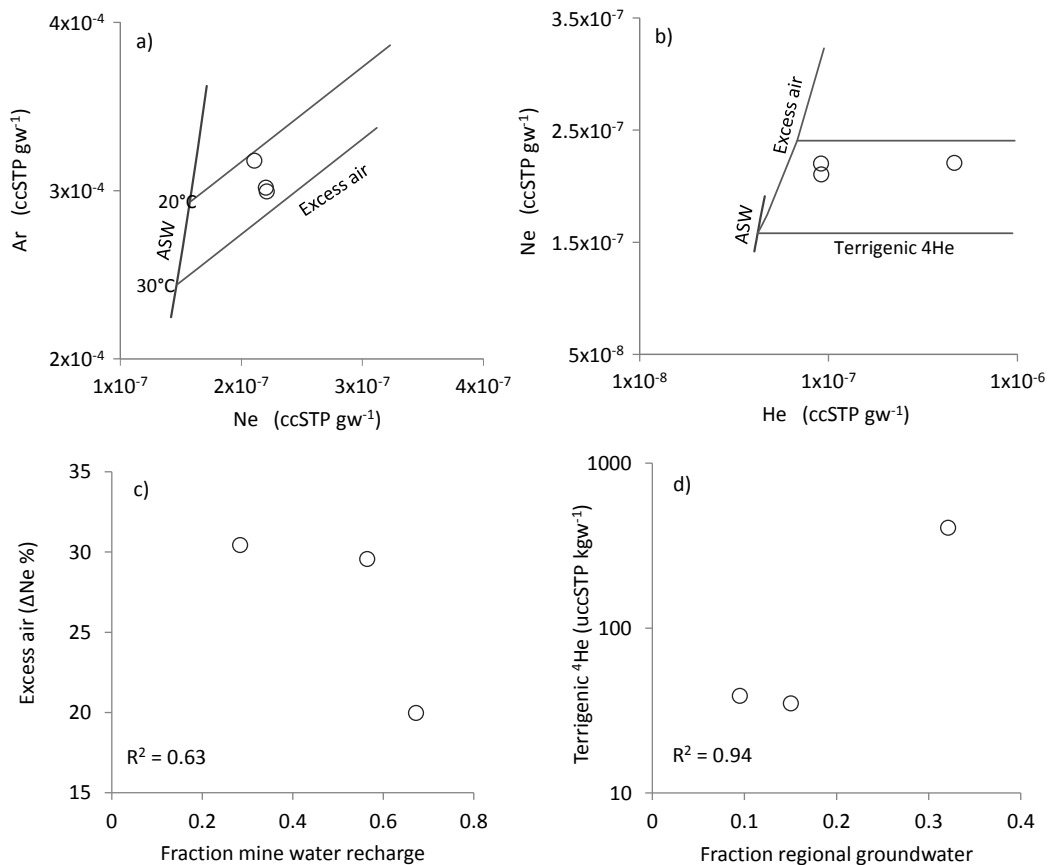
Figure 4.10 a) Ne vs. Ar, showing the influence of recharge temperature and excess air, and b) Ne vs. He, showing excess air and terrigenic ^{4}He, c) Excess air (ΔNe) vs. mean calculated fraction mine water, and d) terrigenic ^{4}He vs. mean calculated fraction regional groundwater.

4.5.6 Extent of recharge by mine water based on stream mass balance

Along Marillana creek, the average daily discharge of mine water from the BHP discharge outlet during August 2011 was 21600 m^3 d^{-1}. Stream flow extended for 8 km downstream of the discharge location. Along Weeli Wolli creek, the average daily discharge from the HD discharge outlet during August 2011 was 70800 m^3 d^{-1}, with an additional 20700 m^3 d^{-1} from the D06 discharge outlet. These discharge volumes caused stream flow to extend 24 km downstream of the HD discharge outlet.

In Marillana creek the best fit to measured chloride data was achieved with an evaporation flux of 0.2 m^2 d^{-1} and a seepage flux of 2.6 m^2 d^{-1}. In Weeli Wolli creek the best fit to measured chloride data was achieved with an evaporation flux of 0.5 m^2 d^{-1} and a seepage flux of 3.3 m^2 d^{-1}. These results suggest that 90% of the discharge to Marillana creek and 85% of the discharge to Weeli Wolli creek recharges to the aquifer. The predicted extent of recharge by mine water, on either side of the creek, was 240 to 730 m at Site 1, 150 to 460 m at Site 2 and 110 to 320 m at Site 3 (Table 4-5).

Table 4-5 Extent of recharge by mine water based on stream mass balance

Site ID	ET loss (E)	Seepage rate (q_g)	Porosity (θ)	Duration of discharge (τ)	Aquifer thickness (b)	Extent mine water recharge (y)
	(m^2 d^{-1})	(m^2 d^{-1})	(v/v)	(years)	(m)	(m either side of stream)
Site 1	0.2	2.6	0.1 - 0.3	10	65	240 – 730
Site 2	0.5	3.3	0.1 - 0.3	5	65	150 – 460
Site 3	0.5	3.3	0.1 - 0.3	4	75	110 – 320

4.6   Discussion

4.6.1 Extent of recharge by mine water

All samples contained mine water, with the largest calculated fractions of mine water within 250 m of the creeks. The spatial limit of recharge by mine water discharge or re-injection was not captured during this study. The locations for piezometer installation were dictated by the locations of pre-existing exploration holes. Additional samples at greater distances from the creek (>550 m) would be required to elucidate the full spatial extent of recharge associated with the disposal of mine water along creek lines.

Previous studies in natural stream systems were able to infer seepage rates from gradients in tracer concentrations away from the stream (Bertin and Bourg, 1994, Beyerle et al., 1999, Stute et al., 1997). Given the uncertainty in calculated mixing fractions, this was not possible in this study. However, because the chloride mass balance in the creeks is well constrained, an estimate of the seepage rates from each creek can be made using longitudinal surveys of chloride concentrations. The predicted extent of recharge by mine water based on the seepage rate from the creeks was consistent with the results from the ternary mixing fractions. The extent of recharge by mine water was estimated to be between 110 to 730 m either side of the creek, with the shortest calculated distance at Site 3 where the calculated fractions of mine water were smaller.

The variation in the calculated extent of mine water recharge is mostly a function of the duration of discharge. This calculation of the extent of mine water recharge depends on aquifer thickness and porosity, and assumes that the full thickness of the aquifer is penetrated. Aquifer thickness is well constrained using drill logs, but porosity is not well constrained, particularly for the fractured CID aquifer. However, the range of values of porosity is much smaller than the possible range of values for hydraulic conductivity, which would be required to calculate the extent of recharge by mine water using measured hydraulic gradients perpendicular to the creek. Determination of the depth of penetration of mine water recharge would require samples from deeper wells than were sampled in this study. This analysis does not consider spatial variation in the seepage flux, which is likely to vary in response to changing geology and hydraulic gradients between the creek and underlying aquifer. A more detailed analysis would be required to determine spatial trends in seepage flux, and the drivers of this variation.

4.6.2   Interception of mine water recharge by dewatering wells

The amount of water that is being recycled locally during dewatering operations can be inferred from the samples collected from dewatering wells. Of the total volume of mine water discharged to the creeks, chloride mass balance suggests that 85 to 90% recharges to the underlying and adjacent aquifers. Mixing fractions based on CFC-12 and ^{14}C suggest that between 10 and 87% of the total volume of water abstracted from dewatering wells is composed of this mine water that recharged through the creeks after disposal. The noble gas data support these results, with strong correlations between the fraction of mine water and

excess air, and the fraction of regional groundwater and terrigenic helium. These correlations are consistent with the conceptual model of recharge mechanisms outlined in Figure 4.1. Recharge during mining operations, (captured by the mine water end-member in ternary mixing calculations) recharges through a connected stream, resulting in lower excess air amounts. Recharge that occurred hundreds to thousands of years ago (captured by the regional groundwater end-member in ternary mixing calculations) has accumulated terrigenic ^{4}He over time. Controlled experiments to determine the relationships between; 1) flood characteristics and excess air formation and 2) the ^{4}He production rates of each aquifer, would be required for a more quantitative analysis to be carried out on the noble gas data.

The abundance of mine water recharge in ongoing abstraction volumes suggests that the overall depletion of the aquifer storage associated with mine dewatering could be significantly reduced by recharge through the creeks subsequent to discharge of mine water. This may increase the volume of groundwater abstraction required to maintain safe mining conditions and, over time, could lead to aquifer salinization through evapo-concentration as the mine water flows along the creeks.

4.6.3 Groundwater age indicators as tracers of groundwater re-circulation

The major limitation of stable isotopes and chloride as tracers of re-circulated groundwater is the lack of clear end-members. At this study site, this is primarily because the enrichment caused by evaporation while exposed at the surface is small relative to the range of values in groundwater. The equilibration of groundwater age indicators in mine water exposed to the atmosphere provides a mechanism for the development of a distinct concentration range in the mine water end-member. This is particularly true for CFC-12, which equilibrates with the atmosphere within 3 to 5 km of the discharge outlets at this study site (approximate flow duration 1 to 3 days). Furthermore, the atmospheric concentrations of these groundwater age indicators have varied over time and the distributions of atmospheric concentrations are known. As a result, if end-members can be defined that represent discrete time intervals, then the distribution of tracer concentrations at the time of recharge can be re-constructed, and used to define the distributions of each end-member.

This approach will work best when the duration of mining is narrow and aligns with known changes in tracer concentrations. For example, if mining had started in 1960 the range of CFC-

12 in the mine water end member would be larger and overlap with the range of CFC-12 in the pre-mining end member. In this case, a binary mixing calculation could be made to differentiate recharge pre-mining and during mining could be made based on the presence or absence of CFC-12. However, this "during mining" end-member would then include natural rainfall recharge and recharge by mine water. If mine operations had started in 1860, CFC-12 would be of limited use as a tracer of mine water recharge because not all mine water would contain CFCs. In this case, a different tracer would be required to differentiate between mine water from natural rainfall recharge.

The application of groundwater age indicators may also be useful for quantifying recharge associated with agricultural irrigation or artificial wetland supplementation. Groundwater age indicators have previously been used to provide a qualitative analysis of recharge associated with agricultural irrigation (Brown et al., 2011). The quantitative methods outlined in this chapter are most likely to succeed where the exposure to the atmosphere is long enough for equilibration to occur, and where the timescale of anthropogenic activity allows for discrete ranges of atmospheric concentrations to be delineated for each end-member. In agricultural or wetland settings, solutes that are associated with anthropogenic recharge, such as nitrate or other contaminants, may provide a cost-effective alternative to isotopic tracers for differentiation recharge sources, but cannot provide information on the aquifer residence time of that recharge (Brown et al., 2011). In this study, uncertainty in mixing ratios was quantified using a Monte Carlo approach. Other studies have used Taylor Series error estimation to quantify uncertainty in mixing ratios (Genereux, 1998). While Monte Carlo analysis can be computationally demanding, it produces more robust results because it does not require assumptions about the distribution of the data to be made, and is less susceptible to extreme data points (Ripley, 2009).

An alternative approach for interpreting groundwater age data is to use a lumped parameter model , or analytical solution to describe the probability density frequency of groundwater ages in the aquifer, or sample (Woolfenden and Ginn, 2009, Soltani and Cvetkovic, 2013, Varni and Carrera, 1998, Maloszewski and Zuber, 1982). This allows for the prediction of tracer concentrations at locations in space and time, if the velocity field is known (Varni and Carrera, 1998, Maloszewski and Zuber, 1982). In steady state systems, the distribution of groundwater ages may be calculated based on the input function and measured concentrations by convolution (Massoudieh et al., 2012). However, application of this type of technique to

interpret tracer data in transient systems like this study site is non-trivial, and would require repeated sampling of groundwater age indicators through time (Massoudieh, 2013).

4.7   Conclusion

In this system that has been modified by mining, groundwater age indicators were more useful than stable isotopes or chloride for constraining the relative contribution of different recharge sources. By measuring CFC-12 and ^{14}C in piezometers and dewatering wells it was possible to calculate ternary mixing fractions of 1) regional groundwater, 2) pre-mining recharge, and 3) mine water in each sample. The calculated mixing fractions demonstrate that mine water is present in all samples, which extend to a distance of 550 m from the creeks. These results are supported by estimates of the extent of recharge by mine water from the chloride mass balance within the creeks.

At this study site, the ore-body aquifer and overlying alluvial aquifers are hydraulically well connected, and a substantial proportion of water abstracted during dewatering operations is effectively being re-circulated locally. Mixing fractions in dewatering wells suggest that mine water recharge accounts for a variable, but potentially significant, proportion of the current abstraction volume. These results are supported by noble gas data, with correlations between excess air and mine water recharge, and between terrigenic ^{4}He and regional groundwater, as would be expected from the conceptual model of the study site. Because of this re-circulation of mine water, the depletion of aquifer storage by mine dewatering operations is offset by recharge through the creeks.

Groundwater age indicators were effective tracers of recharge sources in this system because a) CFC-12 equilibrates rapidly when exposed to the atmosphere, while ^{14}C equilibrates partially with the atmosphere as it flows along the creeks and b) the historical distributions of atmospheric CFC-12 and ^{14}C concentrations are known. The methods applied in this study may also be useful for quantifying recharge associated with agricultural irrigation or artificial wetland supplementation. This approach will be most successful when the duration of mine water discharge, irrigation or wetland supplementation is short, relative to the timescale of variation in atmospheric concentrations.

Chapter 5 Conclusion

5.1   Research Implications

In this thesis, new techniques using environmental isotopes and groundwater age indicators for quantifying surface water-groundwater interaction across a range of spatio-temporal scales and settings have been presented. The new methods demonstrated in this thesis can be used in conjunction with pre-existing methods to improve field-based estimates of surface water-groundwater interaction. This will allow for the broader spectrum of exchange fluxes to be captured, providing valuable information to water users, water resource managers and regulators. A major advantage of the new tracer methods presented in this thesis is that they are able to estimate exchange fluxes over longer spatial and temporal scales than previously published methods. This is important because hydrologic systems are inherently heterogeneous and up-scaling of point-scale measurements is difficult. Uncertainties in each measurement approach can be significant, and these must be accounted for so that the results of field studies can be appropriately integrated into water management practice and policy. Furthermore, the application of mass balance methods outlined in Chapters 2 and 3 requires steady state streamflow conditions, which may be difficult to achieve in settings with regular rainfall or extensive urban drainage networks.

The costs of analysis of isotopic tracers can be substantial, but these costs can be reduced if cheaper methods are used to inform sample collection and analysis of isotopic tracers. For example, in Chapter 3, it was demonstrated that depleted ^{14}C activity in streams caused by groundwater discharge can persist for tens to hundreds of kilometers downstream of the groundwater discharge zone. In this study, the major groundwater discharge zone was easily targeted because it had been delineated during previous studies. Where a field site has not previously been investigated, initial surveys of radon and streamflow will be able to inform analysis of more expensive tracers (e.g. ^{14}C or ^{4}He).

The application of some event markers (eg. ^{3}H, CFCs) as tracers is becoming increasingly difficult as atmospheric concentrations decrease and the inferred residence time becomes non-unique. However, in Chapter 4, by using the combination of the historic atmospheric concentration and known changes in the hydraulic regime at the study site to define end-member concentrations, event markers were able to be utilized to assess the contribution of

re-circulated groundwater to aquifer recharge. Re-circulation of groundwater occurs not just in environments altered by mining, but also in irrigated agricultural landscapes or during artificial supplementation of wetlands. This approach, using historical variation in atmospheric concentrations of gas tracers in combination with changes in hydrologic regime to inform end-member definitions, may also be able to be useful in these settings. If so, then this information will improve our understanding of the effects of changes in climate, land-use or water management practices on surface water-groundwater interaction.

The outcomes of this research have implications for stream ecology, stream rehabilitation and carbon cycling in streams. The new radon-based method presented in Chapter 2 was particularly sensitive to longer scales of hyporheic exchange, that were not captured by previously published methods. If the long-path hyporheic exchange fluxes detected in this study are drivers of nutrient cycling between the stream and streambed, and were not captured in previous studies, then the understanding of stream ecosystem function in these systems is incomplete. Furthermore, given the importance of hyporheic exchange to stream ecosystem function, stream re-alignment or rehabilitation should be carried out in such a way that the full spectrum of return flow paths is facilitated. The presence of long-path return flows in a stream with relatively low sinuosity and few gravel bars was not anticipated, and highlights the benefit of site-specific studies that capture the full spectrum of exchange prior to the commencement of engineering works. Similarly, in Chapter 3 it was demonstrated that depleted ^{14}C activity in streams receiving groundwater can persist for tens to hundreds of kilometres.   Previous studies that used stream ^{14}C to estimate CO_2 efflux from streams to the atmosphere have commonly neglected the influence of groundwater discharge in their analysis. Given the distances that groundwater discharge can influence ^{14}C activities in stream DIC (and possibly DOC), the authors may have incorrectly assumed that the influence of groundwater discharge was negligible in their studies. This may have affected our understanding of carbon cycling in streams and the contribution of streams to the global CO_2 budget.

5.2   Recommendations for future work

This thesis presents new methods for estimating surface water-groundwater exchange using environmental isotopic tracers and groundwater age indicators. Future work will involve the further validation of these new methods and their application in other field sites.

Application of the new radon-based method for quantifying hyporheic exchange in other losing streams, both natural and modified by mining, will be important for determining the frequency of occurrence of long-flow path hyporheic exchange in other systems. In these subsequent studies, concurrent application of the new radon-based method with an injected tracer experiment of longer duration will allow for a more robust validation of the method. The importance of these long hyporheic exchange paths for nutrient cycling and stream ecology is also unclear. Studies that incorporate quantification of the spectrum of hyporheic fluxes with measurement of nutrient distributions will provide valuable insight into nutrient cycling in streams and allow for the ecological significance of these longer return flow paths to be clarified.

Previous studies that incorporated long hyporheic flow paths have usually assumed that they were driven by stream meanders and gravel bars. The new radon method detected long-path hyporheic exchange, even though the creek studied had relatively few meanders and gravel bars. At this site the hydraulic conductivity of the alluvial gravel is likely to be orders of magnitude greater than the hydraulic conductivity of the aquifer materials that the channel is incised into. At this study site, the hydraulic gradients have been modified over time by the discharge of excess mine water. Numerical modeling will allow for the relationships between hydraulic conductivity and hydraulic gradients, both perpendicular and parallel to the creek, and long-path hyporheic exchange to be investigated.

During the development of ^{14}C as a tracer of groundwater discharge to streams, opportunistic sample collection by third parties has meant that the in-situ measurements were limited. Future applications of ^{14}C as a tracer of groundwater discharge in other streams should include in-situ measurement of pCO2, pH and alkalinity by titration, and measurement of stream ^{14}C activity at finer spatial resolution across the discharge zone. Better constraint on the ^{14}C activity at the upstream end of the discharge zone, and measurement of stream ^{14}C activity at finer spatial resolution, will allow for the uncertainty of groundwater ^{14}C activity to be estimated using parameter estimation techniques.

The net depletion of aquifer storage by mine dewatering operations at the study site in this thesis is likely to have been reduced by the recycling of mine water. However, the implications of these dewatering operations (and the related transition from disconnected ephemeral streams to perennial connected streams) on the magnitude and distribution of recharge during natural flood events, is unclear. Further investigation of the implications of this transition is

recommended, with particular consideration of the impact on the water balance of terminal wetland systems.

The amount of excess air formation during diffuse rainfall recharge has previously been shown to be related to the magnitude of water level rise into the unsaturated zone and bank filtration through saturated or unsaturated porous media. However, this published research was conducted in aquifers composed of galciofluvial and fluvial deposits consisting of silt, clay and fine to medium sand. Further controlled experiments investigating the link between excess air amount and stream connection status where recharge occurs through coarse gravel beds, such as in this study, are warranted.

References

AESCHBACH-HERTIG, W., PEETERS, F., BEYERLE, U. & KIPFER, R. 2000. Palaeotemperature reconstruction from noble gases in ground water taking into account equilibration with entrapped air. *Nature,* 405**,** 1040-1044.

AESCHBACH‐HERTIG, W., PEETERS, F., BEYERLE, U. & KIPFER, R. 1999. Interpretation of dissolved atmospheric noble gases in natural waters. *Water Resources Research,* 35**,** 2779-2792.

APPELO, C. & POSTMA, D. 2005. *Geochemistry, groundwater and pollution*, A.A. Blakeema.

BAZEMORE, D. E., ESHLEMAN, K. N. & HOLLENBECK, K. J. 1994. The role of soil water in stormflow generation in a forested headwater catchment: synthesis of natural tracer and hydrometric evidence. *Journal of Hydrology,* 162**,** 47-75.

BECKER, R. H. & CLAYTON, R. N. 1972. Carbon isotopic evidence for the origin of a banded iron-formation in Western Australia. *Geochimica et Cosmochimica Acta,* 36**,** 577-595.

BENCALA, K. E. 1984. Interactions of solutes and streambed sediment: 2. A dynamic analysis of coupled hydrologic and chemical processes that determine solute transport. *Water Resources Research,* 20**,** 1804-1814.

BENCALA, K. E., GOOSEFF, M. N. & KIMBALL, B. A. 2011. Rethinking hyporheic flow and transient storage to advance understanding of stream-catchment connections. *Water Resources Research,* 47, W00H03.

BENCALA, K. E. & WALTERS, R. A. 1983. Simulation of solute transport in a mountain pool-and-riffle stream: a transient storage model. *Water Resources Research,* 19**,** 718-724.

BENNETT, J. P. & RATHBUN, R. E. 1972. *Reaeration in open-channel flow*, US Government Printing Office.

BERTIN, C. & BOURG, A. 1994. Radon-222 and chloride as natural tracers of the infiltration of river water into an alluvial aquifer in which there is significant river/groundwater mixing. *Environmental Science & Technology,* 28**,** 794-798.

BEYERLE, U., AESCHBACH-HERTIG, W., HOFER, M., IMBODEN, D. M., BAUR, H. & KIPFER, R. 1999. Infiltration of river water to a shallow aquifer investigated with 3H/3He, noble gases and CFCs. *Journal of Hydrology,* 220**,** 169-185.

BOANO, F., REVELLI, R. & RIDOLFI, L. 2011. Water and solute exchange through flat streambeds induced by large turbulent eddies. *Journal of Hydrology,* 402**,** 290-296.

BOULTON, A. J., DATRY, T., KASAHARA, T., MUTZ, M. & STANFORD, J. A. 2010. Ecology and management of the hyporheic zone: stream-groundwater interactions of running waters and their floodplains. *Journal of the North American Benthological Society,* 29**,** 26-40.

BOURKE, S. A., COOK, P. G., SHANAFIELD, M., DOGRAMACI, S. & CLARK, J. F. 2014. Characterisation of hyporheic exchange in a losing stream using radon-222. *Journal of Hydrology,* 519**,** 94-105.

BROECKER, W. S., PENG, T. H., MATHIEU, G., HESSLEIN, R. & TORGERSEN, T. 1980. Gas-Exchange Rate Measurements in Natural Systems. *Radiocarbon,* 22**,** 676-683.

BROECKER, W. S. & WALTON, A. 1959. The geochemistry of C-14 in fresh-water systems. *Geochimica et Cosmochimica Acta,* 16**,** 15-38.

BROWN, K. B., MCINTOSH, J. C., RADEMACHER, L. K. & LOHSE, K. A. 2011. Impacts of agricultural irrigation recharge on groundwater quality in a basalt aquifer system (Washington, USA): a multi-tracer approach. *Hydrogeology Journal,* 19**,** 1039-1051.

BUCHANAN, T. J. & SOMERS, W. P. 1969. *Discharge measurements at gaging stations*, US Government Printing Office Washington, DC.

BUSENBERG, E. & PLUMMER, L. N. 1992. Use of Chlorofluorocarbons (CCl_3F and CCl_2F_2) as Hydrologic Tracers and Age-Dating Tools - the Alluvium and Terrace System of Central Oklahoma. *Water Resources Research,* 28**,** 2257-2283.

BUTMAN, D. & RAYMOND, P. A. 2011. Significant efflux of carbon dioxide from streams and rivers in the United States. *Nature Geoscience,* 4**,** 839-842.

CARACO, N., BAUER, J. E., COLE, J. J., PETSCH, S. & RAYMOND, P. 2010. Millennial-aged organic carbon subsidies to a modern river food web. *Ecology,* 91**,** 2385-2393.

CARDENAS, M. B. 2009. Stream-aquifer interactions and hyporheic exchange in gaining and losing sinuous streams. *Water Resources Research,* 45**,** W06429.

CARDENAS, M. B., WILSON, J. L. & ZLOTNIK, V. A. 2004. Impact of heterogeneity, bed forms, and stream curvature on subchannel hyporheic exchange. *Water Resources Research,* 40**,** W08307.

CASTRO, M. C., STUTE, M. & SCHLOSSER, P. 2000. Comparison of He-4 ages and C-14 ages in simple aquifer systems: implications for groundwater flow and chronologies. *Applied Geochemistry,* 15**,** 1137-1167.

CHOI, J., HARVEY, J. W. & CONKLIN, M. H. 2000. Characterizing multiple timescales of stream and storage zone interaction that affect solute fate and transport in streams. *Water Resources Research,* 36**,** 1511-1518.

CHOI, J., HULSEAPPLE, S., CONKLIN, M. & HARVEY, J. 1998. Modeling CO2 degassing and pH in a stream-aquifer system. *Journal of Hydrology,* 209**,** 297-310.

CLARET, C. & BOULTON, A. 2009. Integrating hydraulic conductivity with biogeochemical gradients and microbial activity along river–groundwater exchange zones in a subtropical stream. *Hydrogeology Journal,* 17**,** 151-160.

CLARK, I. & FRITZ, P. 1997. *Environmental isotopes in hydrology*, Lewis Publishers, Boca Raton, Florida.

CLARK, J. F., SCHLOSSER, P., WANNINKHOF, R., SIMPSON, H. J., SCHUSTER, W. S. F. & HO, D. T. 1995. Gas Transfer Velocities for SF6 and He-3 in a Small Pond at Low Wind Speeds. *Geophysical Research Letters,* 22**,** 93-96.

COLE, J. J. & CARACO, N. F. 2001. Carbon in catchments: connecting terrestrial carbon losses with aquatic metabolism. *Marine and Freshwater Research,* 52**,** 101-110.

COLE, J. J., PRAIRIE, Y. T., CARACO, N. F., MCDOWELL, W. H., TRANVIK, L. J., STRIEGL, R. G., DUARTE, C. M., KORTELAINEN, P., DOWNING, J. A., MIDDELBURG, J. J. & MELACK, J. 2007. Plumbing the global carbon cycle: Integrating inland waters into the terrestrial carbon budget. *Ecosystems,* 10**,** 171-184.

COOK, P. & HERCZEG, A. 2000. *Environmental tracers in subsurface hydrology*, Kluwer Academic.

COOK, P. G. 2013. Estimating groundwater discharge to rivers from river chemistry surveys. *Hydrological Processes,* 27**,** 3694-3707.

COOK, P. G., FAVREAU, G., DIGHTON, J. C. & TICKELL, S. 2003. Determining natural groundwater influx to a tropical river using radon, chlorofluorocarbons and ionic environmental tracers. *Journal of Hydrology,* 277**,** 74-88.

COOK, P. G., LAMONTAGNE, S., BERHANE, D. & CLARK, J. F. 2006. Quantifying groundwater discharge to Cockburn River, southeastern Australia, using dissolved gas tracers Rn-222 and SF6. *Water Resources Research,* 42**,** W10411.

CRAIG, H. 1957. The Natural Distribution of Radiocarbon and the Exchange Time of Carbon Dioxide Between Atmosphere and Sea. *Tellus,* 9**,** 1-17.

CRANSWICK, R. H. & COOK, P. G. *In review*. Scales and magnitude of hyporheic, river – aquifer and bank storage exchange fluxes. *Hydrological Processes*.

DEFORET, T., MARMONIER, P., RIEFFEL, D., CRINI, N., GIRAUDOUX, P. & GILBERT, D. 2009. Do parafluvial zones have an impact in regulating river pollution? Spatial and temporal dynamics of nutrients, carbon, and bacteria in a large gravel bar of the Doubs River (France). *Hydrobiologia,* 623**,** 235-250.

DENT, C. L., GRIMM, N. B., MARTÍ E., EDMONDS, J. W., HENRY, J. C. & WELTER, J. R. 2007. Variability in surface-subsurface hydrologic interactions and implications for nutrient retention in an arid-land stream. *Journal of Geophysical Research,* 112**,** G04004.

DOCTOR, D. H., KENDALL, C., SEBESTYEN, S. D., SHANLEY, J. B., OHTE, N. & BOYER, E. W. 2008. Carbon isotope fractionation of dissolved inorganic carbon (DIC) due to outgassing of carbon dioxide from a headwater stream. *Hydrological Processes,* 22**,** 2410-2423.

DOGRAMACI, S., HEDLEY, P. & FIRMANI, G. *In prep*. Connecting a disconnected creek: A case study from the semi-arid Hamersley Basin.

DOGRAMACI, S., SKRZYPEK, G., DODSON, W. & GRIERSON, P. F. 2012. Stable isotope and hydrochemical evolution of groundwater in the semi-arid Hamersley Basin of subtropical northwest Australia. *Journal of Hydrology,* 475**,** 281-293.

FINDLAY, S. 1995. Importance of Surface-Subsurface Exchange in Stream Ecosystems: The Hyporheic Zone. *Limnology and Oceanography,* 40**,** 159-164.

FREEZE, R. A. & CHERRY, J. A. 1977. *Groundwater*, Prentice Hall.

GARDNER, W. P., HARRINGTON, G. A., SOLOMON, D. K. & COOK, P. G. 2011. Using terrigenic He-4 to identify and quantify regional groundwater discharge to streams. *Water Resources Research,* 47, W06523.

GENEREUX, D. 1998. Quantifying uncertainty in tracer‐based hydrograph separations. *Water Resources Research,* 34**,** 915-919.

GENEREUX, D. & HEMOND, H. 1992. Determination of gas exchange rate constants for a small stream on Walker Branch Watershed, Tennessee. *Water Resources Research,* 28**,** 2365-2374.

GOOSEFF, M. N. 2010. Defining hyporheic zones–advancing our conceptual and operational definitions of where stream water and groundwater meet. *Geography Compass,* 4**,** 945-955.

GOOSEFF, M. N., MCKNIGHT, D. M., RUNKEL, R. L. & VAUGHN, B. H. 2003. Determining long time-scale hyporheic zone flow paths in Antarctic streams. *Hydrological Processes,* 17**,** 1691-1710.

HAGEDORN, B. & CARTWRIGHT, I. 2010. The CO2 system in rivers of the Australian Victorian Alps: CO2 evasion in relation to system metabolism and rock weathering on multi-annual time scales. *Applied Geochemistry,* 25**,** 881-899.

HARRINGTON, G., COOK, P. & HERCZEG, A. 2002. Spatial and temporal variability of ground water recharge in central Australia: a tracer approach. *Ground Water,* 40**,** 518-527.

HARVEY, J. W. & WAGNER, B. J. 2000. Quantifying hydrologic interactions between streams and their subsurface hyporheic zones. *In:* JONES, J. B. & MULHOLLAND, P. J. (eds.) *Streams and Ground Waters.* Elsevier.

HARVEY, J. W., WAGNER, B. J. & BENCALA, K. E. 1996. Evaluating the reliability of the stream tracer approach to characterize stream-subsurface water exchange. *Water Resources Research,* 32**,** 2441-2451.

HEDGES, J. I., ERTEL, J. R., QUAY, P. D., GROOTES, P. M., RICHEY, J. E., DEVOL, A. H., FARWELL, G. W., SCHMIDT, F. W. & SALATI, E. 1986. Organic C-14 in the Amazon River System. *Science,* 231**,** 1129-1131.

HENDY, C. H. 1971. Isotopic Geochemistry of Speleothems .1. Calculation of Effects of Different Modes of Formation on Isotopic Composition of Speleothems and Their Applicability as Palaeoclimatic Indicators. *Geochimica et Cosmochimica Acta,* 35**,** 801-824.

HOEHN, E. & CIRPKA, O. A. 2006. Assessing residence times of hyporheic ground water in two alluvial flood plains of the Southern Alps using water temperature and tracers. *Hydrology and Earth System Sciences,* 10**,** 553-563.

HOEHN, E. & VON GUNTEN, H. 1989. Radon in groundwater: A tool to assess infiltration from surface waters to aquifers. *Water Resources Research,* 25**,** 1795-1803.

HOLMES, R. M., FISHER, S. G. & GRIMM, N. B. 1994. Parafluvial Nitrogen Dynamics in a Desert Stream Ecosystem. *Journal of the North American Benthological Society,* 13**,** 468-478.

HOLOCHER, J., PEETERS, F., AESCHBACH-HERTIG, W., HOFER, M., BRENNWALD, M., KINZELBACH, W. & KIPFER, R. 2002. Experimental investigations on the formation of excess air in quasi-saturated porous media. *Geochimica et Cosmochimica Acta,* 66**,** 4103-4117.

INGRAM, R. G., HISCOCK, K. M. & DENNIS, P. F. 2007. Noble gas excess air applied to distinguish groundwater recharge conditions. *Environmental Science & Technology,* 41**,** 1949-1955.

JOERIN, C., BEVEN, K. J., IORGULESCU, I. & MUSY, A. 2002. Uncertainty in hydrograph separations based on geochemical mixing models. *Journal of Hydrology,* 255**,** 90-106.

JONES, J. B. & MULHOLLAND, P. J. 2000. *Streams and Ground Waters,* New York, Academic Press.

KALBUS, E., REINSTORF, F. & SCHIRMER, M. 2006. Measuring methods for groundwater, surface water and their interactions: a review. *Hydrology and Earth System Sciences Discussions,* 3**,** 1809-1850.

KEMPE, J. 1983. Review of water pollution problems and control strategies in the South African mining industry. *Water Science & Technology,* 15**,** 27-58.

KENDALL, C. & MCDONNELL, J. J. 1999. *Isotope tracers in catchment hydrology*, Elsevier.

KEPPEL, M. N., POST, V. E. A., LOVE, A. J., CLARKE, J. D. A. & WERNER, A. D. 2012. Influences on the carbonate hydrochemistry of mound spring environments, Lake Eyre South region, South Australia. *Chemical Geology,* 296–297**,** 50-65.

KIPFER, R., AESCHBACH-HERTIG, W., BAUR, H., HOFER, M., IMBODEN, D. & SIGNER, P. 1994. Injection of mantle type helium into Lake Van (Turkey): The clue for quantifying deep water renewal. *Earth and Planetary Science Letters,* 125**,** 357-370.

KIPFER, R., AESCHBACH-HERTIG, W., PEETERS, F. & STUTE, M. 2002. Noble gases in lakes and ground waters. *Noble Gases in Geochemistry and Cosmochemistry,* 47**,** 615-700.

LAMONTAGNE, S. & COOK, P. 2007. Estimation of hyporheic water residence time in situ using 222 Rn disequilibrium. *Limnolology and Oceanography: Methods,* 5**,** 407-416.

LAUTZ, L. K., KRANES, N. T. & SIEGEL, D. I. 2010. Heat tracing of heterogeneous hyporheic exchange adjacent to in stream geomorphic features. *Hydrological Processes,* 24**,** 3074-3086.

LEANEY, F. & HERCZEG, A. 2006. A rapid field extraction method for determination of radon-222 in natural waters by liquid scintillation counting. *Limnology and Oceanography: Methods,* 4**,** 254-259.

LEWIS, D., GRIMM, N., HARMS, T. & SCHADE, J. 2007. Subsystems, flowpaths, and the spatial variability of nitrogen in a fluvial ecosystem. *Landscape Ecology,* 22**,** 911-924.

LYNCH-STIEGLITZ, J. 1995. The influence of air-sea exchange on the isotopic composition of oceanic carbon: Observations and modeling. *Global biogeochemical cycles,* 9**,** 653-665.

MALOSZEWSKI, P. & ZUBER, A. 1982. Determining the Turnover Time of Groundwater Systems with the Aid of Environmental Tracers .1. Models and Their Applicability. *Journal of Hydrology,* 57**,** 207-231.

MASSMANN, G. & SÜLTENFUß, J. 2008. Identification of processes affecting excess air formation during natural bank filtration and managed aquifer recharge. *Journal of Hydrology,* 359**,** 235-246.

MASSOUDIEH, A. 2013. Inference of long‐term groundwater flow transience using environmental tracers: A theoretical approach. *Water Resources Research,* 49**,** 1-14.

MASSOUDIEH, A., SHARIFI, S. & SOLOMON, D. K. 2012. Bayesian evaluation of groundwater age distribution using radioactive tracers and anthropogenic chemicals. *Water Resources Research,* 48, W09529.

MAYORGA, E., AUFDENKAMPE, A. K., MASIELLO, C. A., KRUSCHE, A. V., HEDGES, J. I., QUAY, P. D., RICHEY, J. E. & BROWN, T. A. 2005. Young organic matter as a source of carbon dioxide outgassing from Amazonian rivers. *Nature,* 436**,** 538-541.

MAZOR, E. 2003. *Chemical and isotopic groundwater hydrology*, CRC press.

MCINTYRE, R. E. S., ADAMS, M. A., FORD, D. J. & GRIERSON, P. F. 2009. Rewetting and litter addition influence mineralisation and microbial communities in soils from a semi-arid intermittent stream. *Soil Biology & Biochemistry,* 41**,** 92-101.

MEREDITH, E. L. & KUZARA, S. L. 2012. Identification and Quantification of Base Flow Using Carbon Isotopes. *Ground Water,* 50**,** 959-965.

MILLS, G. A. & UREY, H. C. 1940. The Kinetics of Isotopic Exchange between Carbon Dioxide, Bicarbonate Ion, Carbonate Ion and Water1. *Journal of the American Chemical Society,* 62**,** 1019-1026.

MULLINGER, N. J., BINLEY, A. M., PATES, J. M. & CROOK, N. P. 2007. Radon in Chalk streams: Spatial and temporal variation of groundwater sources in the Pang and Lambourn catchments, UK. *Journal of Hydrology,* 339**,** 172-182.

MULLINGER, N. J., PATES, J. M., BINLEY, A. M. & CROOK, N. P. 2009. Controls on the spatial and temporal variability of 222Rn in riparian groundwater in a lowland Chalk catchment. *Journal of Hydrology,* 376**,** 58-69.

O'CONNOR, B. L. & HARVEY, J. W. 2008. Scaling hyporheic exchange and its influence on biogeochemical reactions in aquatic ecosystems. *Water Resources Research,* 44, W12423.

OSTER, H., SONNTAG, C. & MUNNICH, K. O. 1996. Groundwater age dating with chlorofluorocarbons. *Water Resources Research,* 32**,** 2989-3001.

PALMER, S., HOPE, D., BILLETT, M., DAWSON, J. & BRYANT, C. 2001. Sources of organic and inorganic carbon in a headwater stream: Evidence from carbon isotope studies. *Biogeochemistry,* 52**,** 321-338.

PARKHURST, D. L. & APPELO, C. 1999. User's guide to PHREEQC (Version 2): A computer program for speciation, batch-reaction, one-dimensional transport, and inverse geochemical calculations.

PAYN, R., GOOSEFF, M., MCGLYNN, B., BENCALA, K. & WONDZELL, S. 2009. Channel water balance and exchange with subsurface flow along a mountain headwater stream in Montana, United States. *Water Resources Research,* 45, W11427.

PEARSON, F. Use of C-13/C-12 ratios to correct radiocarbon ages of material initially diluted by limestone. Proceedings of the 6th International Conference on Radiocarbon and Tritium Dating, Pulman, WA, 1965.

PETERSON, E. W. & SICKBERT, T. B. 2006. Stream water bypass through a meander neck, laterally extending the hyporheic zone. *Hydrogeology Journal,* 14**,** 1443-1451.

RAYMOND, P. & COLE, J. 2001. Gas exchange in rivers and estuaries: Choosing a gas transfer velocity. *Estuaries and Coasts,* 24**,** 312-317.

RAYMOND, P. A. & BAUER, J. E. 2001. Riverine export of aged terrestrial organic matter to the North Atlantic Ocean. *Nature,* 409**,** 497-500.

RAYMOND, P. A., BAUER, J. E., CARACO, N. F., COLE, J. J., LONGWORTH, B. & PETSCH, S. T. 2004. Controls on the variability of organic matter and dissolved inorganic carbon ages in northeast US rivers. *Marine Chemistry,* 92**,** 353-366.

RAYMOND, P. A., CARACO, N. F. & COLE, J. J. 1997. Carbon dioxide concentration and atmospheric flux in the Hudson River. *Estuaries,* 20**,** 381-390.

RAYMOND, P. A. & HOPKINSON, C. S. 2003. Ecosystem modulation of dissolved carbon age in a temperate marsh-dominated estuary. *Ecosystems,* 6**,** 694-705.

RICHEY, J. E., MELACK, J. M., AUFDENKAMPE, A. K., BALLESTER, V. M. & HESS, L. L. 2002. Outgassing from Amazonian rivers and wetlands as a large tropical source of atmospheric CO_2. *Nature,* 416**,** 617-620.

RIPLEY, B. D. 2009. *Stochastic simulation*, John Wiley & Sons.

RUNKEL, R. L. 1998. One-dimensional transport with inflow and storage (OTIS): A solute transport model for streams and rivers. US Department of the Interior, US Geological Survey.

SCANLON, B. R., HEALY, R. W. & COOK, P. G. 2002. Choosing appropriate techniques for quantifying groundwater recharge. *Hydrogeology Journal,* 10**,** 18-39.

SEARLE, J. A., HAMMOND, M. J. & BATHOLS, G. 2011. Perth Shallow Groundwater Systems Investigation: Lake Nowergup. *Hydrogeological record series HG40.* Department of Water, Western Australia, ISBN 978-1-921736-14-8.

SHANAFIELD, M. & COOK, P. G. 2014. Transmission losses, infiltration and groundwater recharge through ephemeral and intermittent streambeds: A review of applied methods. *Journal of Hydrology,* 511**,** 518-529.

SMERDON, B. D., PAYTON GARDNER, W., HARRINGTON, G. A. & TICKELL, S. J. 2012. Identifying the contribution of regional groundwater to the baseflow of

a tropical river (Daly River, Australia). *Journal of Hydrology,* 467-465**,** 107-115.

SOLOMON, D. K. 2000. 4He in groundwater. *In:* COOK, P. G. & HERCZEG, A. L. (eds.) *Environmental tracers in subsurface hydrology.* Kluwer Academic.

SOLTANI, S. S. & CVETKOVIC, V. 2013. On the distribution of water age along hydrological pathways with transient flow. *Water Resources Research,* 49**,** 5238-5245.

SOPHOCLEOUS, M. 2002. Interactions between groundwater and surface water: the state of the science. *Hydrogeology Journal,* 10**,** 348-348.

STIEGLITZ, T. C., CLARK, J. F. & HANCOCK, G. J. 2013. The mangrove pump: The tidal flushing of animal burrows in a tropical mangrove forest determined from radionuclide budgets. *Geochimica et Cosmochimica Acta,* 102**,** 12-22.

STOLP, B., SOLOMON, D., SUCKOW, A., VITVAR, T., RANK, D., AGGARWAL, P. & HAN, L. 2010. Age dating base flow at springs and gaining streams using helium-3 and tritium: Fischa-Dagnitz system, southern Vienna Basin, Austria. *Water Resources Research,* 46**,** W07503.

STONEDAHL, S. H., HARVEY, J. W., WORMAN, A., SALEHIN, M. & PACKMAN, A. I. 2010. A multiscale model for integrating hyporheic exchange from ripples to meanders. *Water Resources Research,* 46**,** W12539.

STOREY, R. G., HOWARD, K. W. & WILLIAMS, D. D. 2003. Factors controlling riffle-scale hyporheic exchange flows and their seasonal changes in a gaining stream: A three-dimensional groundwater flow model. *Water Resources Research,* 39**,** 1034.

STUIVER, M. & POLACH, H. A. 1977. Reporting of C-14 Data - Discussion. *Radiocarbon,* 19**,** 355-363.

STUTE, M., DEÁK, J., RÉVÉSZ, K., BÖHLKE, J., DESEÖ, É., WEPPERNIG, R. & SCHLOSSER, P. 1997. Tritium/3He dating of river infiltration: An example from the Danube in the Szigetkoez area, Hungary. *Ground Water,* 35**,** 905-911.

SWANSON, T. E. & CARDENAS, M. B. 2010. Diel heat transport within the hyporheic zone of a pool-riffle-pool sequence of a losing stream and evaluation of models for fluid flux estimation using heat. *Limnology and Oceanography,* 55**,** 1741-1754.

TICKELL, S. J. 2011. Assessment of major spring systems in the Oolloo Dolostone, Daly River. *Northern Territory Department of Land Resource Management, Technical Report No. 22/2011D.*

TRISKA, F. J., DUFF, J. H. & AVANZINO, R. J. 1993. Patterns of Hydrological Exchange and Nutrient Transformation in the Hyporheic Zone of a Gravel-Bottom Stream - Examining Terrestrial Aquatic Linkages. *Freshwater Biology,* 29**,** 259-274.

VARNI, M. & CARRERA, J. 1998. Simulation of groundwater age distributions. *Water Resources Research,* 34**,** 3271-3281.

WANNINKHOF, R., LEDWELL, J. R., BROECKER, W. S. & HAMILTON, M. 1987. Gas exchange on Mono Lake and Crowley Lake, California. *Journal of Geophysical Research,* 92**,** 14567-14580.

WARNER, M. & WEISS, R. 1985. Solubilities of chlorofluorocarbons 11 and 12 in water and seawater. *Deep Sea Research Part A. Oceanographic Research Papers,* 32**,** 1485-1497.

WEISS, R. F. 1974. Carbon dioxide in water and seawater: the solubility of a non-ideal gas. *Marine Chemistry,* 2**,** 203-215.

WINTER, T. C., HARVEY, J. W., FRANKE, O. L. & ALLEY, W. M. 1998. Ground water and surface water: a single resource. *US Geological Survey Circular 1139.* U.S. Geological Survey.

WOOLFENDEN, L. R. & GINN, T. R. 2009. Modeled ground water age distributions. *Ground water,* 47**,** 547-557.

WORMAN, A., PACKMAN, A. I., JOHANSSON, H. & JONSSON, K. 2002. Effect of flow-induced exchange in hyporheic zones on longitudinal transport of solutes in streams and rivers. *Water Resources Research,* 38, 1001.

ZEEBE, R. E., WOLF-GLADROW, D. A. & JANSEN, H. 1999. On the time required to establish chemical and isotopic equilibrium in the carbon dioxide system in seawater. *Marine Chemistry,* 65**,** 135-153.

ZHANG, J., QUAY, P. D. & WILBUR, D. O. 1995. Carbon isotope fractionation during gas-water exchange and dissolution of CO2. *Geochimica et Cosmochimica Acta,* 59**,** 107-114.

Appendix 1 Derivation of carbon isotope mass balance

A1.1. *Derivation of equation for rate of change in ¹⁴C/¹²C in an evaporating pan of water*

In an evaporating pan of water that is in chemical equilibrium with the atmosphere, the mass balance of ¹²C in TDIC is given by;

$$V \frac{\partial}{\partial t} {}^{12}C_{TDIC} = {}^{12}C_{TDIC} AE \qquad (A1.1.1)$$

where V is the volume of water [L³], A is the surface area of the pan [L²], E is the evaporation rate (L T⁻¹).

If the water in the pan is not in isotopic equilibrium with the atmosphere, the mass balance of ¹⁴C in TDIC is given by;

$$V \frac{\partial}{\partial t} {}^{14}C_{TDIC} = {}^{14}C_{TDIC} AE + \alpha_k k_{co_2} A({}^{14}CO_{2eq} - {}^{14}CO_2) \qquad (A1.1.2)$$

where ${}^{14}CO_2$ is the concentration of ¹⁴CO₂ in the water at time t [M L⁻³], and ${}^{14}CO_{2eq}$ is the ¹⁴CO₂ concentration of water in the pan when it is at isotopic equilibrium with the atmosphere [M L⁻³] α_k is the kinetic fractionation factor associated with the varying gas transfer velocities of ¹²CO₂ and ¹⁴CO₂, and k_{CO2} is the gas transfer velocity of ¹²CO₂. The value of this α_k is very close to 1 (0.9992 at 20 °C), and is neglected in subsequent analysis.

The rate of change of the isotopic ratio ¹⁴C/¹²C in TDIC, referred to as R_{TDIC}, is described by;

$$\frac{\partial}{\partial t} R_{TDIC} = \frac{\partial}{\partial t} \frac{{}^{14}C_{TDIC}}{{}^{12}C_{TDIC}} \qquad (A1.1.3)$$

Given the quotient rule;

$$\frac{\partial}{\partial t} \frac{{}^{14}C_{TDIC}}{{}^{12}C_{TDIC}} = \frac{{}^{12}C_{TDIC} \frac{\partial}{\partial t} {}^{14}C_{TDIC} - {}^{14}C_{TDIC} \frac{\partial}{\partial t} {}^{12}C_{TDIC}}{({}^{12}C_{TDIC})^2} \qquad (A1.1.4)$$

Rearranging and substituting A1.1.1 , A1.1.2 and A1.1.3 into equation A1.1.4 gives;

$$\frac{\partial}{\partial t} R_{TDIC}$$
$$= \frac{{}^{12}C_{TDIC}({}^{14}C_{TDIC} \frac{AE}{V} + k_{CO2} \frac{A}{V}({}^{14}CO_{2eq} - {}^{14}CO_2)) - {}^{14}C_{TDIC}({}^{12}C_{TDIC} \frac{AE}{V})}{({}^{12}C_{TDIC})^2} \qquad (A1.1.5)$$

Cancelling ¹²C$_{TDIC}$ terms gives;

$$\frac{\partial}{\partial t} R_{TDIC} = \frac{{}^{14}C_{TDIC} \frac{AE}{V} + k_{CO2} \frac{A}{V}({}^{14}CO_{2eq} - {}^{14}CO_2) - {}^{14}C_{TDIC} \frac{AE}{V}}{{}^{12}C_{TDIC}} \qquad (A1.1.6)$$

Which rearranges to give;

$$\frac{\partial}{\partial t}R_{TDIC} = \frac{^{14}C_{TDIC}}{^{12}C_{TDIC}}\frac{AE}{V} + k_{CO2}\frac{A}{V}\frac{1}{^{12}C_{TDIC}}\left(^{14}CO_{2eq} - {}^{14}CO_2\right) - \frac{^{14}C_{TDIC}}{^{12}C_{TDIC}}\frac{AE}{V} \qquad (A1.1.7)$$

The first and third terms cancel, giving;

$$\frac{\partial}{\partial t}R_{TDIC} = k_{CO2}\frac{A}{V}\frac{1}{^{12}C_{TDIC}}\left(^{14}CO_{2eq} - {}^{14}CO_2\right) \qquad (A1.1.8)$$

This is mathematically equivalent to;

$$\frac{\partial}{\partial t}R_{TDIC} = k_{CO2}\frac{A}{V}\frac{^{12}CO_2}{^{12}C_{TDIC}}\left(\frac{^{14}CO_{2eq}}{^{12}CO_2} - \frac{^{14}CO_2}{^{12}CO_2}\right) \qquad (A1.1.9)$$

If the water in the pan is at chemical equilibrium with the atmosphere, then $^{12}CO_2$ is equal to $^{12}CO_{2eq}$, and this equation can be written as;

$$\frac{\partial}{\partial t}R_{TDIC} = k_{CO2}\frac{A}{V}\frac{^{12}CO_2}{^{12}C_{TDIC}}\left(\frac{^{14}CO_{2eq}}{^{12}CO_{2eq}} - \frac{^{14}CO_2}{^{12}CO_2}\right) \qquad (A1.1.10)$$

Using the R notation for isotopic ratios, this simplifies to;

$$\frac{\partial}{\partial t}R_{TDIC} = k_{CO2}\frac{A}{V}\frac{^{12}CO_2}{^{12}C_{TDIC}}\left(R_{CO2eq} - R_{CO2}\right) \qquad (A1.1.11)$$

Because 99% of total C is ^{12}C, it can be assumed that $^{12}CO_2$ equals the total CO_2 and similarly, that $^{12}C_{TDIC}$ equals the total TDIC, which leads to;

$$\frac{\partial}{\partial t}R_{TDIC} = k_{CO2}\frac{A}{V}\frac{CO_2}{TDIC}\left(R_{CO2eq} - R_{CO2}\right) \qquad (A1.1.12)$$

which can be used to simulate the isotopic equilibration of water in the pan, either in units of permil or pMC.

A1.2. Derivation of equation for rate of change in $^{14}C/^{12}C$ in a stream in chemical equilibrium with the atmosphere

The mass balance of ^{12}C in TDIC in a stream at chemical equilibrium with the atmosphere is given by;

$$Q\frac{\partial}{\partial x}{}^{12}C_{TDIC} = Ew\,{}^{12}C_{TDIC} - q_{gw}({}^{12}C_{TDIC} - {}^{12}C_{TDICgw}) \qquad (A1.2.1)$$

where Q is the stream discharge rate of water [$L^3\,T^{-1}$], w is stream width [L], E is the evaporation rate ($L\,T^{-1}$). If the water in the stream is not in isotopic equilibrium with the atmosphere, the mass balance of ^{14}C in TDIC is given by;

$$Q\frac{\partial}{\partial x}{}^{14}C_{TDIC} = Ew\,{}^{14}C_{TDIC} - q_{gw}({}^{14}C_{TDIC} - {}^{14}C_{TDICgw})$$
$$+ kw({}^{14}CO_{2eq} - {}^{14}CO_2) \qquad (A1.2.2)$$

where $^{14}CO_2$ is the concentration of $^{14}CO_2$ in the stream at time t [$M\,L^{-3}$], and $^{14}CO_{2eq}$ is the $^{14}CO_2$ concentration of the stream when it is at isotopic equilibrium with the atmosphere [$M\,L^{-3}$].

The rate of change of the isotopic ratio $^{14}C/^{12}C$ in TDIC in the stream, referred to as R_{TDIC}, is described by;

$$\frac{\partial}{\partial x}R_{TDIC} = \frac{\partial}{\partial x}\frac{{}^{14}C_{TDIC}}{{}^{12}C_{TDIC}} \qquad (A1.2.3)$$

Given the quotient rule;

$$\frac{\partial}{\partial x}\frac{{}^{14}C_{TDIC}}{{}^{12}C_{TDIC}} = \frac{{}^{12}C_{TDIC}\frac{\partial}{\partial t}{}^{14}C_{TDIC} - {}^{14}C_{TDIC}\frac{\partial}{\partial t}{}^{12}C_{TDIC}}{({}^{12}C_{TDIC})^2} \qquad (A1.2.4)$$

Rearranging and substituting A2.1, A2.2 and A2.3 into equation A2.4 gives;

$$\frac{\partial}{\partial x}R_{TDIC} = \frac{{}^{12}C_{TDIC}\left({}^{14}C_{TDIC}\frac{wE}{Q} - \frac{q_{gw}}{Q}({}^{14}C_{TDIC} - {}^{14}C_{TDICgw}) + k\frac{w}{Q}({}^{14}CO_{2eq} - {}^{14}CO_2)\right)}{({}^{12}C_{TDIC})^2}$$
$$- \frac{{}^{14}C_{TDIC}\left({}^{12}C_{TDIC}\frac{wE}{Q} - \frac{q_{gw}}{Q}({}^{12}C_{TDIC} - {}^{12}C_{TDICgw})\right)}{({}^{12}C_{TDIC})^2} \qquad (A1.2.5)$$

Similar to the evaporating pan of water, the evaporation terms cancel, and the equation reduces to;

$$\frac{\partial}{\partial x} R_{TDIC} =$$

$$\frac{^{12}C_{TDIC}\left(k\frac{w}{Q}(^{14}CO_{2eq}-^{14}CO_2)-\frac{q_{gw}}{Q}(^{14}C_{TDIC}-^{14}C_{TDICgw})\right)-^{14}C_{TDIC}\left(-\frac{q_{gw}}{Q}(^{12}C_{TDIC}-^{12}C_{TDICgw})\right)}{(^{12}C_{TDIC})^2} \qquad (A1.2.6)$$

Which, if the stream is at chemical equilibrium with the atmosphere, can be rearranged to give the familiar gas transfer term and two groundwater discharge terms.

$$\frac{\partial}{\partial x} R_{TDIC} = \quad k_{CO2}\frac{w}{Q}\frac{^{12}CO_2}{^{12}C_{TDIC}}\left(\frac{^{14}CO_{2eq}}{^{12}CO_{2_{eq}}}-\frac{^{14}CO_2}{^{12}CO_2}\right)-\frac{1}{^{12}C_{TDIC}}(\frac{q_{gw}}{Q}(^{14}C_{TDIC}-^{14}C_{TDICgw})$$

$$+\frac{^{14}C_{TDIC}}{^{12}C_{TDIC}^2}(\frac{q_{gw}}{Q}(^{12}C_{TDIC}-^{12}C_{TDICgw}) \qquad (A1.2.7)$$

Focussing now on the groundwater terms, which are;

$$\frac{^{14}C_{TDIC}}{^{12}C_{TDIC}^2}(\frac{q_{gw}}{Q}(^{12}C_{TDIC}-^{12}C_{TDICgw})-\frac{1}{^{12}C_{TDIC}}(\frac{q_{gw}}{Q}(^{14}C_{TDIC}-^{14}C_{TDICgw}) \qquad (A1.2.8)$$

Expanding and collecting like terms gives;

$$\frac{q_{gw}}{Q}\left(\frac{^{14}C_{TDIC}}{^{12}C_{TDIC}}-\frac{^{14}C_{TDIC}}{^{12}C_{TDIC}}\frac{^{12}C_{TDICgw}}{^{12}C_{TDIC}}+\frac{^{14}C_{TDICgw}}{^{12}C_{TDIC}}-\frac{^{14}C_{TDIC}}{^{12}C_{TDIC}}\right) \qquad (A1.2.9)$$

The second and fourth terms cancel, giving;

$$\frac{q_{gw}}{Q}\left(\frac{^{14}C_{TDICgw}}{^{12}C_{TDIC}}-\frac{^{14}C_{TDIC}}{^{12}C_{TDIC}}\frac{^{12}C_{TDICgw}}{^{12}C_{TDIC}}\right) \qquad (A1.2.10)$$

Which is equivalent to;

$$-\frac{q_{gw}}{Q}\frac{^{12}C_{TDICgw}}{^{12}C_{TDIC}}\left(\frac{^{14}C_{TDICgw}}{^{12}C_{TDICgw}}-\frac{^{14}C_{TDIC}}{^{12}C_{TDIC}}\right) \qquad (A1.2.11)$$

Substituting equation A1.2.11 into A1.2.7 and using R notation, the change in isotopic ratio along the stream is given by;

$$\frac{\partial}{\partial x} R_{TDIC} = k_{CO2}\frac{w}{Q}\frac{^{12}CO_2}{^{12}C_{TDIC}}\left(R_{CO2eq}-R_{CO2}\right)$$

$$-\frac{q_{gw}}{Q}\frac{^{12}C_{TDICgw}}{^{12}C_{TDIC}}\left(R_{TDIC}-R_{TDICgw}\right) \qquad (A1.2.12)$$

If ^{12}C is assumed to be equal to the total TDIC, this equation becomes;

$$\frac{\partial}{\partial x} R_{TDIC} =$$

$$k_{CO2}\frac{w}{Q}\frac{CO_2}{TDIC}\left(R_{CO2eq}-R_{CO2}\right)-\frac{q_{gw}}{Q}\frac{TDIC_{gw}}{TDIC}\left(R_{TDIC}-R_{TDICgw}\right) \qquad (A1.2.13)$$

which can be used to simulate the change in isotopic ratio of the stream, either in permil, or pMC.

Appendix 2 Locations of piezometers, creek samples and dewatering wells, and associated hydrochemistry data

Table A2-1 Locations of creek samples, piezometers and dewatering wells

	Site ID	Sample ID	Easting	Northing	Distance from creek
			(m) MGA Z50	(m) MGA Z50	(m)
Creeks	Site 1	BHP1800*	722121	7478690	0
		MC22500	725376	7480242	0
	Site 2	BFN Creek	738711	7479836	0
	Site 3	WW1	733262	7473804	0
		WWXING	729364	7467778	0
Alluvial	Site 1	PZ03	721669	7478287	30
aquifer		JSW003	722371	7478803	30
	Site 2	WW3	733368	7473592	30
		BFS002	732937	7472476	250
		BFS003	733028	7472319	550
		BFS006	733101	7472248	325
	Site 3	BFN001	738794	7479780	100
		BFN002	738794	7479780	100
		BFN003	739077	7479498	500
CID	Site 1	PZ02	721668	7478289	100
aquifer		JSW008	722612	7478667	300
	Site 2	BFS001	732902	7472444	100
		BFS005	733101	7472248	325
		BFS007	733316	7472040	550
Dewatering		SB004	732924	7473698	150
wells		PC005	726348	7480555	50
		MC008	730197	7478627	0

Table A2-2 Hydrochemistry data: creek samples, piezometers and dewatering wells

Sample ID	Sample Date	pH	Total Alkalinity as CaCO3	Bicarbonate Alkalinity as HCO3	Chloride	Sulphate	Bromide	Calcium	Magnesium	Potassium	Sodium	Silicon	Iron
			mg/L	mg/L	mg/L	mg/L	mg/L	mg/L	mg/L	mg/L	mg/L	mg/L	mg/L
BFN Creek	27-Jul-12	8.4	330	403	102	35	0.52	68.7	55.8	9.8	65.6	12.73	<0.02
BFN001	26-Jul-12	7.8	290	353	112	54	0.56	72.5	47.9	8.1	63.1	21.30	<0.02
BFN002	26-Jul-12	8.1	403	492	110	52	0.59	47.9	68.1	14.7	105.6	28.56	<0.02
BFN003	27-Jul-12	7.9	330	402	111	56	0.59	75.0	57.7	9.6	62.9	20.35	<0.02
BFS001	25-Sep-12	7.9	288	351	83	55	0.46	55.4	39.6	6.7	45.1	12.63	<0.02
BFS002	05-Oct-12	7.8	271	330	81	59	0.46	42.4	34.2	5.8	37.9	9.61	<0.02
BFS003	27-Jul-12	7.9	303	369	82	43	0.44	68.0	47.4	8.6	53.1	13.30	<0.02
BFS005	25-Sep-12	7.9	290	354	83	57	0.47	54.2	43.3	7.8	45.1	12.54	<0.02
BFS006	05-Oct-12	7.9	300	366	85	57	0.47	44.8	40.8	6.9	41.1	11.47	<0.02
BFS007	24-Sep-12	7.9	335	409	110	72	0.62	50.5	55.2	10.4	56.2	17.89	<0.02
BHP1800	25-Oct-11	7.9	264	287	122	62	0.65	39.6	48.8	8.6	83.9	25.81	<0.02
D05	07-Oct-12	8.1	279	341	106	44	0.57	40.9	35.8	6.1	51.2	27.80	<0.02
JSW003	08-Oct-12	8.0	308	376	123	53	0.70	40.1	39.5	5.9	64.3	18.20	<0.02
JSW008	29-Jul-12	7.6	238	290	67	41	0.33	48.9	28.1	5.3	57.0	23.91	<0.02
MC008	07-Oct-12	7.8	276	336	107	48	0.56	41.5	34.9	5.7	52.5	21.38	<0.02
MC22500	24-Oct-11	8.0	293	329	113	62	0.67	65.0	50.7	8.7	64.7	11.69	<0.02
PC005	06-Oct-12	7.7	248	302	140	63	0.77	41.1	38.5	5.2	66.9	19.57	<0.02
PZ02	04-Oct-12	7.7	245	298	136	64	0.75	51.3	44.6	6.4	71.0	22.63	<0.02
PZ03	04-Oct-12	8.3	269	328	121	57	0.66	37.1	35.5	6.8	55.4	20.53	<0.02
SB004	06-Oct-12	7.9	323	394	92	58	0.52	48.4	44.7	7.4	43.1	13.92	<0.02
WW1	27-Jul-12	8.4	333	406	83	59	0.45	58.4	57.4	9.6	51.7	14.29	<0.02
WWXING	08-Oct-12	8.3	312	378	79	55	0.46	43.8	45.8	7.6	38.2	11.93	<0.02

Table A2-3 Noble gas data

Sample	Kr	Xe	Ar	Ne	He
	ccSTP gw^{-1}	ccSTP gw^{-1}	ccSTP gw^{-1}	ccSTP gw^{-1}	ccSTP gw^{-1}
SB004	5.9×10^{-8}	7.6×10^{-9}	3.0×10^{-4}	2.2×10^{-7}	9.1×10^{-8}
PC005	6.1×10^{-8}	7.7×10^{-9}	3.2×10^{-4}	2.1×10^{-7}	9.1×10^{-8}
MC008	6.6×10^{-8}	8.7×10^{-9}	3.0×10^{-4}	2.2×10^{-7}	4.6×10^{-7}

Table A2-4 Calculated recharge temperature, excess air (ΔNe) and terrigenic ^{4}He (^{4}He$_{Terr}$)

Sample	Noble gases parameter estimates are based on	Recharge Temperature	ΔNe	^{4}He$_{Terr}$
		°C	‰	µccSTP kgw^{-1}
SB004	Ar, Ne	23.2	29.6	35
	Kr, Xe, Ar, Ne	27.3	26.2	34
PC005	Ar, Ne	18.8	20.0	39
	Kr, Xe, Ar, Ne	23.2	17.4	38
MC008	Ar, Ne	23.7	30.5	406
	Kr, Xe, Ar, Ne	29.0	28.3	405

Appendix 3 Abstracts of related conference presentations

A3.1. *National Ground Water Association (NGWA) Groundwater Summit, May 2012, Garden Grove, California USA*

Title: Transient storage models underestimate the depth of the hyporheic zone

Sarah A. Bourke, Flinders University; Peter G. Cook, Dr., CSIRO; Margaret Shanafield, PhD, National Centre for Groundwater Research and Training; Shawan Dogramaci, PhD, Rio Tinto Iron Ore;

Hyporheic exchange is commonly estimated using transient storage models to interpret data from tracer experiments. Velocities within the hyporheic zone can also be estimated using streambed temperature and radon profiles. We propose an additional method to estimate hyporheic exchange using radon activities within the stream itself. In losing streams, the stream radon concentration is determined by the balance of gas exchange with the atmosphere and radon introduced through hyporheic exchange. If the gas exchange rate is known, the hyporheic exchange flux can be estimated using a mass balance model.
We compared estimates of hyporheic exchange using these methods on a losing stream in the arid, sub-tropical Pilbara region of Western Australia. The transient storage model OTIS suggests the average storage zone area is 25 m^2. Assuming the contribution from stagnant zones is negligible; this implies a hyporheic zone thickness of 0.15 m beneath the stream. Vertical profiles of radon concentration showed either a low concentration zone within the top 0.1 m suggesting rapid exchange with the stream, or elevated concentrations within the top 0.3 m suggesting the upwelling of older water. Similarly, streambed temperature profiles show a change in vertical velocity between 0.3 and 0.5 m depth, implying a hyporheic exchange zone within the top 0.5 m of the streambed.

In contrast to these estimates, mass balance modeling suggests that the hyporheic zone needs to be 10 m thick to maintain the radon concentration within the stream at 3 Bq/L. This suggests the presence of hyporheic flow paths with residence times of days to weeks that were not captured by the tracer test or streambed profiles. This study highlights the multi-scale nature of hyporheic exchange and demonstrates that reliance on transient storage modeling could significantly underestimate the depth of the hyporheic zone.

Title: Carbon-14 as a tracer of groundwater discharge to streams

Bourke, S.A.[1,2*], Harrington, G.A.[1,3], Cook, P.G.[1,2], Post, V.E.A.[1], Dogramaci, S.[4]

[1]National Centre for Groundwater Research and Training, Flinders University, Bedford Park, S.A. Australia; [2]Commonwealth Scientific and Industrial Research Organization (CSIRO), Division of Land and Water, Floreat, WA, Australia; [3]Commonwealth Scientific and Industrial Research Organization (CSIRO), Division of Land and Water, Glen Osmond, SA, Australia; [4]Rio Tinto Iron Ore, 162-168 St Georges Tce, Perth, WA 6000, Australia

In this paper we demonstrate the use of the carbon-14 activity of dissolved inorganic carbon (hereafter referred to as ^{14}C) as a tracer of groundwater discharge to streams. Excess carbon dioxide (CO_2) in the emerging groundwater degasses until equilibrium with atmospheric CO_2 is reached; increasing pH and enriching the residual ^{14}C by fractionation. In addition, the ^{14}C gradient between groundwater and the atmosphere drives a slower process of isotopic equilibration. We have measured the rates of chemical and isotopic equilibration experimentally by exposing 250 L of old groundwater to the atmosphere in an evaporation pan. Chemical equilibrium was achieved within 2 days, during which the ^{14}C increased from 6 pmC to 16 pmC. The influence of fractionation during the initial CO_2 degassing on isotopic equilibrium rates was negligible. Isotopic equilibrium took over 2 months, with ^{14}C in the evaporation pan increasing to 108 pmC over 71 days. This increase in ^{14}C was simulated using a mass balance model with an effective ^{14}C gas transfer velocity of 0.015 m/d.

Field testing of the method was conducted at two sites. Firstly, we measured the evolution of ^{14}C in dewater discharge as it flows along an ephemeral creek channel in the Pilbara, Western Australia. Measured ^{14}C increased from 11 to 31 pmC along the 10km reach, which corresponds to a travel time of about 2 days. The measured increase was simulated using a mass balance model with an effective ^{14}C gas transfer velocity of 0.05 m/d. Secondly, we measured ^{14}C at six sites along the Daly River, Northern Territory. Here we observed a decrease in ^{14}C of 7 pmC across a major groundwater discharge zone and were able to simulate the observed ^{14}C using a gas transfer velocity of 0.18 m/d.

The potential for groundwater discharge to be detectable in other streams using ^{14}C depends on the magnitudes of groundwater discharge, alkalinity and ^{14}C relative to stream values.

Paper 1

Title: Interpretation of groundwater age tracers (CFC-12, ^{14}C, ^{4}He) in a mining-influenced stream-aquifer system with transient recharge dynamics

Sarah A. Bourke[1,2]*, Peter G. Cook [1,3], Rolf Kipfer [4] Shawan Dogramaci [5],

[1] National Centre for Groundwater Research and Training (NCGRT), School of the Environment Flinders University, GPO Box 2100, South Australia, Australia; [2] Commonwealth Scientific and Industrial Research Organization (CSIRO), Division of Land and Water, Floreat, Private Bag 5 Wembley 6913 WA, Australia [3] Commonwealth Scientific and Industrial Research Organization (CSIRO), Division of Land and Water, Glen Osmond, Adelaide SA 5064, Australia; [4] Department of Water Resources and Drinking Water, Eawag: Swiss Federal Institute of Aquatic Science and Technology, Ueberlandstrasse 133, 8600 Dubendorf, Switzerland; [5] Rio Tinto Iron Ore, 162-168 St Georges Tce, Perth, WA 6000, Australia

Interpretation of groundwater age indicators often requires consideration of the mixing of groundwater with varying residence times. Quantification of mixing can be approached through measurement of multiple groundwater age indicators with varying ranges of temporal sensitivity, and their interpretation using lumped parameter models. However, in systems altered by mining, where recharge mechanisms are highly transient in space and time, lumped parameter models do not adequately represent the complexity of the system.

In the Pilbara region of Western Australia, water abstracted during dewatering of ore-body aquifers is disposed of by discharging it into ephemeral streams and allowing it to recharge the aquifer. Because this water is essentially being recycled, stable isotopes and chloride are not useful tracers of the impact of this dewatering discharge. In contrast, gas tracers that respond rapidly to exposure to the atmosphere are more useful tracers for constraining the influence of dewatering discharge on the aquifer water balance. In this study we measured CFC-12, ^{14}C and noble gases in production wells and transects of piezometers perpendicular to the stream. Even in samples from wells screened over intervals of 1 m, we observe combinations of tracer concentrations that indicate mixing of groundwater with contrasting residence times. For example, all samples contained measureable CFC-12 concentrations, including those with appreciable terrigenic ^{4}He.

Interpretation of these data requires consideration of the history of mining activity in the area. Stream ^{14}C activities, which now range from 50 to 75 pMC, are a function of the dewatering discharge, and are no longer in equilibrium with the atmosphere. As a result, groundwater that recharged prior to mining operations can have higher ^{14}C activities than groundwater that recharged through the stream in the last 10 years. The dewatering discharge has caused the stream to transition from a disconnected ephemeral system, to a connected perennial stream system, which may result in lower, or negligible, excess air amounts in recently recharged waters. We calculate ternary mixing ratios from the CFC-12 and ^{14}C data to estimate the fractions of regional groundwater, pre-mining stream recharge and during-mining dewatering recharge in each water sample. These results are cross-checked against the calculated excess air and terrigenic [4]He amounts. These data suggest that the influence of dewatering discharge extends at most 500 m, and in some places less than 50 m laterally from the stream. This implies that the majority of the dewatering discharge is being recycled locally or flows along the alluvial channel aquifer associated with the stream.

Paper 2

Title: Carbon-14 as a tracer of groundwater discharge to streams

Bourke, S.A.[1,2*], Harrington, G.A.[1,3], Cook, P.G.[1,2], Post, V.E.A.[1], Dogramaci, S.[4]

[1]National Centre for Groundwater Research and Training, Flinders University, Bedford Park, S.A. Australia; [2]Commonwealth Scientific and Industrial Research Organization (CSIRO), Division of Land and Water, Floreat, WA, Australia; [3]Commonwealth Scientific and Industrial Research Organization (CSIRO), Division of Land and Water, Glen Osmond, SA, Australia; [4]Rio Tinto Iron Ore, 162-168 St Georges Tce, Perth, WA 6000, Australia

The provenance of groundwater discharge to a stream can be determined by measuring the response of multiple groundwater age tracers within the stream across the discharge zone. The sampling interval required to detect groundwater discharge is limited by the rate of equilibration with the atmosphere downstream of the discharge zone, which is determined by the gas transfer velocity. Carbon-14 (^{14}C) equilibration is driven by CO_2 exchange, which is a small component of the dissolved inorganic carbon in most stream systems, and therefore the rate of equilibration is slower than for other gaseous age tracers. In this paper we use a step-wise approach to develop and demonstrate the use of ^{14}C as a tracer in streams receiving groundwater discharge.

Excess carbon dioxide (CO_2) in the emerging groundwater degasses until equilibrium with atmospheric CO_2 is reached; increasing pH and enriching the residual ^{14}C by fractionation. In addition, the ^{14}C gradient between groundwater and the atmosphere drives a slower process of isotopic equilibration. We have measured the rates of this chemical and isotopic equilibration experimentally by exposing 250 L of old groundwater to the atmosphere in an evaporation pan. Chemical equilibrium was achieved within 2 days, during which the ^{14}C increased from 6 to 16 pMC. The influence of fractionation during the initial CO_2 degassing on isotopic equilibrium rates was negligible. Isotopic equilibrium took over 2 months, with ^{14}C in the evaporation pan increasing to 108 pMC over 71 days. This increase in ^{14}C was simulated using a mass balance model with an effective ^{14}C gas transfer velocity of 0.013 m d^{-1}.

Field testing of the method was conducted at two sites. Firstly, we measured the evolution of ^{14}C in dewater discharge as it flows along an ephemeral creek channel in the Pilbara, Western Australia. Measured ^{14}C increased from 11 to 31 pMC along the 10km reach, which corresponds to a travel time of about 2 days. The measured increase was simulated using a mass balance model with an effective ^{14}C gas transfer velocity of 0.025 m d^{-1}. Secondly, we measured ^{14}C at six sites along the Daly River, Northern Territory. Here we observed a decrease of 7 pMC across a major groundwater discharge zone and were able to simulate the observed ^{14}C using a gas transfer velocity of 0.14 m d^{-1}. We quantify the total groundwater influx using measurements of stream discharge and radon-222. This allows us to estimate the ^{14}C activity of the groundwater discharge at 64 pMC.

The potential for groundwater discharge to be detectable in other streams using ^{14}C depends on the magnitudes of groundwater discharge, dissolved inorganic carbon, and ^{14}C relative to stream values.